The Abdus Salam
International Centre for Theoretical Physics

United Nations
Educational, Scientific and
Cultural Organization

IAEA
International Atomic Energy Agency

2332-30

School on Synchrotron and FEL Based Methods and their Multi-Disciplinary Applications

19 - 30 March 2012

Infrared spectroscopy and microscopy

Lisa Vaccari
ELETTRA - Sincrotrone Trieste

Strada Costiera 11, 34151 Trieste, Italy - Tel.+39 040 2240 111; Fax +39 040 224 163 - sci_info@ictp.it

Infrared spectroscopy and microscopy

Lisa Vaccari
SISSI beamline @ Elettra Laboratory

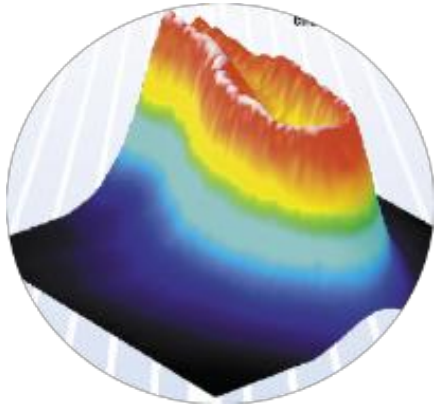

SR & FEL School
19-30 March 2012

Talk outline

- The infrared spectral region
- Basics on vibrational spectroscopy
- Instrumentation
  - FTIR spectrometer
  - Vis-IR microscope
- InfraRed Synchrotron Radiation (IRSR)
  - IRSR Sources
  - IRSR Advantages
  - IR Beamline design
- SR-IRMS applications in the MIR domain
  - Space science
  - Earth science
  - Cultural Heritage
  - Biological and biomedical applications of SR-IRMS: from archeology to living cell analysis
    - Biology and biochemistry: the spectroscopic point of view
      - Microspectroscopic Evidence of Cretaceous Bone Proteins
      - Prion disorders
      - SR-IRMS of living cells: toward a label free single-cell based assay
        - » SR-IRMS of living versus fixed single-cells
        - » Real-time chemical imaging of bacterial activity in biofilms
        - » Dual element ATR mapping
- Summary and conclusions

The infrared spectral region

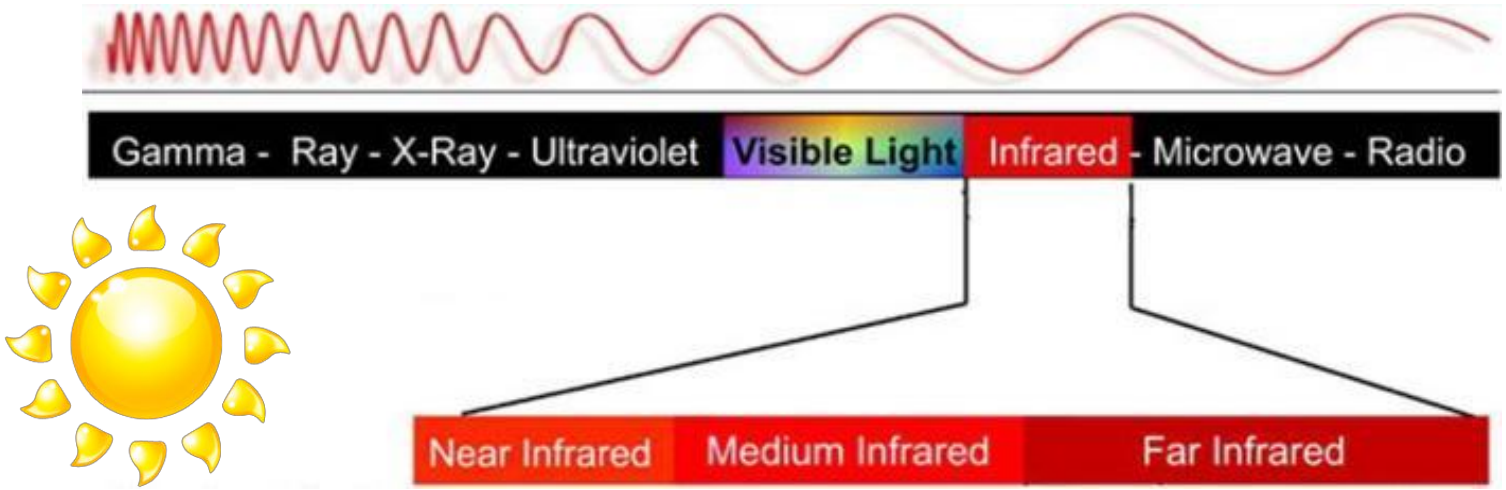

	NIR	MIR		FIR
λ (μm)	0.74	3	30	300
ν (THz)	400	100	10	1
$\overline{\nu}$ (cm^{-1})	~13000	~3333	~333	~33
E (eV)	1.65	0.413	0.041	0.004
E (Kcal/mol)	37	10	1	0.1

The IR spectral range is a wide region of long wavelengths

Basics on vibrational spectroscopy

IR spectroscopy is an absorption spectroscopy

Direct resonance between vibrational transition frequency and photon frequency

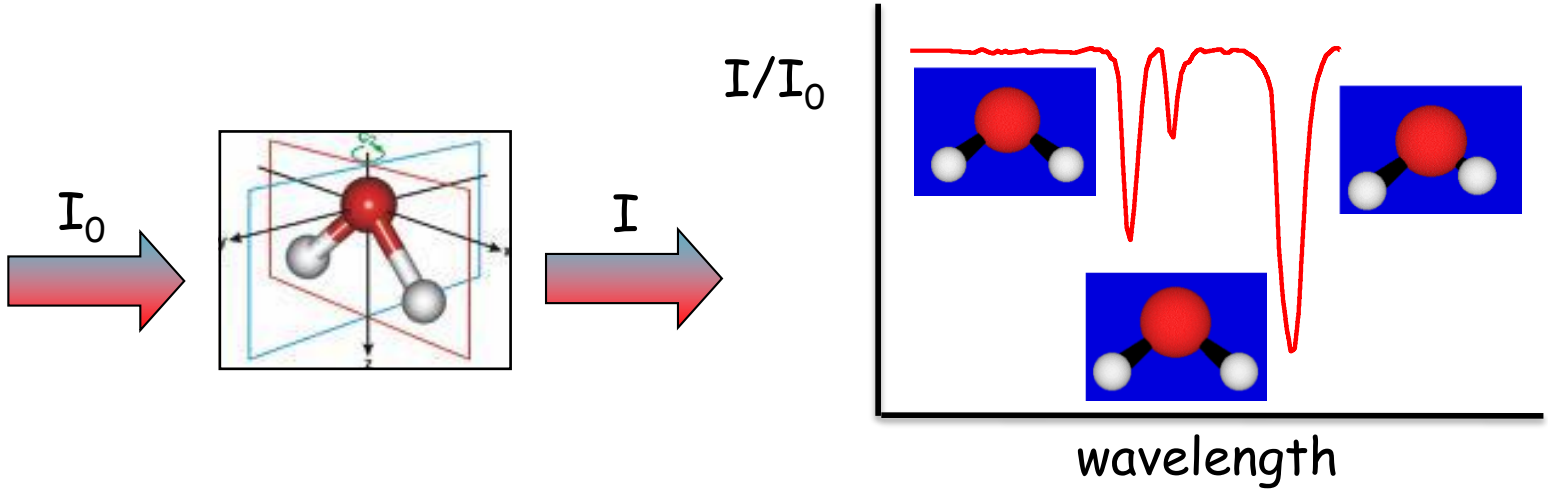

Vibrational (stretching) frequencies

For a diatomic molecule or molecular fragment

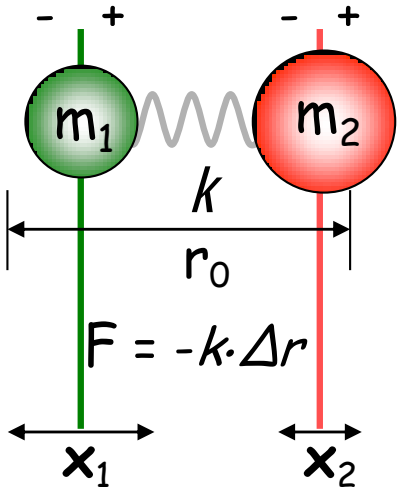

$$\nu = \frac{1}{2\pi}\sqrt{\frac{k}{\mu}}$$

$$\mu = \text{Reduced mass} = \frac{m_1 m_2}{m_1 + m_2}$$

$$K = \text{Spring constant}$$

$$\Delta r = \text{Displacement}$$

Vibrational energies

Harmonic approximation

$$E_{vib} = h\nu_0(n+1/2), \quad \nu_0 = \text{fudamental vibrational frequency} = \frac{1}{2\pi}\sqrt{\frac{k}{\mu}}$$

Anharmonicity

$$E_{vib} = h\nu_0[(n+1/2) - x_o(n+1/2)^2 + \text{higher terms}]$$

$$x_0 = \text{anharmonic constant}$$

Harmonic oscillator

$$\Delta n = 1$$

Anharmonic oscillator

$$\Delta n = \text{integer}$$

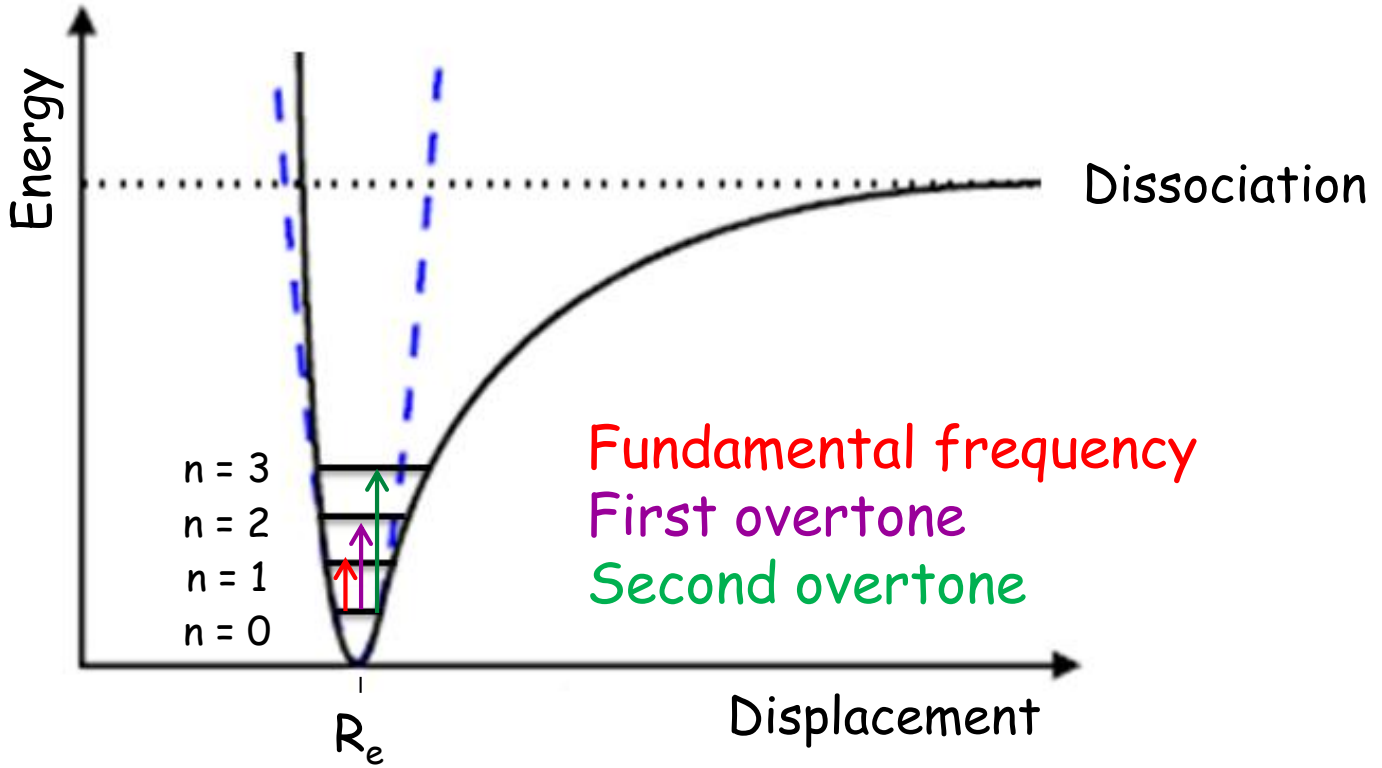

Fundamental modes of vibrations for polyatomic molecules

Linear N-atom molecule: 3N-5 modes of vibration

Non linear N-atom molecule: 3N-6 modes of vibration

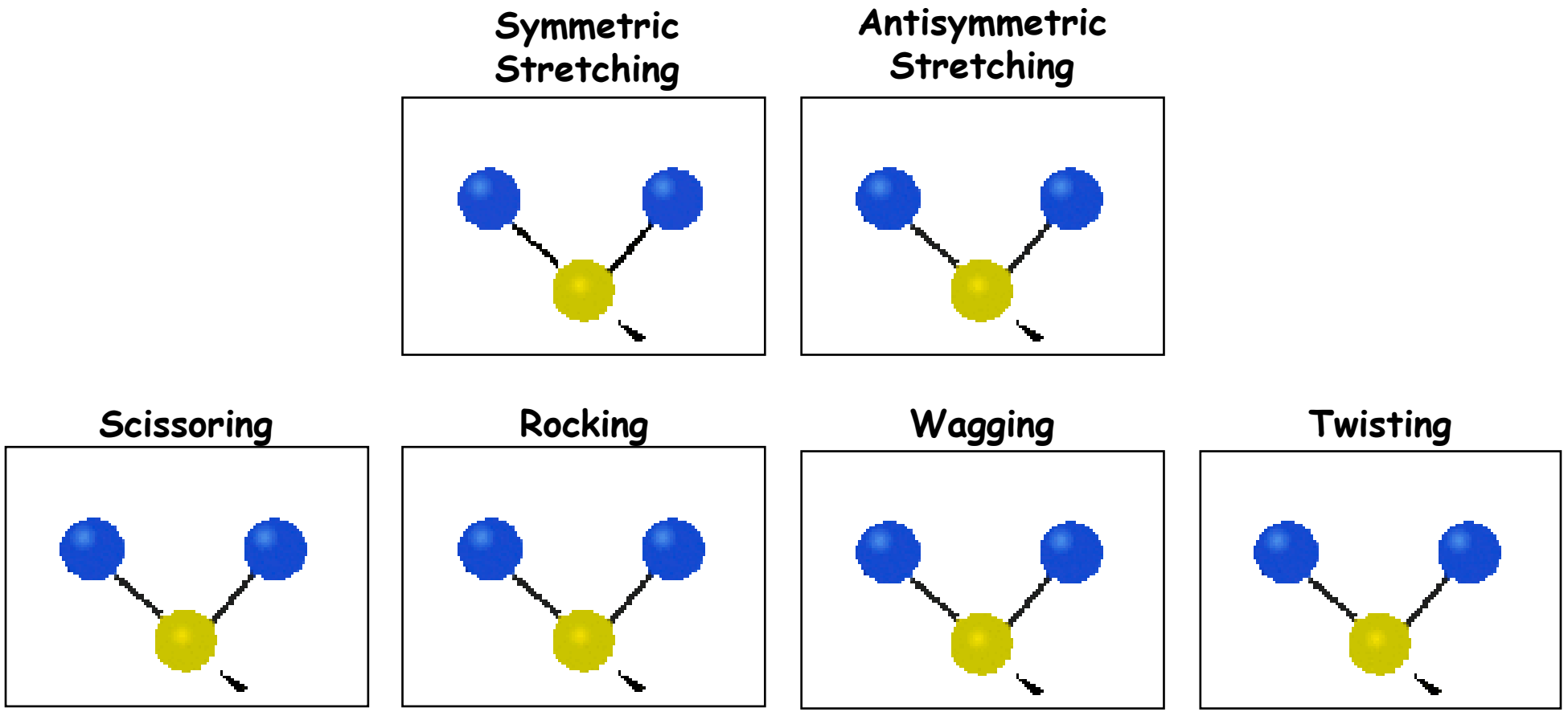

Only the vibrational modes that produce a change of the molecular dipole moment are IR active

The liquid water absorption spectrum

Overtones and combination bands

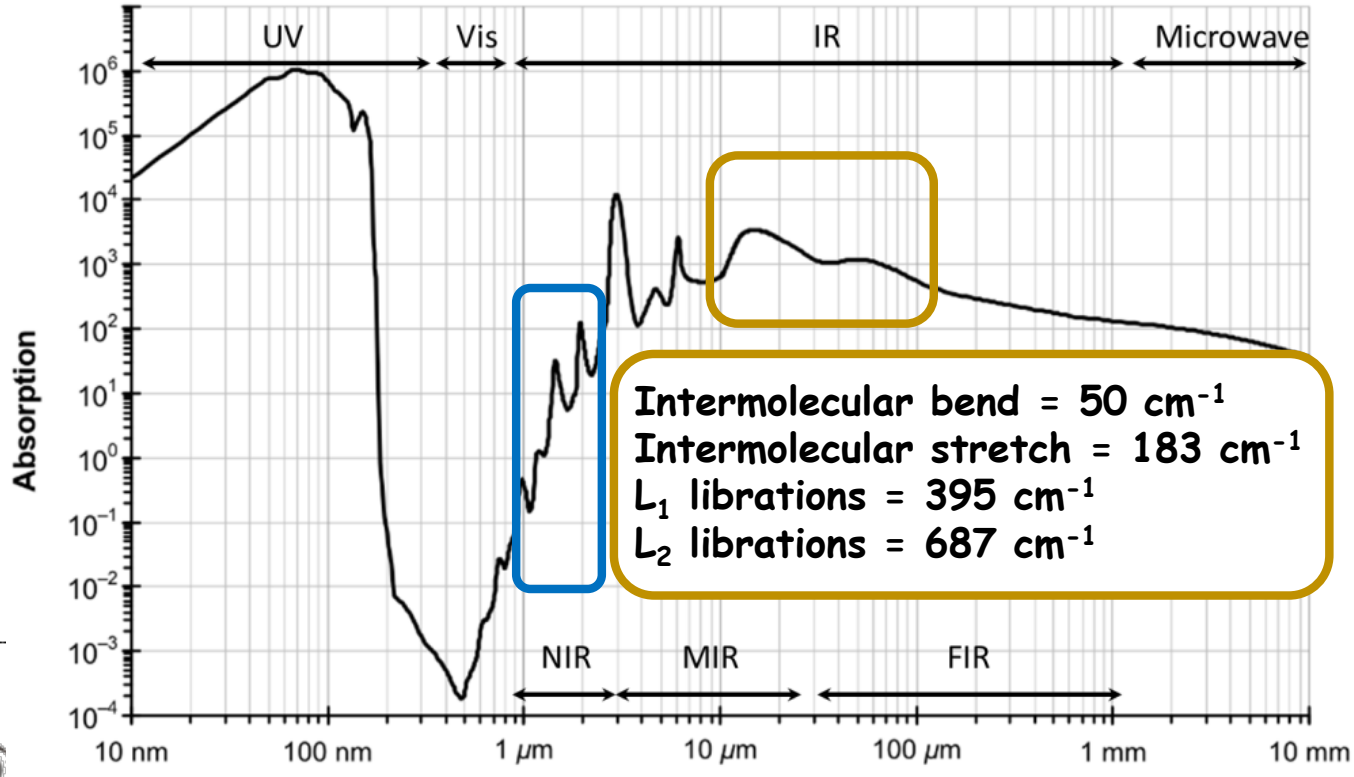

Intermolecular bend = 50 cm^{-1}
Intermolecular stretch = 183 cm^{-1}
L_1 librations = 395 cm^{-1}
L_2 librations = 687 cm^{-1}

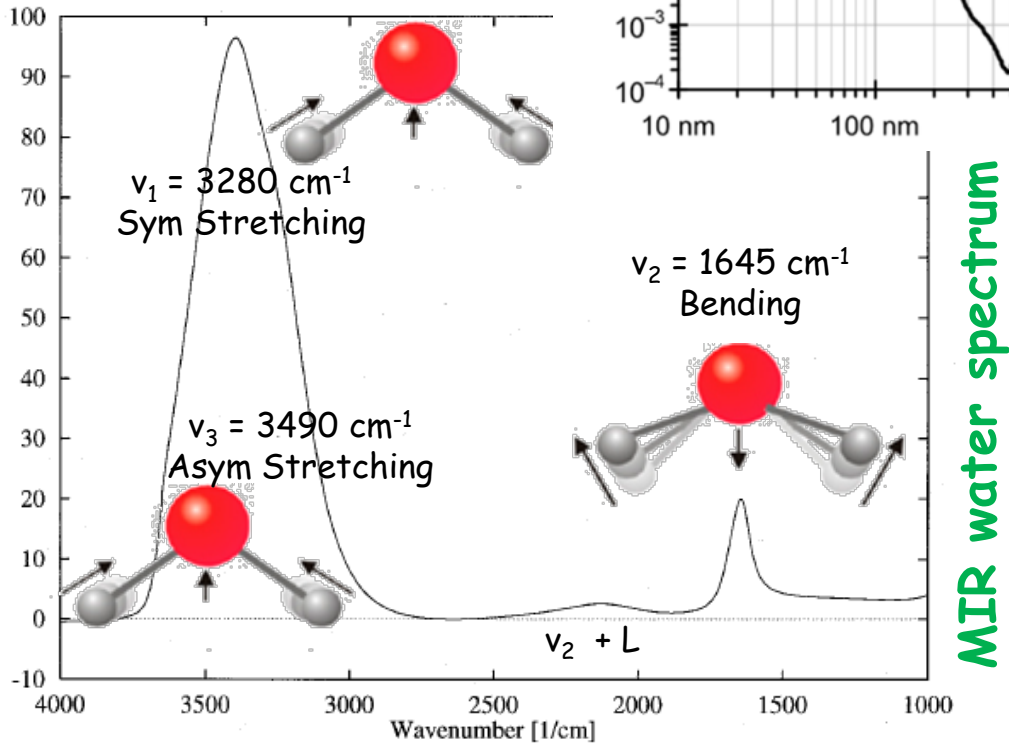

MIR water spectrum

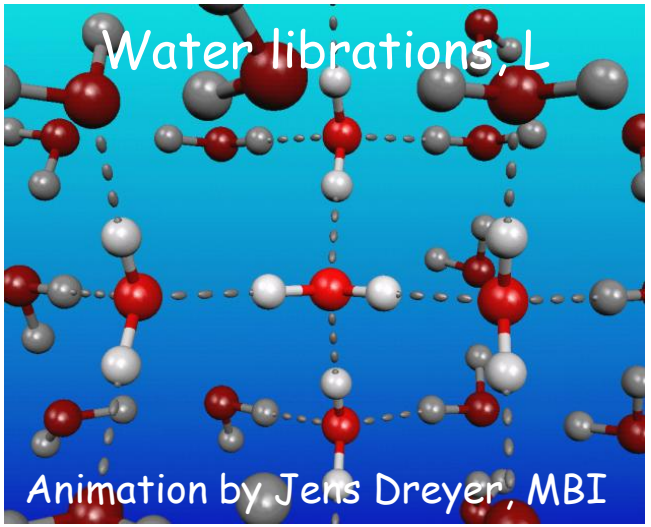

Spectral information

From peak position, intensity and width

- Atoms involved in the vibration
- Strength of the atomic bond(s) : single, double, triple bond
- Bond(s) conformation: cis/trans isomers, molecular conformations, ….
- Chemical environment
- Atomic bond orientation

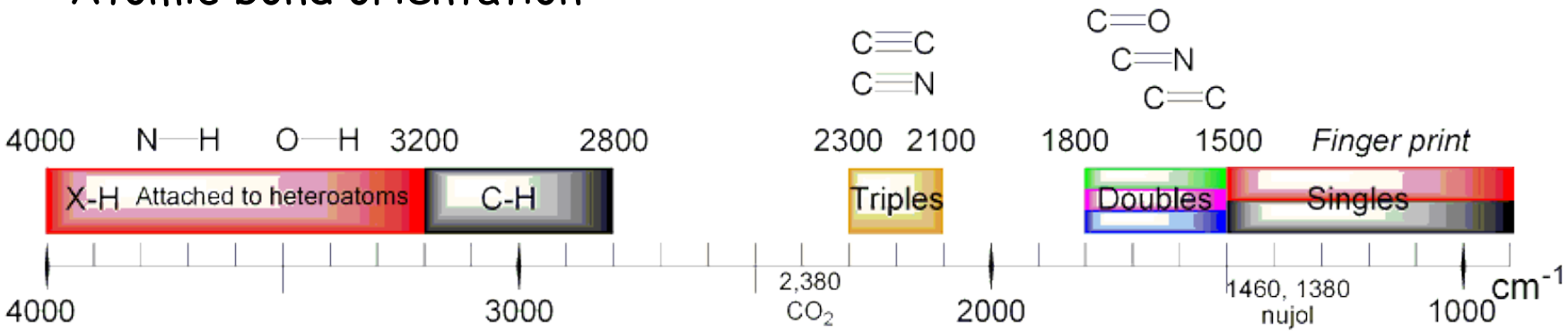

- Drude term (FIR)
- Semiconductor gaps (NIR-Vis)
- Excitons
- Polarons

Instrumentation
FTIR spectrometerrometer

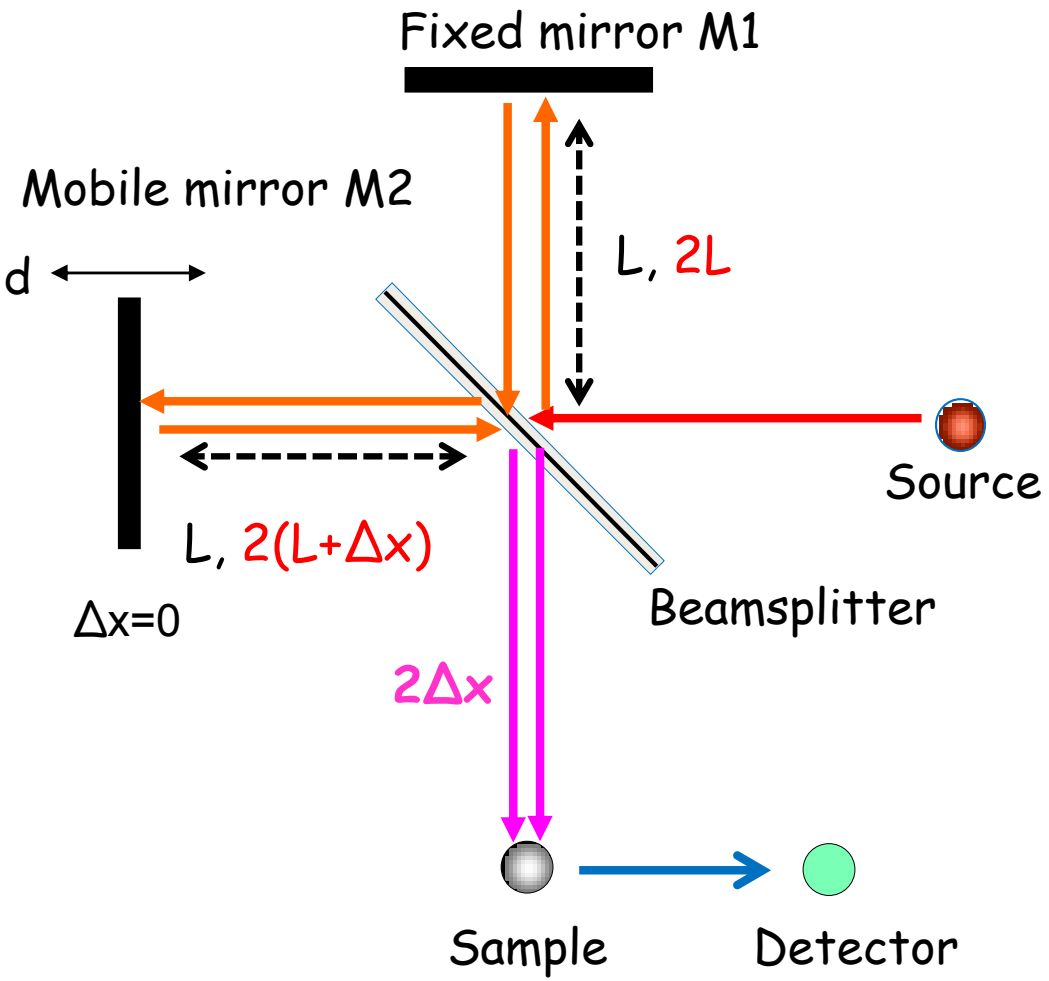

Conventional sources

NIR: Tungsten lamp
MIR: Glow bar (SiC)
FIR: Hg-Arc

Beamsplitters

NIR: CaF_2
MIR: KBr
FIR: Mylar, Silicon

Detectors

NIR – InGaAs, InSb, Ge, Si room temperature detectors
MIR: Room temperature DLaTGS
Nitrogen cooled MCT
FIR – He Cooled Silicon Bolometer
Room temperature DLaTGS

Spectral Resolution

$\Delta\nu \sim 1/\Delta x(cm^{-1}) \sim 0.001\ cm^{-1} \sim 1meV$

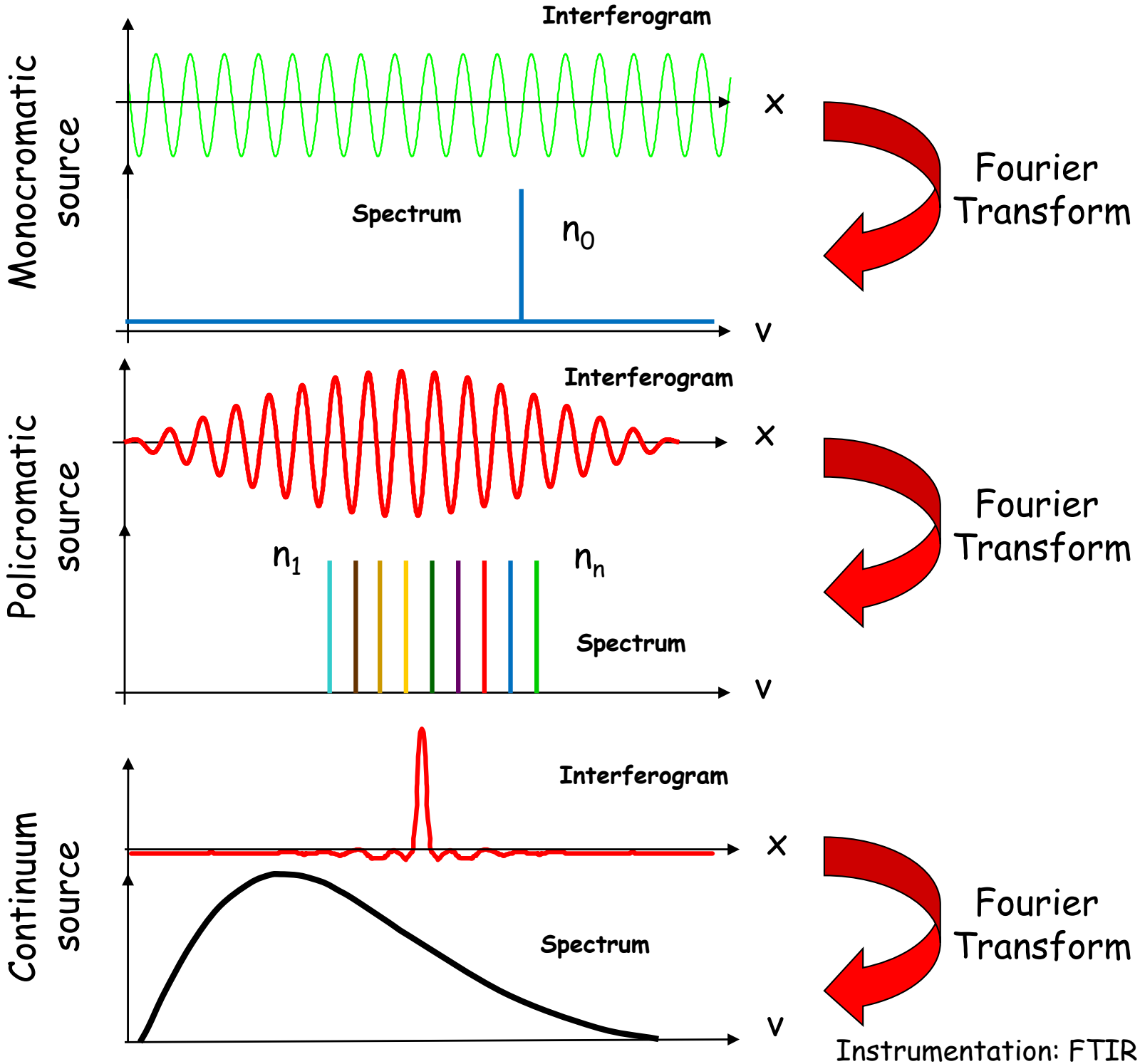
Monocromatic source
Interferogram
x
Spectrum
n_0
v
Fourier Transform
Policromatic source
Interferogram
x
n_1
n_n
Spectrum
v
Fourier Transform
Continuum source
Interferogram
x
Spectrum
v
Fourier Transform

Advantages of FTIR interferometers

- Jacquinot's throughput advantage
  - All source wavelengths are measured simultaneously in an interferometer, whereas in a dispersive spectrometer they are measured successively. A complete spectrum can be collected very rapidly and many scans can be averaged in the time taken for a single scan of a dispersive spectrometer.
- Fellgett's advantage (Multiplex advantage)
  - For the same resolution, the energy throughput in an interferometer can be higher than in a dispersive spectrometer, where it is restricted by the slits.
- Connes' accuracy advantage
  - The wavenumber scale of an interferometer is derived from a HeNe laser that acts as an internal reference for each scan. The wavenumber of this laser is known very accurately (632.8 nm) and is very stable. As a result, the wavenumber calibration of interferometers is much more accurate and has much better long term stability than the calibration of dispersive instruments.

As a result, a FTIR spectrum can be measured with the same signal-to-noise ratio than a dispersive spectrum in a much shorter time (seconds rather than minutes) and spectral subtractions can be carried out without frequency errors

Spectral acquisition

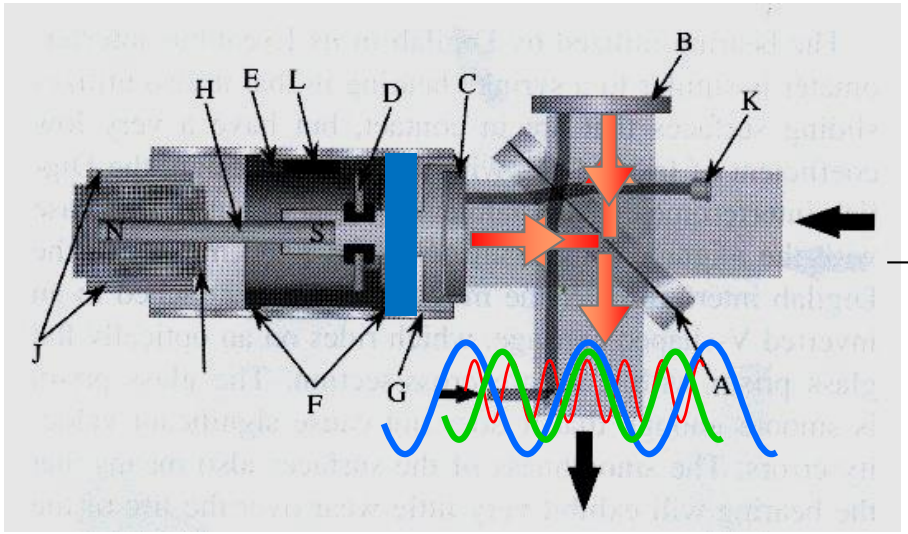

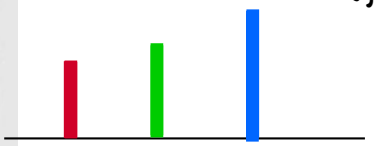

ν

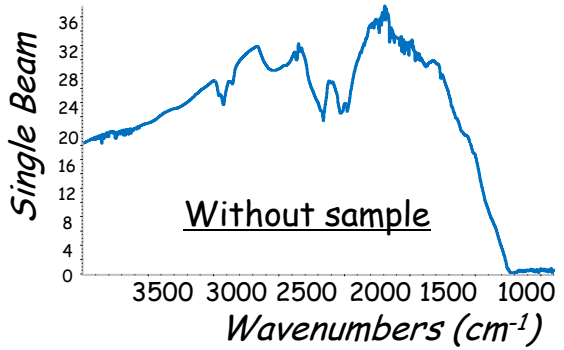

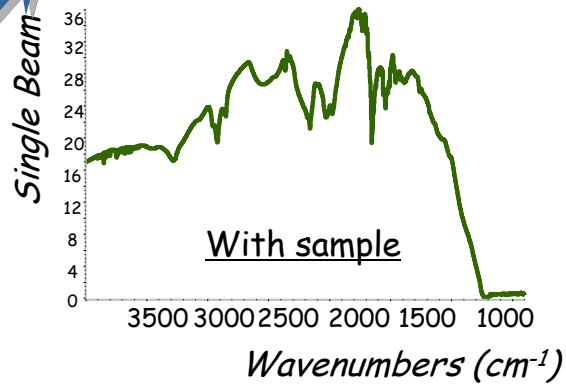

Fast Fourier Transform

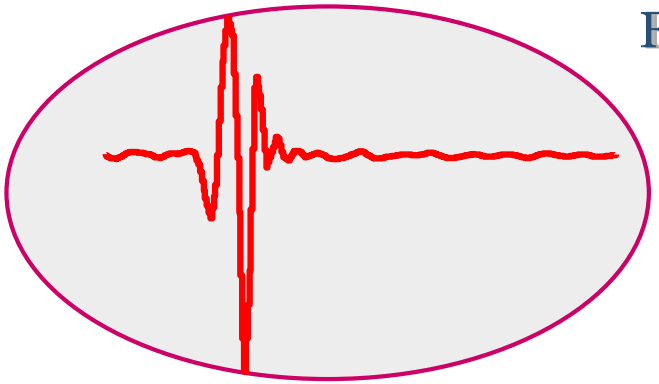

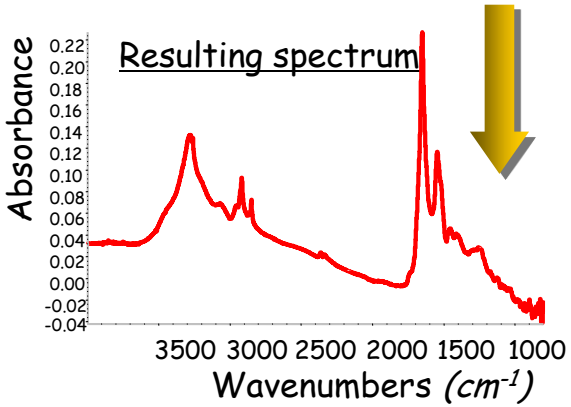

Instrumentation: FTIR spectrometer_4

Sampling techniques

- TRANSMISSION

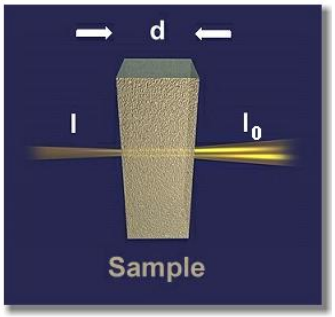

Lambert-Beer Law

$$A = -\log_{10}(I/I_0) = \varepsilon dc$$

$$[\varepsilon] = L \cdot mol^{-1} \cdot cm^{-1},\ [c] = mol \cdot L^{-1},\ [d] = cm$$

- REFLECTION

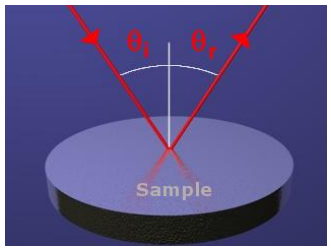

Typical angle of incidence = 10-30°
The refraction behavior of the bulk sample is investigated

  - SPECULAR
  - DIFFUSE

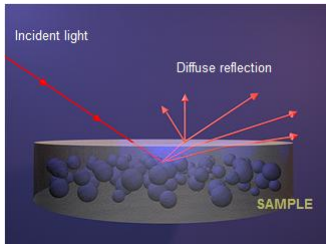

The diffusive-reflection spectrum is defined by the absorption-scattering behavior of the sample

  - ATR

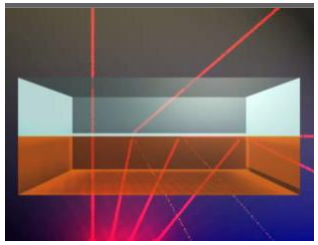

$$dp\ (\text{penetration depth}) = \frac{\lambda}{2\pi n_1 \sqrt{(\sin^2\theta - n_{21}^{\ 2})}}$$

1 = crystal, 2 = sample

(Attenuated Total Reflection)

  - GRAZING INCIDENCE

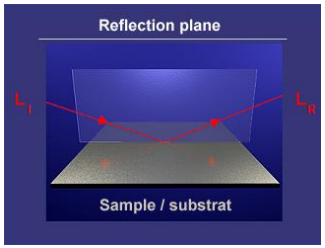

Typical angle of incidence = 50-85°
The surface properties of the sample are investigated

Instrumentation: FTIR spectrometer_5

Instrumentation
Vis-IR microscopes

Spatially resolved chemical information on heterogeneous samples are obtained by coupling FTIR spectrometers with specially designed Vis-IR microscopes

Schwarzschild objective

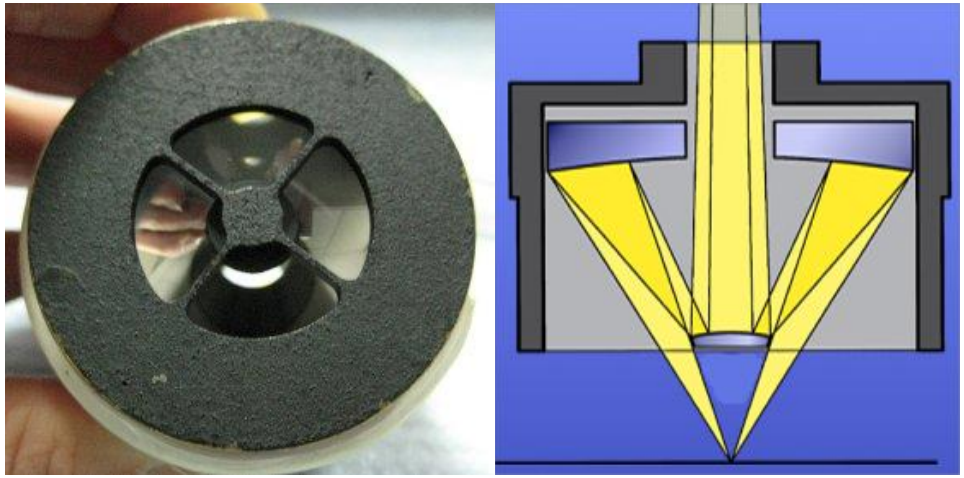

The highest achievable lateral resolution, δ, is diffraction limited

Objective NA	Wavelength	δ
0.4	10 μm (1000cm^{-1})	~15 μm
	2.5 μm (4000cm^{-1})	~ 4 μm
0.65	10 μm (1000cm^{-1})	~ 9,5 μm
	2.5 μm (4000cm^{-1})	~ 2,5 μm

$$\delta \approx 0.61 \lambda / NA$$

FTIR mapping versus FTIR imaging

Mapping layout

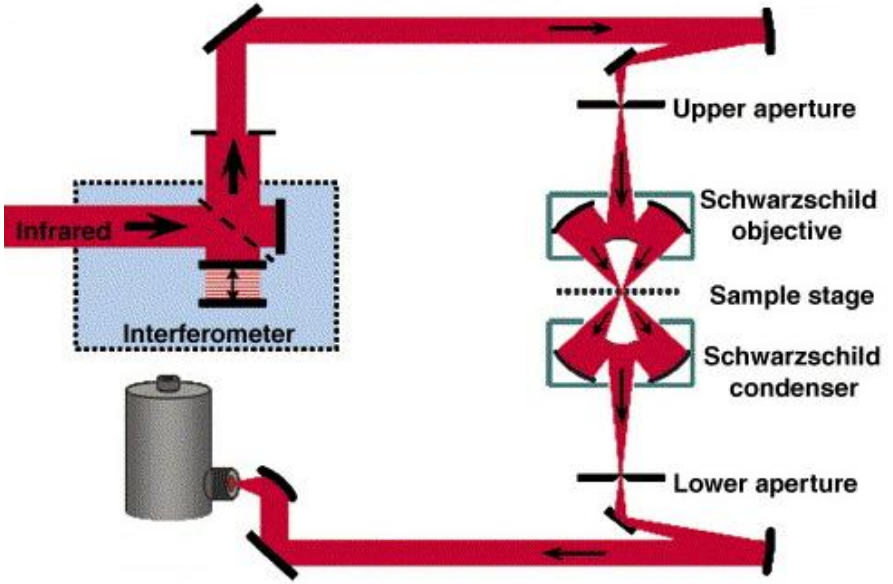

Single point detector

Optical sample image

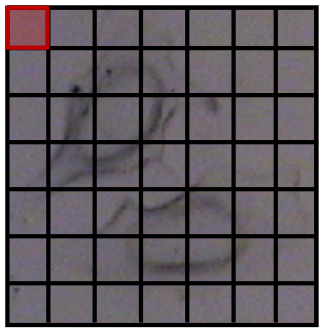

- The map pixel size is provided by the aperture settings
- Sequential acquisition: Slow imaging of large sample areas
- Low detector noise, high SNR

Chemical sample image

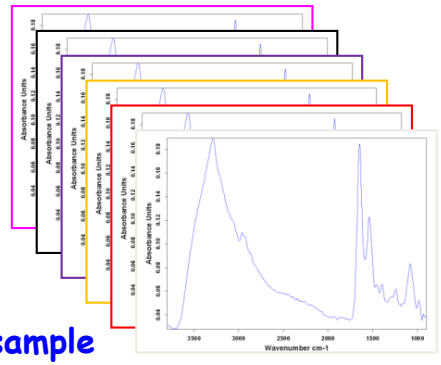

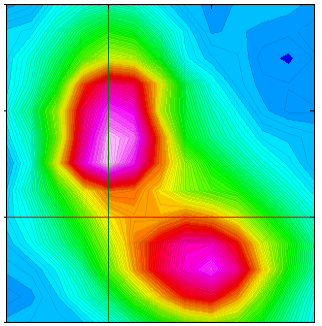

Imaging layout

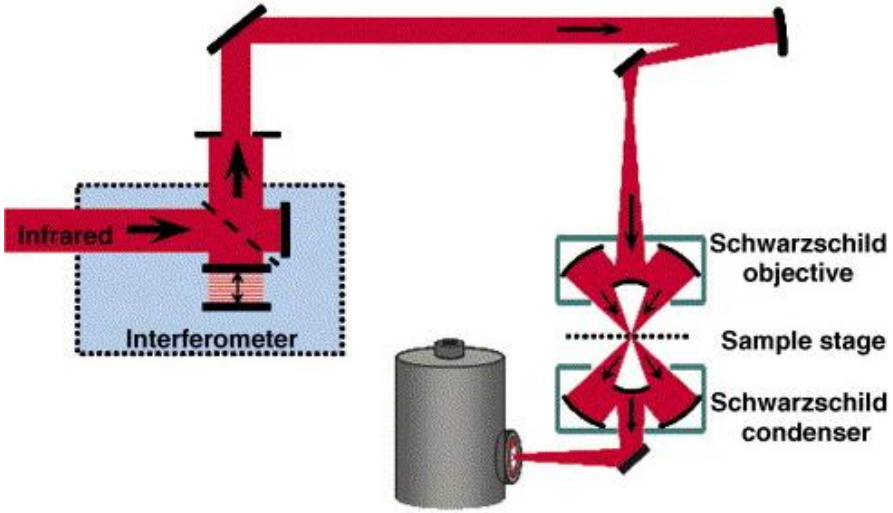

Detector array at focal plane

Optical sample image

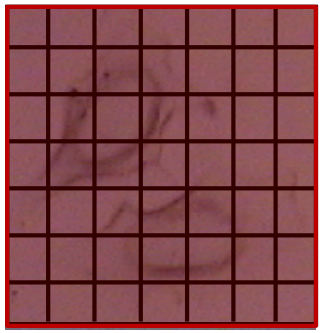

- The image pixel size is provided by the individual pixel of the detector
- Parallel acquisition: Fast imaging of large sample areas
- High detector noise, low SNR

Adapted from: L.Miller, P. Dumas, BBA 1758:846, 2006

InfRared Synchrotron Radiation (IRSR) _ Sources

Standard Bending radiation

Emitted during the circular trajectory in the bending magnet (BM) due to the constant magnetic field, B

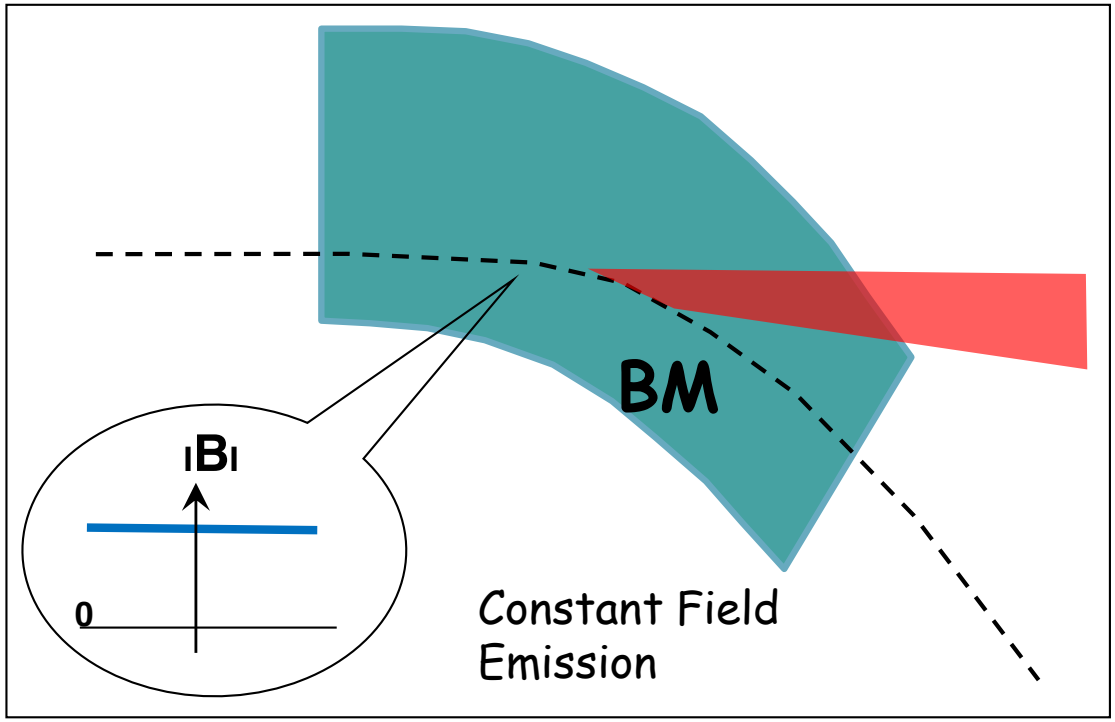

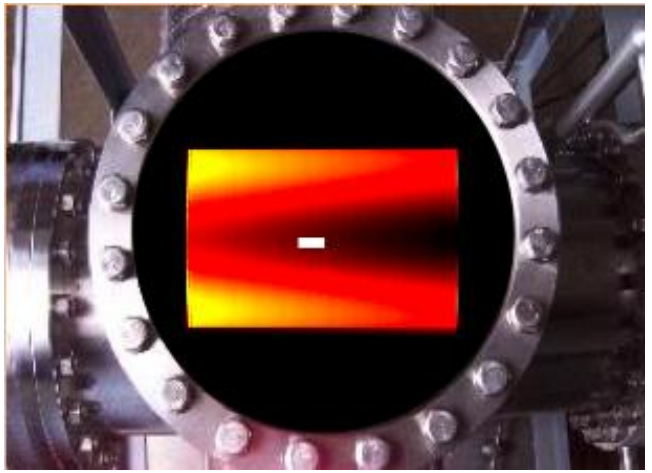

Natural opening angle

$\Theta_{V\text{-}NAT}$ (rad) = 1.66 (λ / ρ)$^{1/3}$

P (λ) = 4.4 10^{14} x I x Θ_H x *bw* x (ρ/λ)$^{1/3}$ photons s^{-1}

I is the current in amperes,

Θ_H **(rads)** the horizontal collection angle,

bw the bandwidth in per cent, **λ** the wavelength, and **ρ** the radius of the bending

Edge Emission

Emitted at the entrance (exit) of a bending magnet due to the rapid variation of the B field

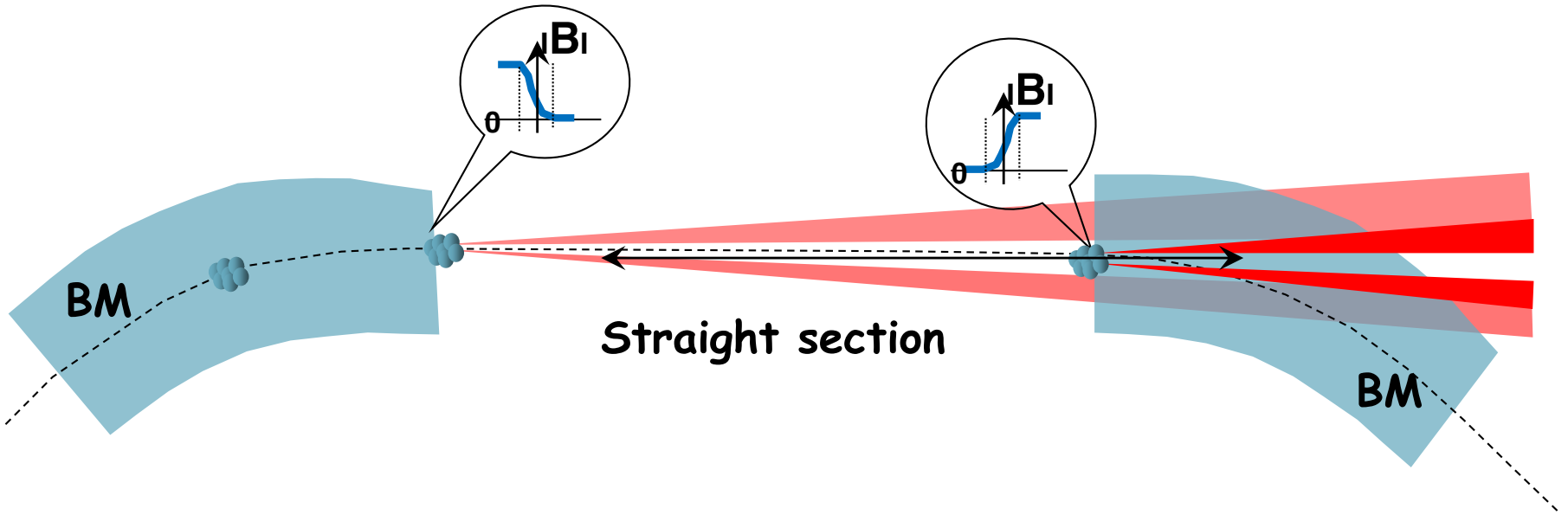

In the Far-Field approximation:

$$P = \alpha \times I \times \gamma^4 \Theta^2/(1+ \gamma^2\ \Theta^2)^2 \text{ photons } s^{-1}$$

I is the current in amperes,
Θ (rads) the emission angle
(concentrated in $\Theta_{max} \sim 1/\ \gamma \sim 10$ mrads)

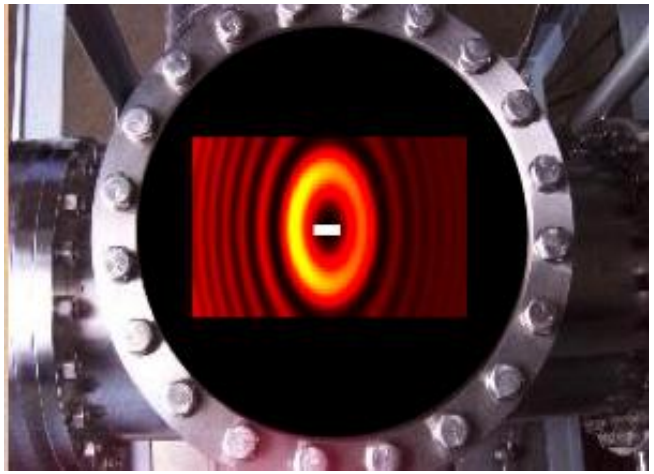

InfRared Synchrotron Radiation (IRSR) _ Advantages

The IRSR Flux and Brilliance depend on:

- -beam current
- -source size/emittance
- -extraction aperture
- -transmission optics

Instead scarcely depend on the machine energy

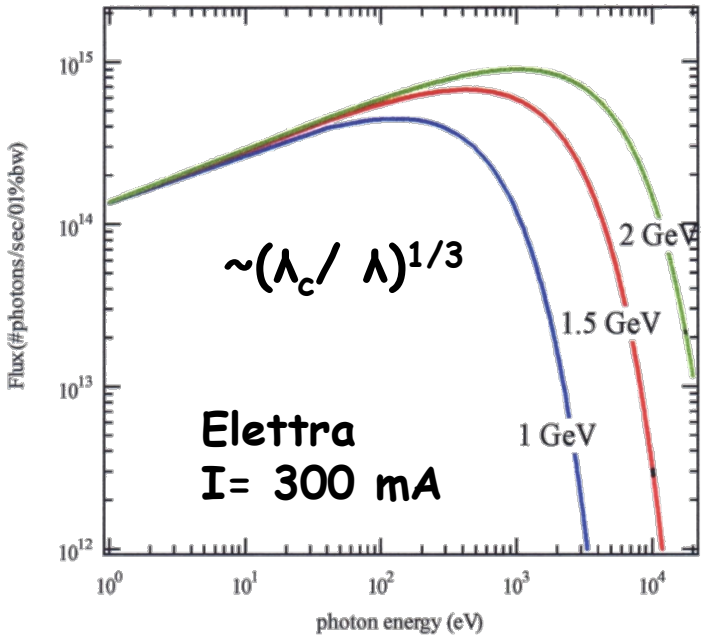

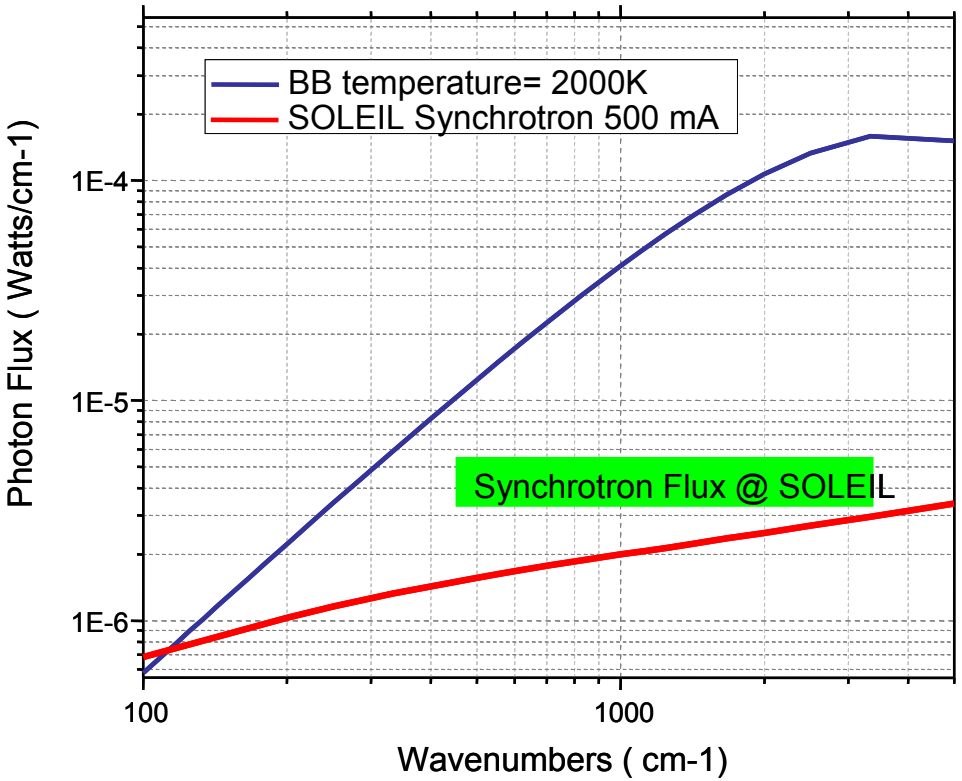

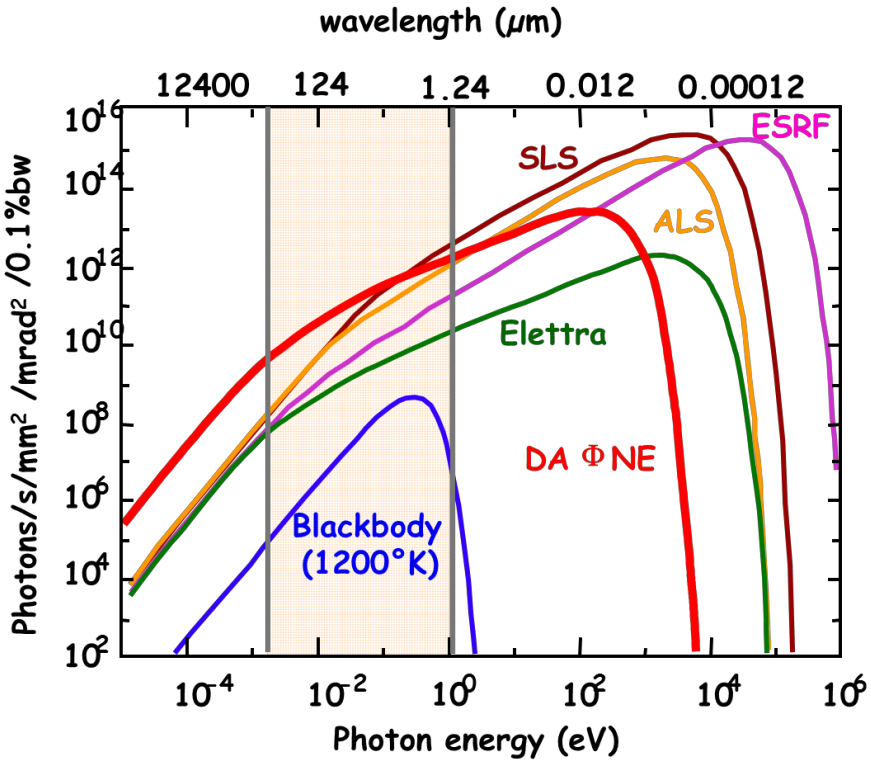

InfRared Synchrotron Radiation (IRSR)
Advantages

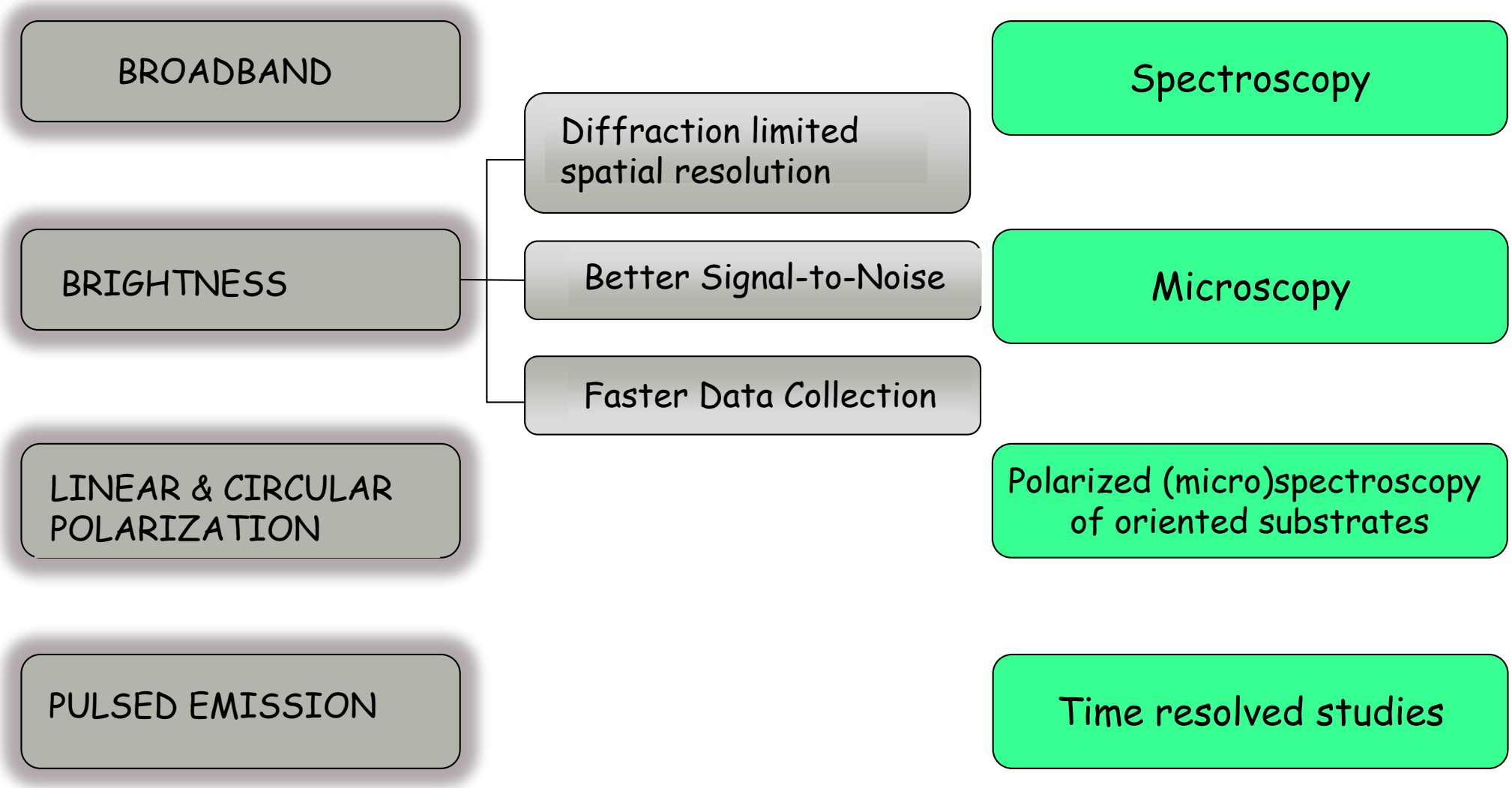

IR beamline design

Conventional IR beamline layout: SISSI@Elettra

Radiation is collected over a solid angle of
65 mrad (H) × 25 mrad (V)

M1 Plane mirror
M2 Ellipsoidal mirror
M3 Plane mirror
M4 Ellipsoidal mirror

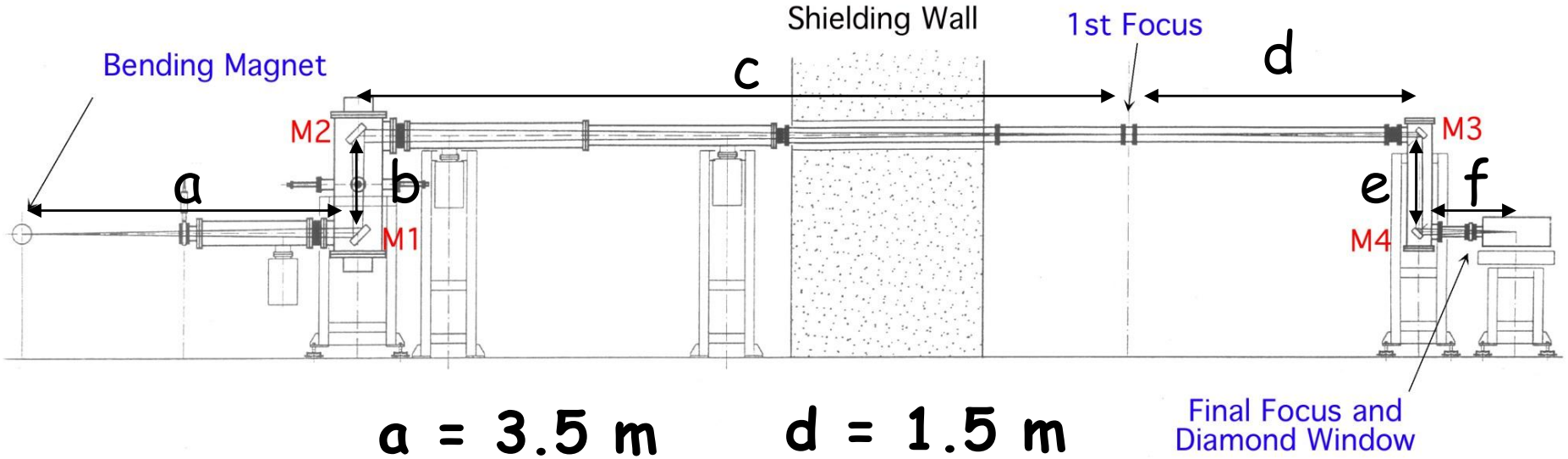

a = 3.5 m d = 1.5 m

b = 1.0 m e = 1.0 m

c = 11.5 m f = 2.5 m

SISSI first chamber

The water-cooled extraction mirror (M1)

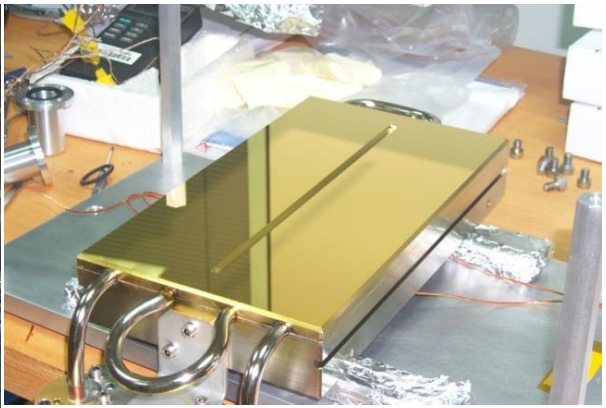

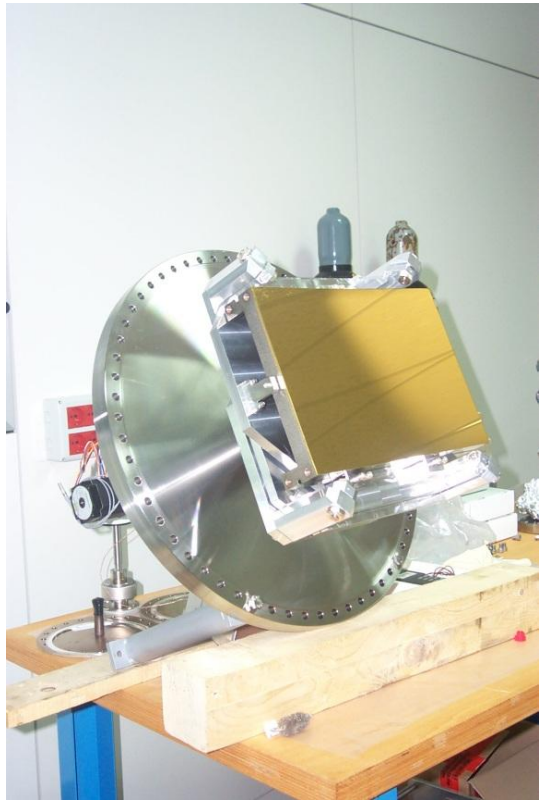

The focusing Ellipsoidal mirror (M2)

Intensity distribution on the extraction mirror (photons*0.1%bw/mm^2)

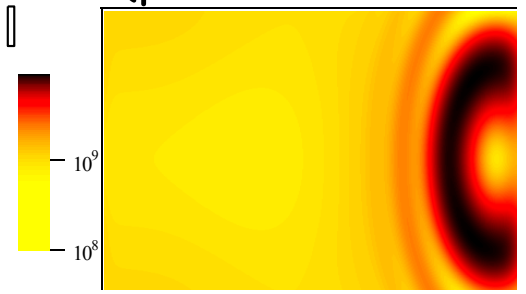

10 meV
~ 80 cm^{-1}

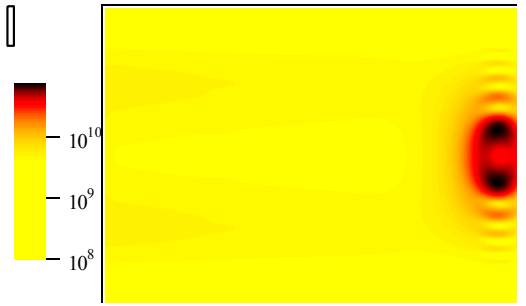

100 meV
~ 805 cm^{-1}

500 meV
~ 4000 cm^{-1}

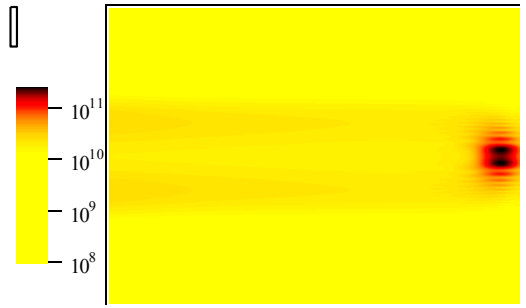

1 eV
~ 8000 cm^{-1}

IR beamline design_2

MIR performances of SISSI@Elettra

Diffraction-limited lateral resolution is practically achievable only by exploiting the brightness advantage of SR

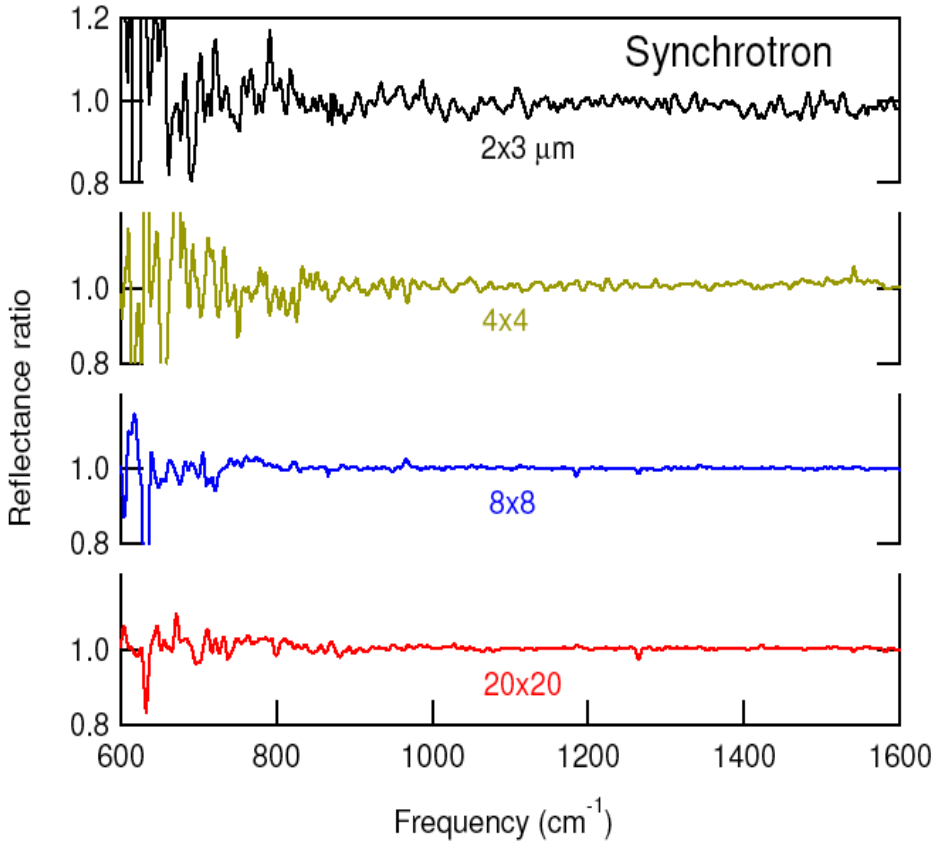

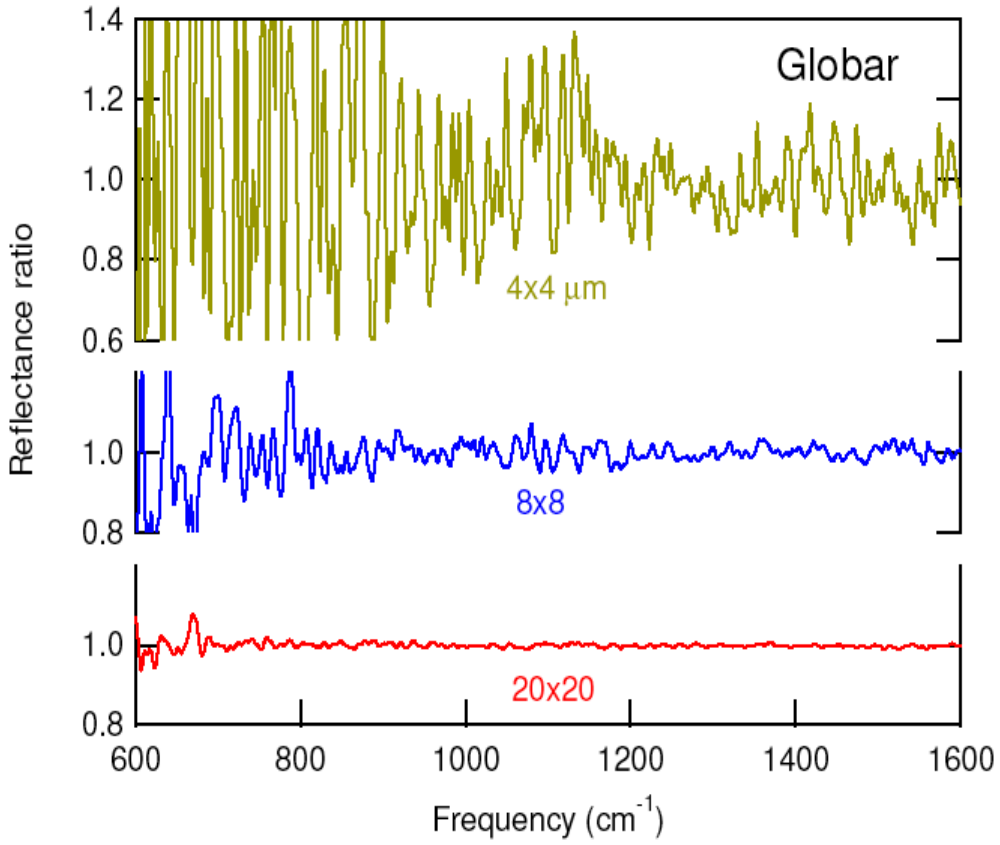

N_2 cooled MCT detector, 128 scans, 4 cm^{-1} spectral resolution

Figure of merit of SISSI@Elettra

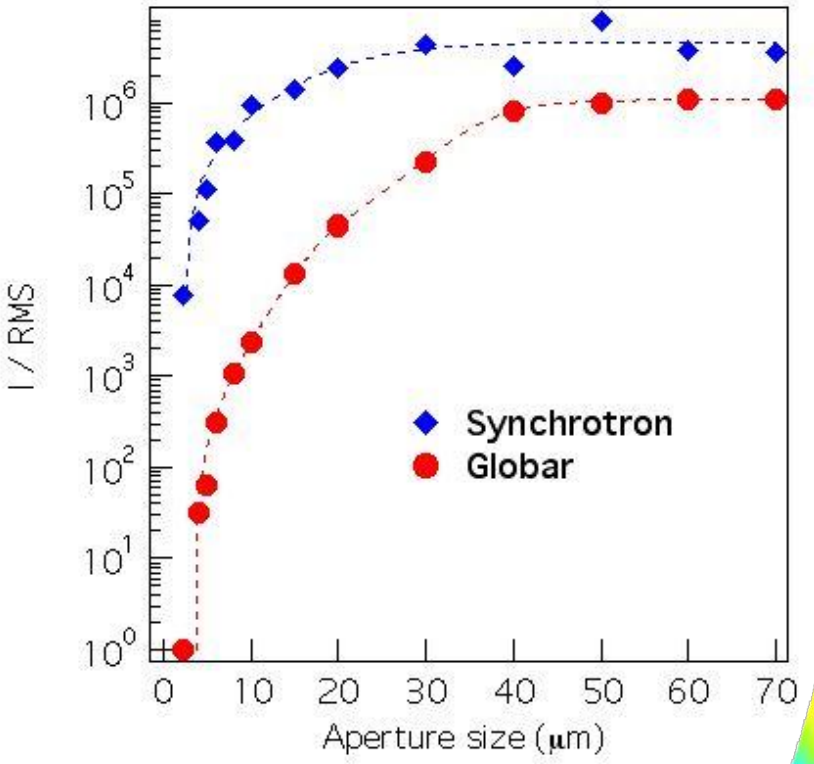

MIR

MCT detector, 128 scans,
4 cm^{-1}

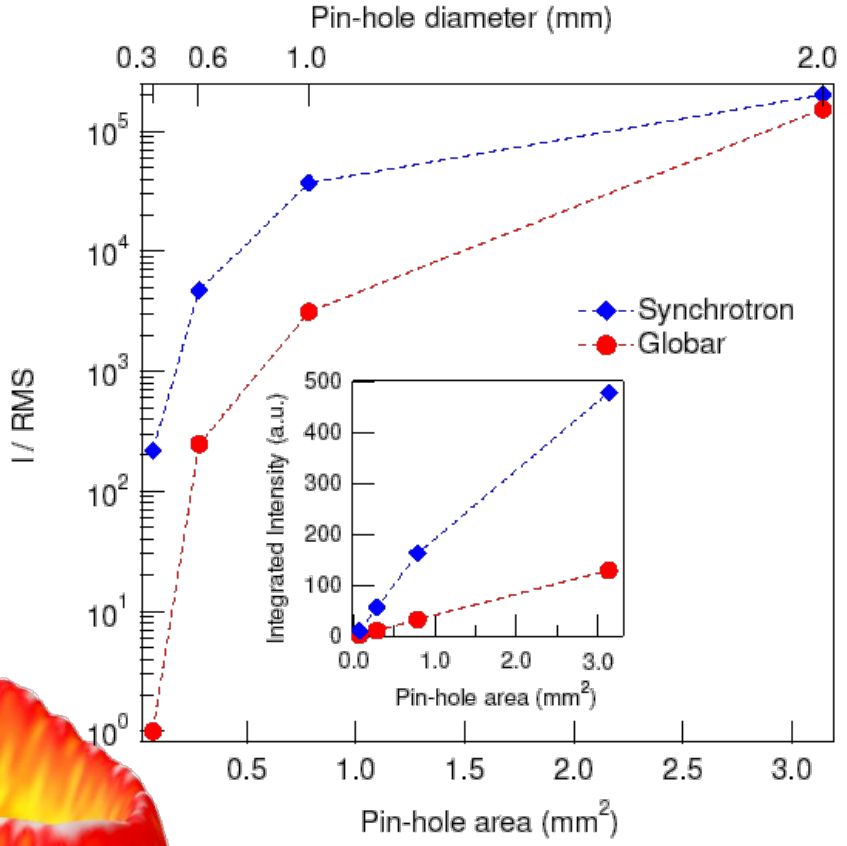

FIR

Si bolometer, 128 scans,
4 cm^{-1}

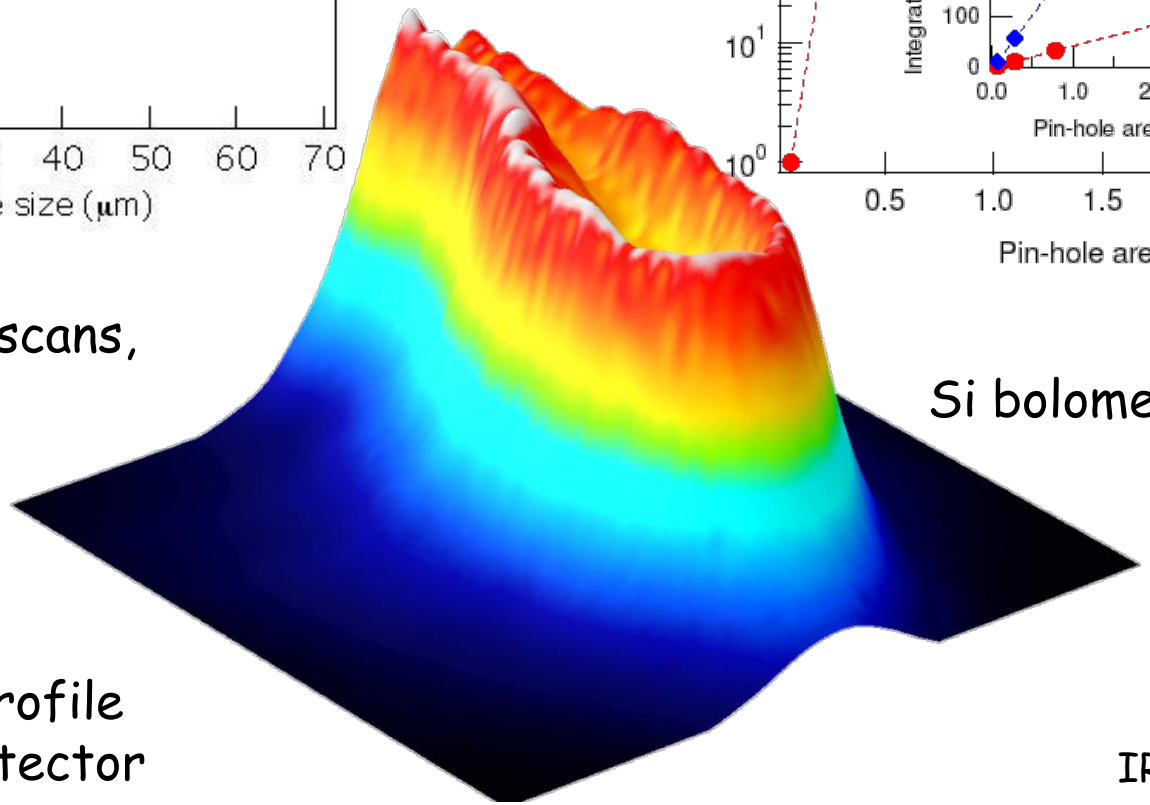

SISSI MIR beam profile
imaged with FPA detector

Beamline branches simultaneously working

At SISSI beamline, the two branches can not operate simultaneously

More recent beamlines in newer III generation SR facilities split BM and ER radiation contributions for the simultaneous operation of two branches

SMIS @ Soleil

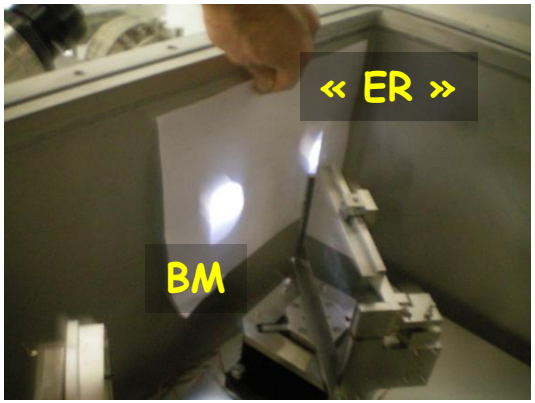

Microscope 2
Branche ER

Microscope 1
Branche BM

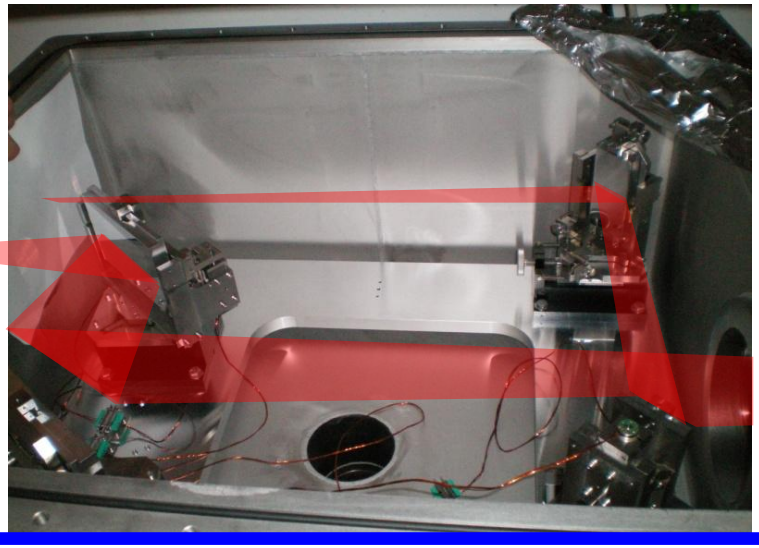

More recent IR beamline layout: IRENI@Synchrotron Radiation Center, Wisconsin-Madison

The FTIR imaging approach: high SNR and fast acquisition speed

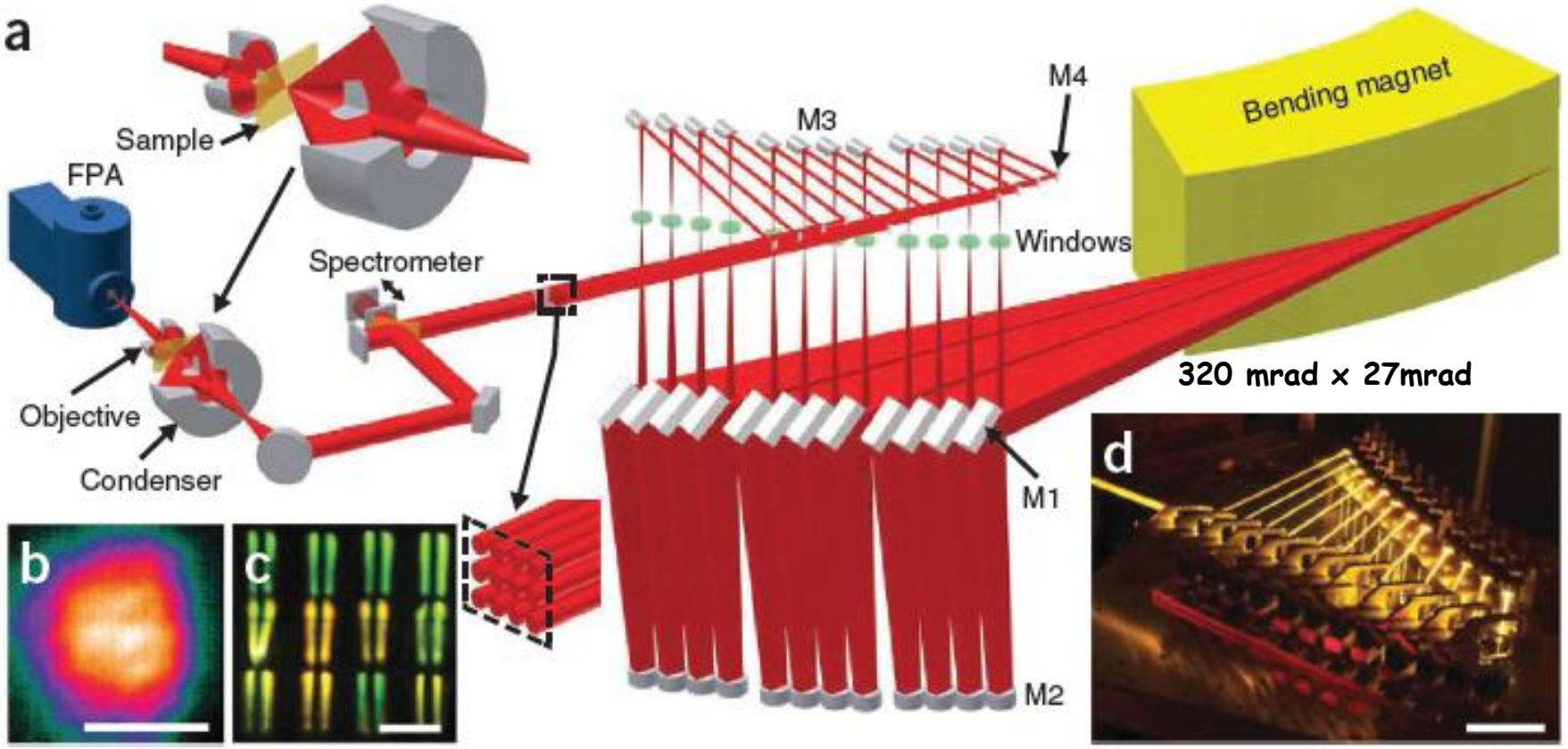

From M.J. Nasse *et al.*, Nature methods, 8:413 (2011)

IRSR Beamlines in the World

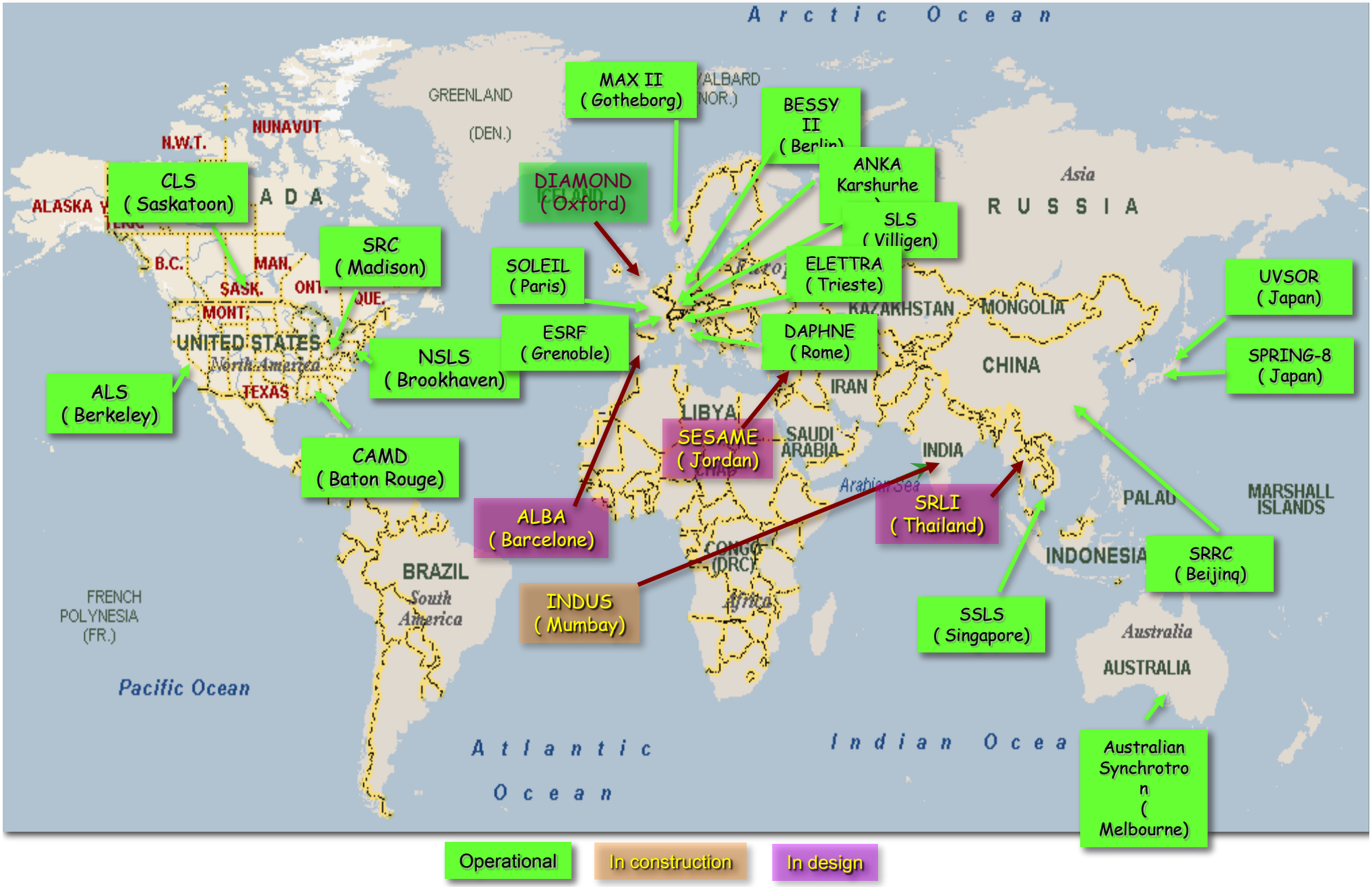

Syncrotron Radiation applications in the MIR domain

- Space science
- Earth science
- Cultural Heritage
- Biological and biomedical applications of SR-IRMS: from archeology to living cell analysis

  Biology and biochemistry: the spectroscopic point of view
  - Microspectroscopic Evidence of Cretaceous Bone Proteins
  - Prion disorders

  SR-IRMS of living cells: toward a label free single-cell based assay
  - Living versus fixed single cell SR-IRMS
  - Real-time chemical imaging of bacterial activity in biofilms
  - Dual-element ATR microscopy
- And many others…..

Synchrotron infrared microscopy of micron-sized extraterrestrial grains

The study of extraterrestrial micronsized particles is a topic of major interest in astrophysics and planetology. Among the various microanalysis tools available, SR Infrared Microspectrometry is of particular interest, as it is a non-destructive technique, well suited to provide mineralogical and chemical information on micrometer scales.

Caractherization of Orgueil chondrite

A large stony carbonaceous meteorite that disintegrated and fell in fragments near the French town of Orgueil on May 14, 1864

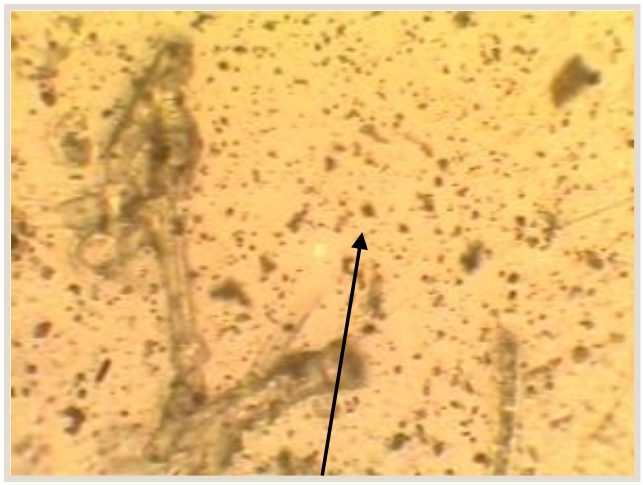

"Orgueil" particle sample prepared by crushing the material between two glass slide and following transfer on a KBr window

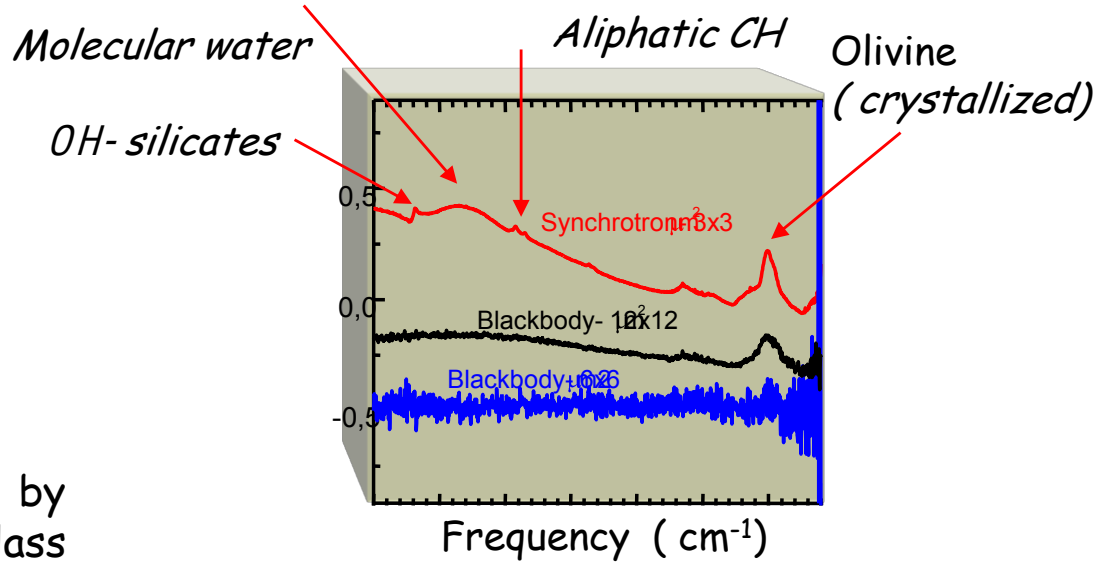

Chemical image of –OH water distribution inside Orgueill particles, 3X3µm lateral resolution

Optical snapshot

Integrated absorbance [3800-3000 cm^{-1}]

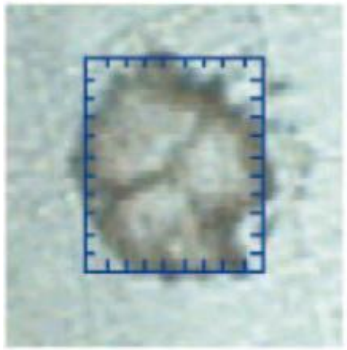

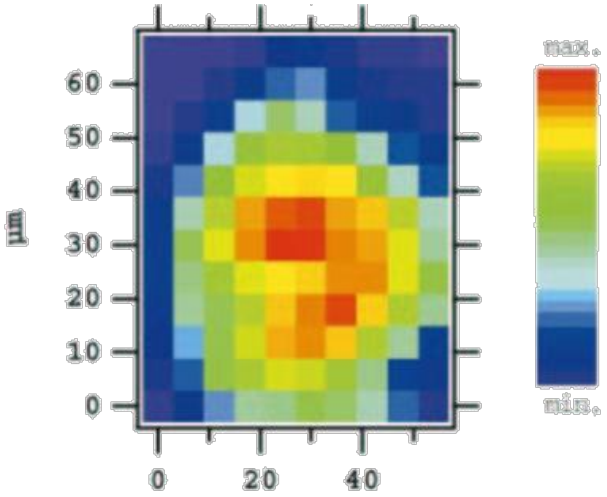

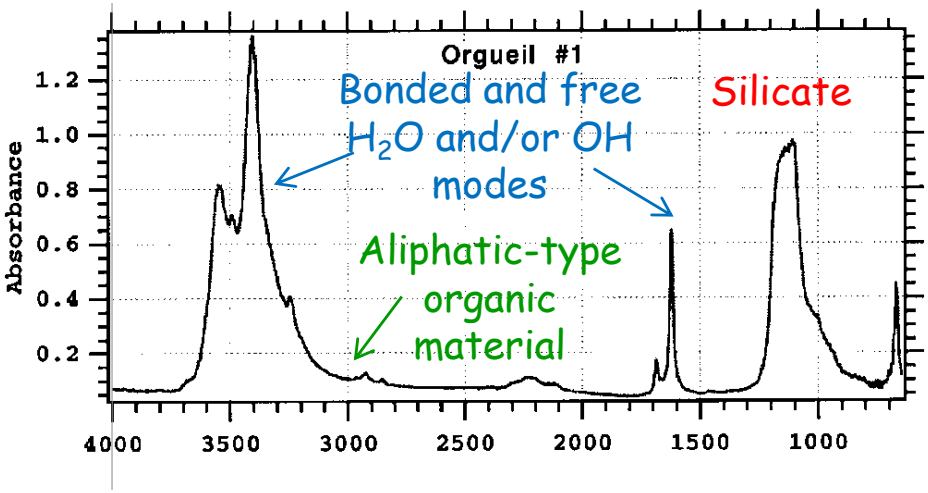

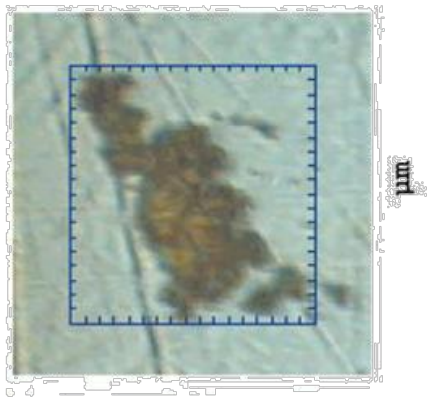

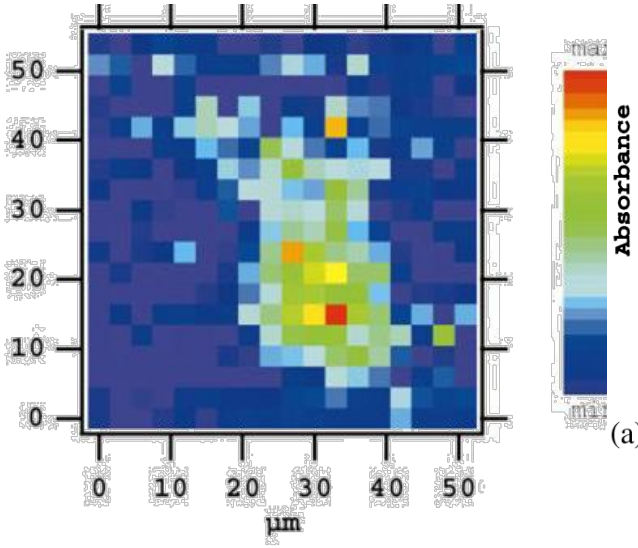

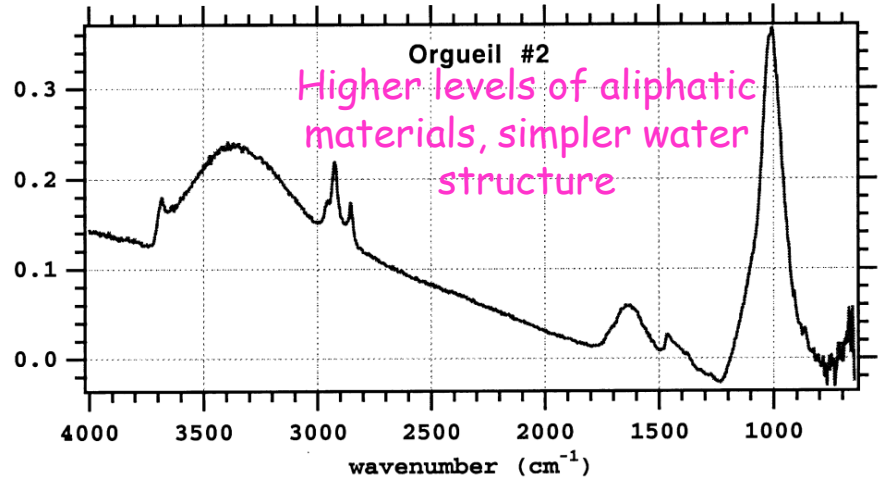

(a)

From P.I. Raynala;E. Quiricoa, J. Borga, et al., Planetary and Space Science 48 (2000) 1329

The STARDUST MISSION

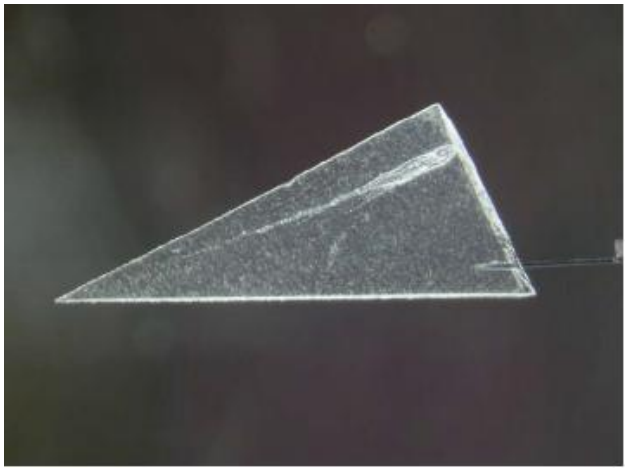

Optical snapshot of the original aerogel surface exposed to the comet

"The primary goal of the Stardust mission was to collect samples of a comet (**81P/Wild2**) and return them to Earth for laboratory analysis. Comets are ancient bodies of frozen ice and dust that formed beyond the orbit of the most distant planet. They were expected to contain materials that the solar system formed from, preserved in ice for billions of years. Before the mission, there were very good reasons to believe that we knew what comets would be made of and there was a general expectation was that the particles collected from comet Wild 2 would be mainly be dust that formed around other stars, dust that was older than the Sun. Such particles are called stardust or pre-solar grains and this was the main reason why the mission was named Stardust."

January 2004- January 2006)

[from: http://stardust.jpl.nasa.gov/news/news116.html]

C2009,7,62

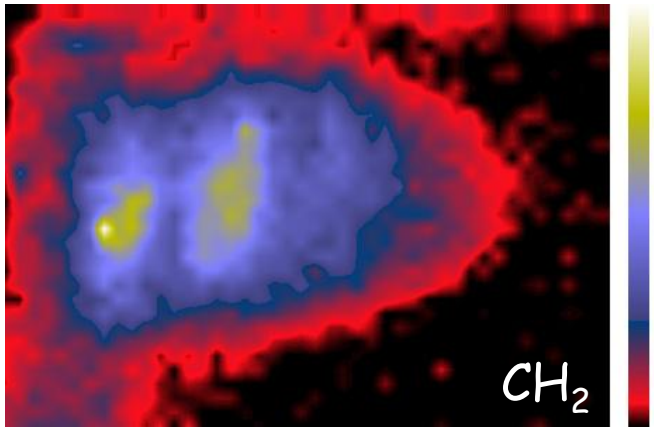

C2009,4,59

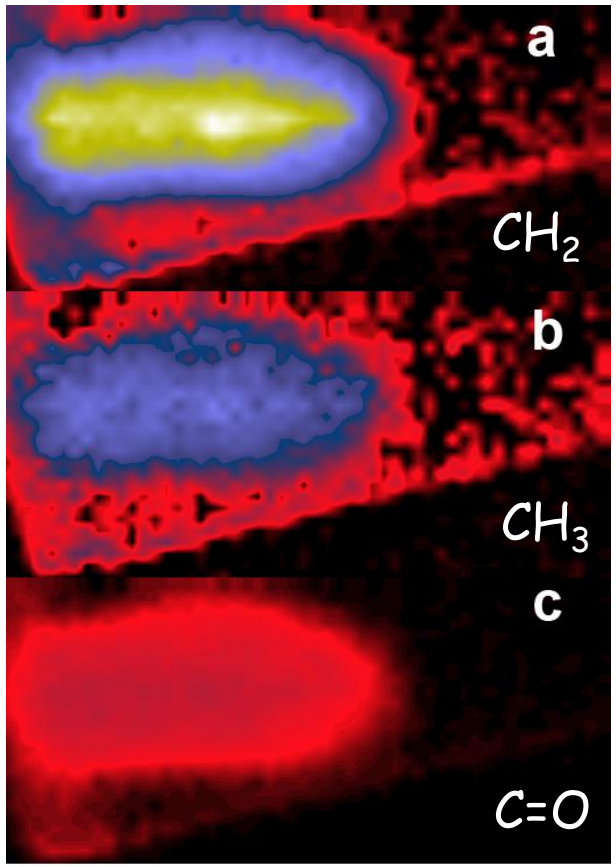

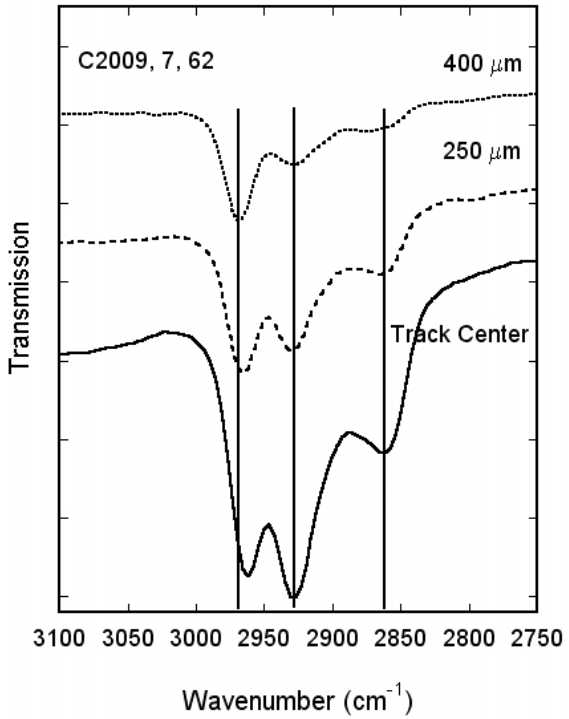

Infrared spectroscopy maps of some tracks, made by cometary dust from 81P/Wild 2 impacting Stardust aerogel, reveal an interesting distribution of volatile organic material [-CH_2- rich].

It is clear that the population of cometary particles impacting the Stardust aerogel collectors also include grains that contained little or none of this volatile organic component. This observation is consistent with the highly heterogeneous nature of the collected grains, as seen by a multitude of other analytical techniques.

S. Bajt, S. A. Sandford, G. J. Flynn et al., 2009 MAPS 44, 471

Earth science: mimicking extreme conditions

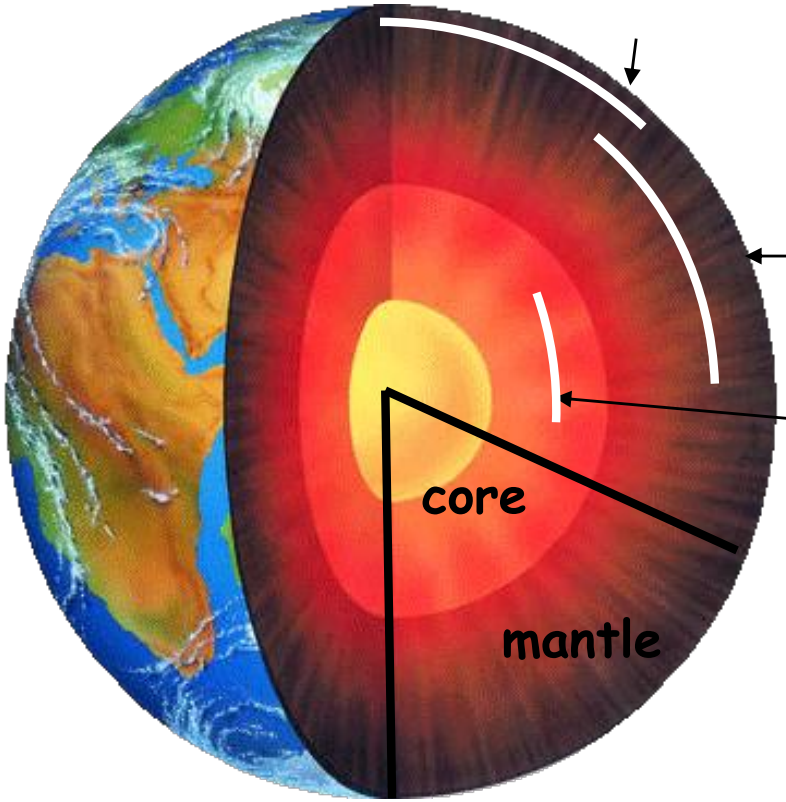

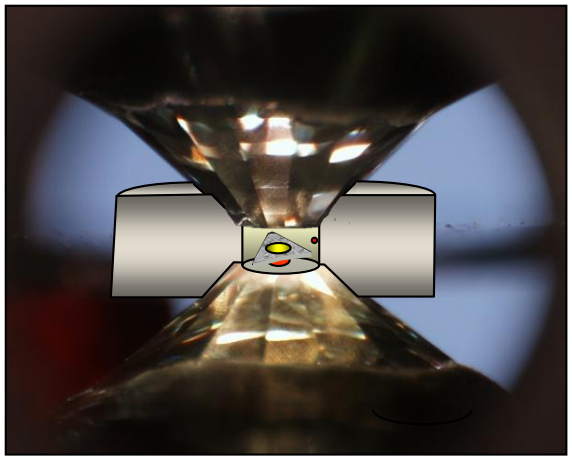

DAC
Diamond Anvil cell

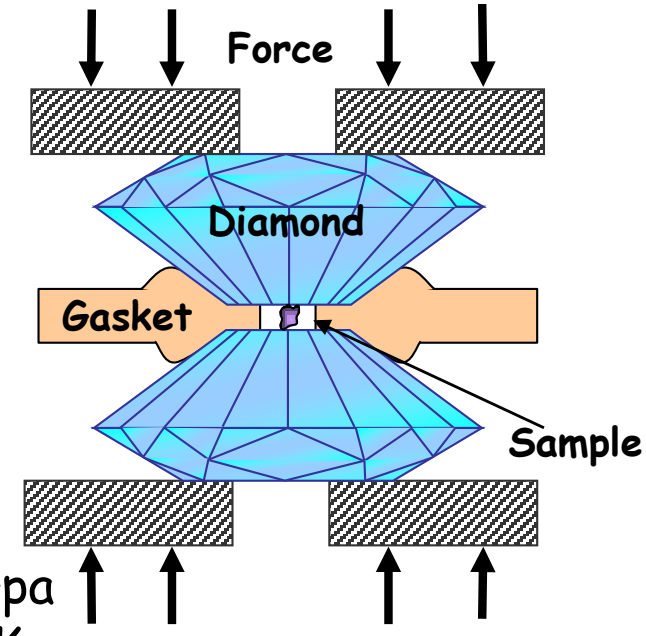

Pressure range: 0.1 Gpa – 30 Gpa
Temperature range: from 4.3K

Effect of H_2O on upper mantle phase transition in $MgSiO_3$

A short introduction

The **X discontinuity** is an intermittently observed upper mantle discontinuity, that lies at a depth of 250-350 km. This boundary is most typically observed in regions of active mantle dynamics, including subduction zones and volcanic hotspots. The X-discontinuity is not a global feature, but it is geologically widespread beneath stable continents.

Upper mantle and transition zone seismic discontinuities are among the most important physical observable of the mantle for remotely interpreting temperature, compositions and mineralogy of the Earth's interior.

Whereas depths and topography of the global discontinuities correspond to well-characterized phase transformations in $(Mg,Fe)_2SiO_4$ polymorphs, the X-discontinuity has eluded obvious explanations. It is difficult to explain its behavior in terms of a single mineralogical phase transition in part because of its depth variability.

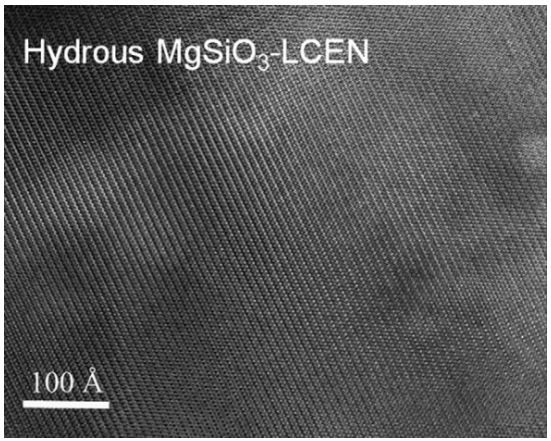

The pressure variation alone at the X discontinuity can not exhaustively explain its properties

The effects of water content in clinoenstatite (a monoclinic magnesium-iron pyroxene with Mg substantially in excess of iron) was studied by infrared spectroscopy on enstatite, $MgSiO_3$-pyroxene.

Jacobsen, SD, Liu Z, Ballaran TB, Littlefield EF, Ehm L, and Hemley RJ (2010) *Physics of the Earth and Planetary Interiors* 183:234-244.

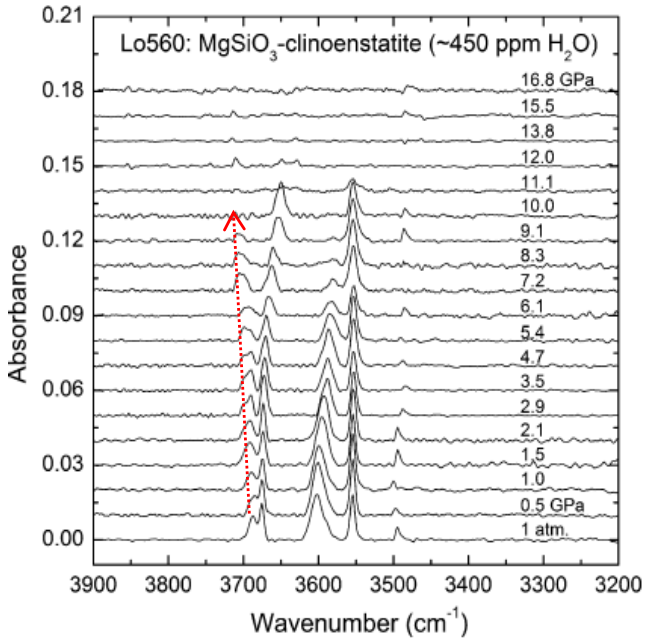

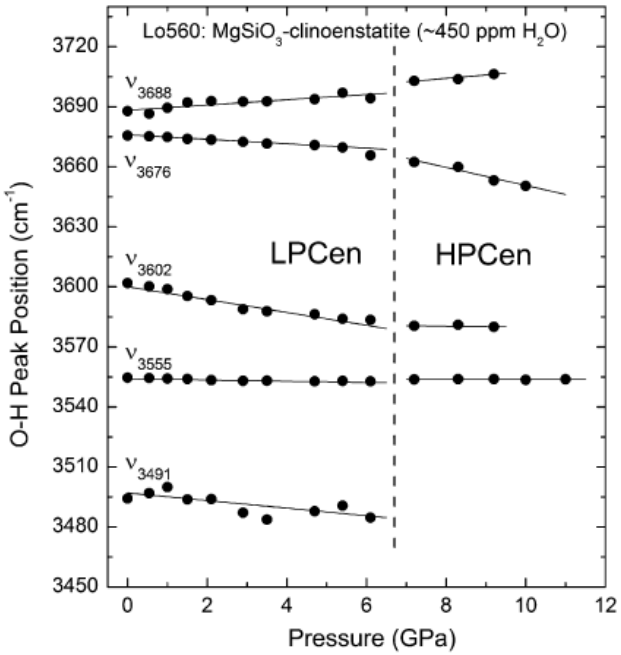

Room pressure OH-bearing clinoenstatite –OH stretching bands:
3688, **3676**, **3602**, **3555**, and **3491** cm^{-1}

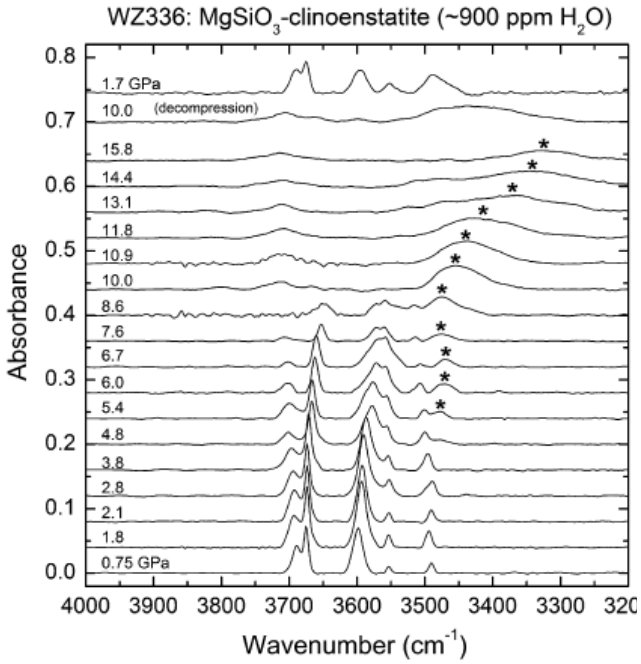

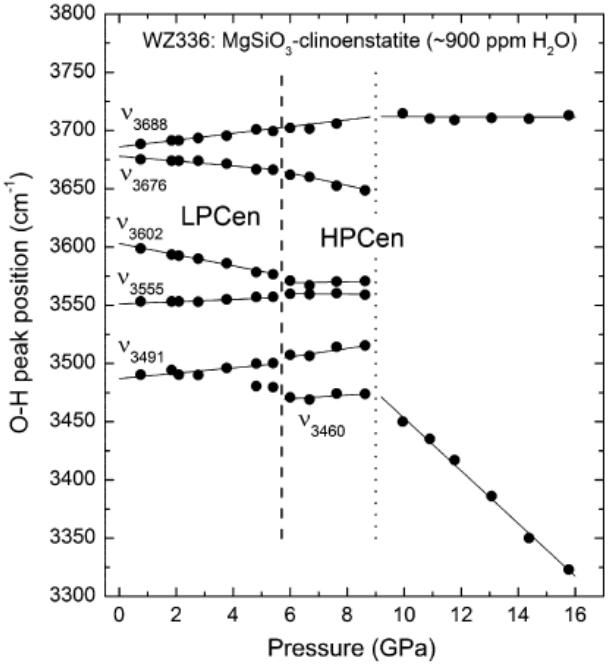

Main results

A decrease in the transition pressure on compression by about 1.3GPa for 900ppm H_2O was observed. Whereas most hydrogen bonds in the structure become shorter (stronger) on compression, a few exceptions occur.

The dominant band at 3602 cm^{-1} decrease to background absorbance up to 8,3GPa for 450ppm weight H_2O, and a new OH-stretching band at 3480 cm^{-1} appears above 4.8GPa for 900ppm weight H_2O.

Current trends in Cultural Heritage Science using synchrotron-based FTIR micro-spectroscopy

BMM35 Fragment of a wall painting in cave, in the Bamiyan site, Afghanistan.
Buddhist painting techniques, around 5th-9th centuries

1 – yellowish transparent layer
2 – green layer
3 – black layer
4 – white ground
5 – transparent brownish layer

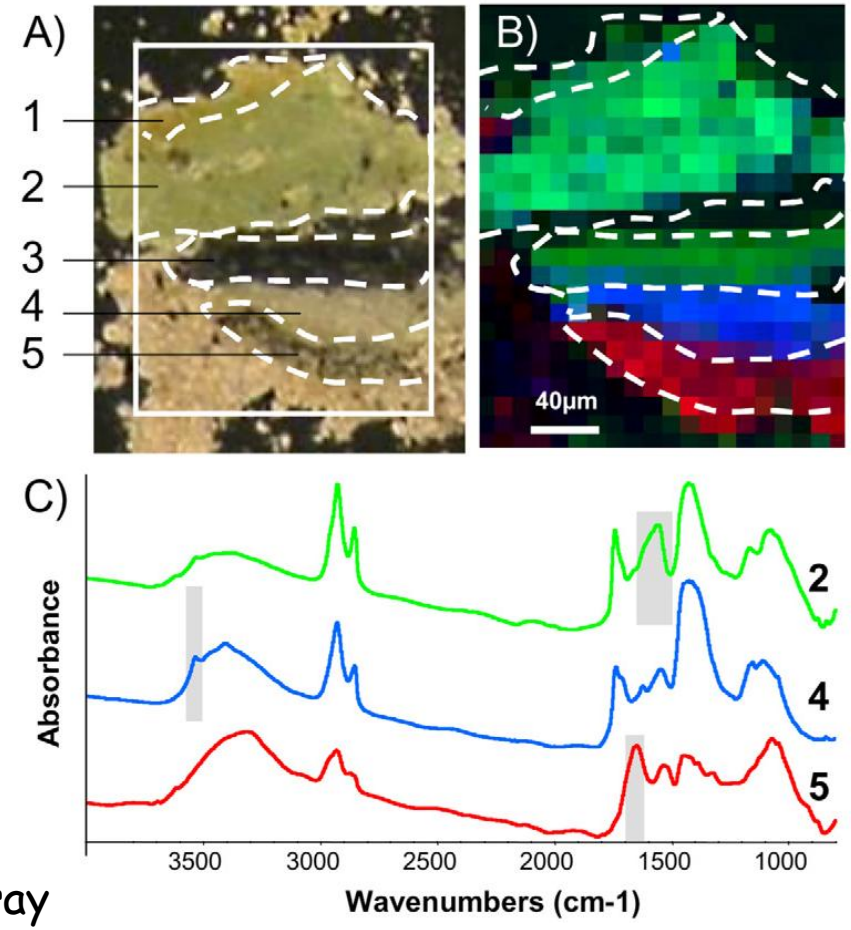

Carboxylates
(C=O stretching 1550 cm^{-1})
reaction of oil esters with some inorganic compounds;
mix of lead and copper soaps

Hydrocerussite ($Pb_3(CO_3)_2(OH)_2$)
(OH stretching 3524 cm^{-1})
Lead carbonates entering into lead white composition

Protein-based (Amide band 1650 cm^{-1})
Use of egg white or animal glue

Experimental conclusions are supported by micro-Xray diffraction and fluorescence for elemental analysis

From Cotte M, Dumas P, Taniguchi Y, Checroun E, et.al., C.R. Physique 10 (2009)

Biology and Biochemistry: The spectroscopic point of view

Biology is the branch of natural science that studies life and living organisms.

The building blocks of life are the **cells**

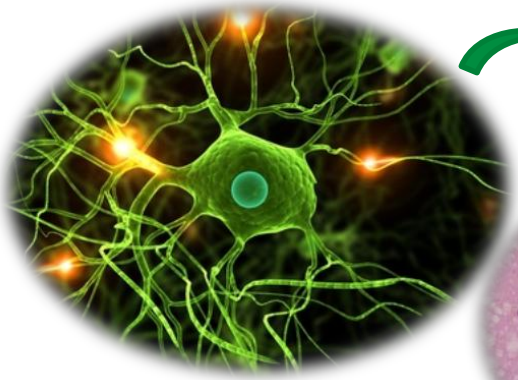

Cell

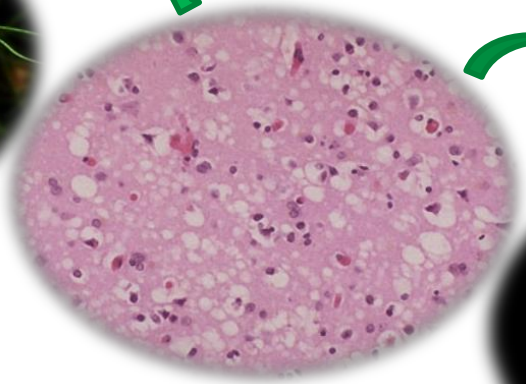

Tissue

Organ

Organism

The study of the chemical processes in living organisms is the subject of **Biochemistry**

It deals with the <u>structures</u> and <u>functions</u> of cellular components such as **proteins**, **carbohydrates**, **lipids**, **nucleic acids** and other **biomolecules**

The eukaryotic cell spectrum

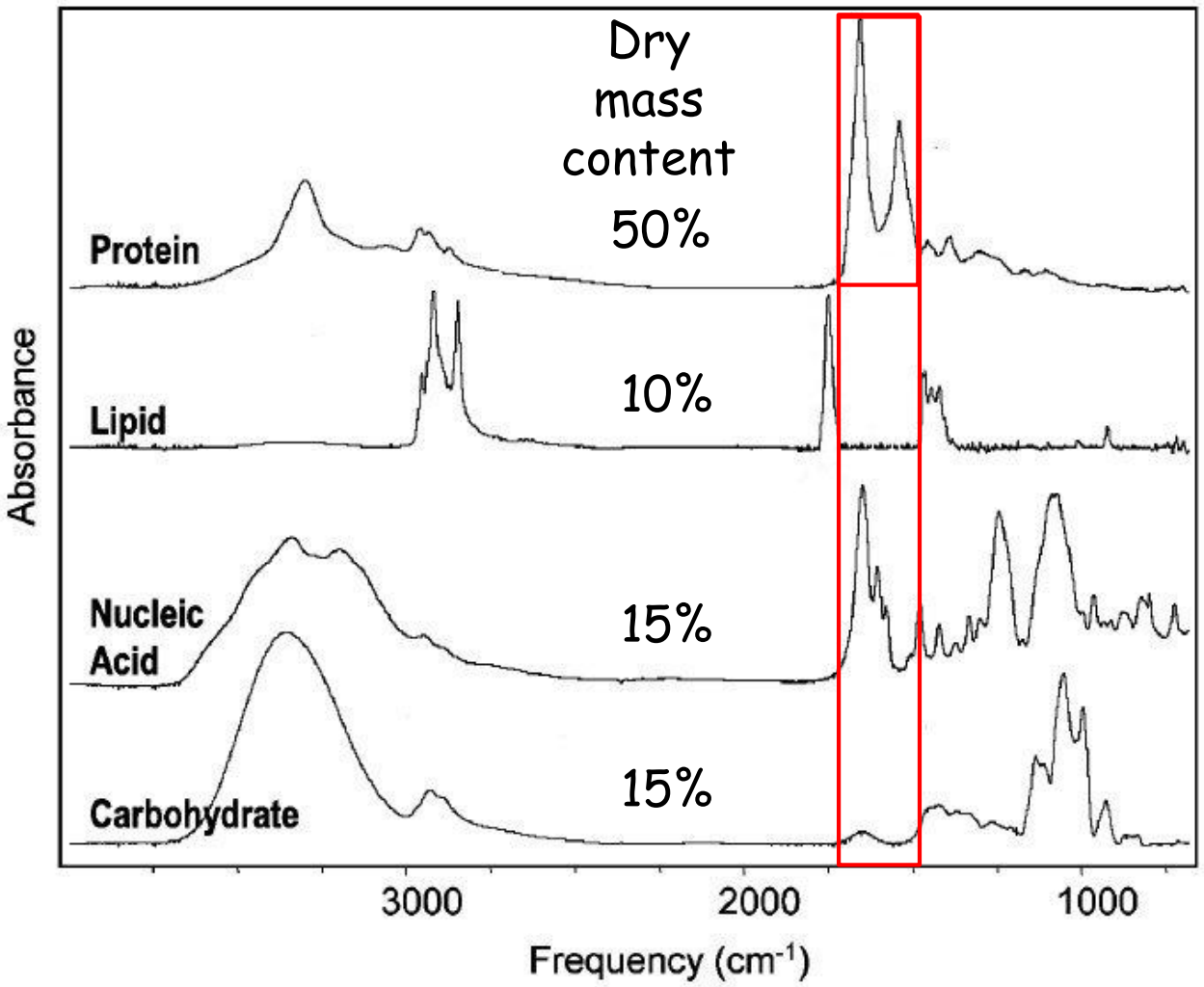

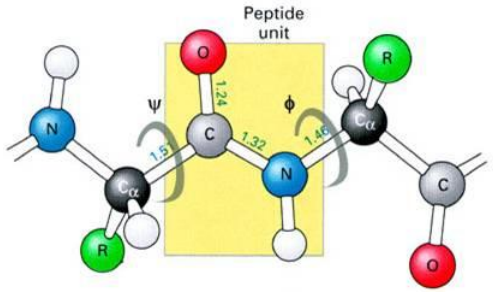

1700-1600

1705-1690 : ν *C=O* RNA

1660-1650 : ν *C=O* DNA

1660-1650 : ν *C=O* RNA

1700-1600: Amide I

80% ν *C=O* + 10% ν *C-N* +10% δ N-H

1600-1500

1600-1500: Amide II

40% ν *C-N* + 60% δ N-H

Adapted from: L. M. Miller, G.D. Smith and G. L. Carr, *Journal of Biological Physics*, 29 (2-3), 219-230, **2003**

The eukaryotic cell spectrum

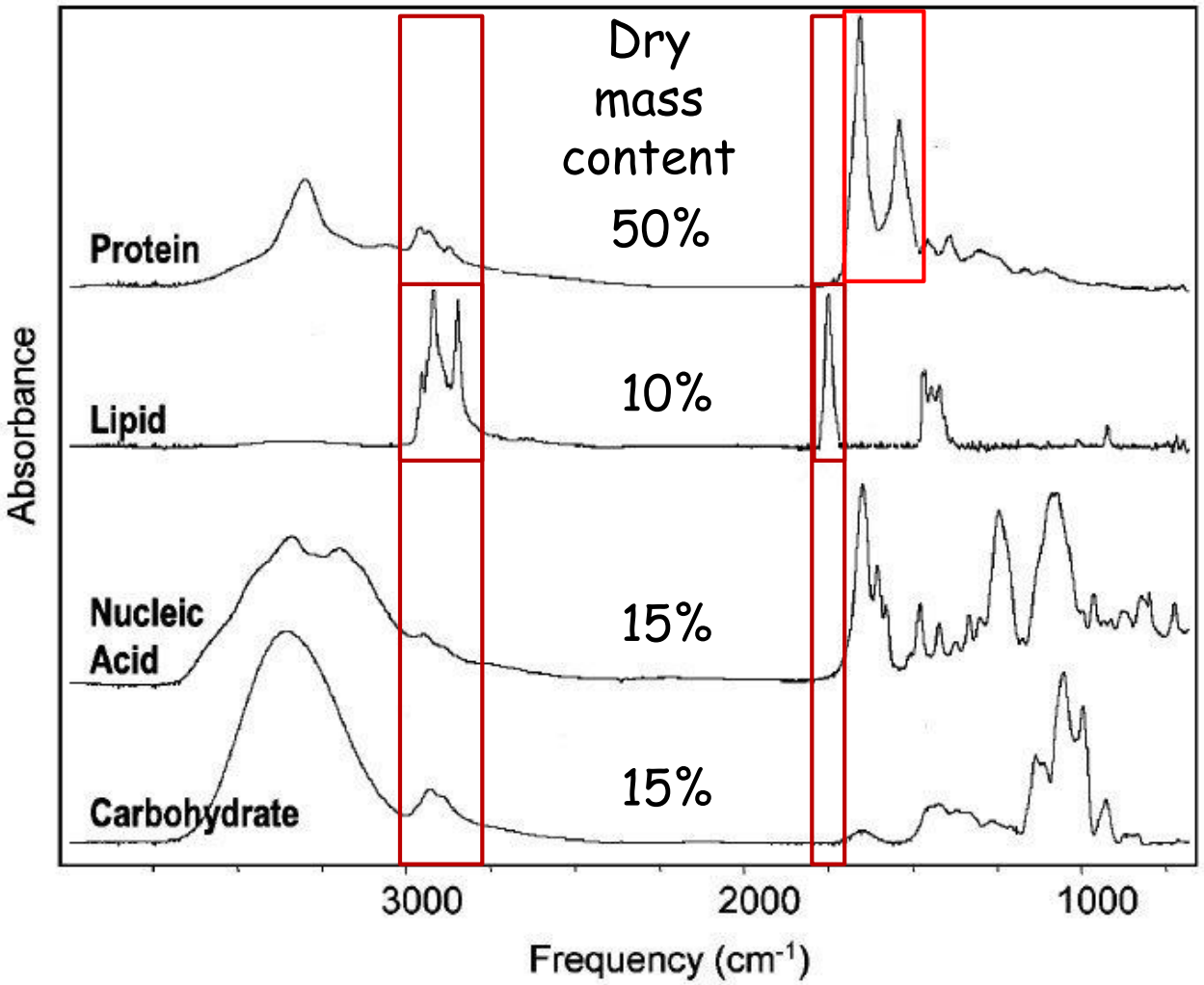

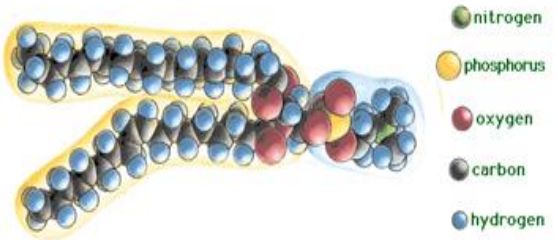

Saturated Acyl chains

2950-2960 : ν_{as} (CH_3)

2915-2925 : ν_{as} (CH_2)

2867-1877 : ν_s (CH_3)

2845-2855 : ν_s (CH_2)

Unsaturated Acyl chains

> 3000 : ν (=CH)

Ester Band

1700-1750 : ν (C=O)

The eukaryotic cell spectrum

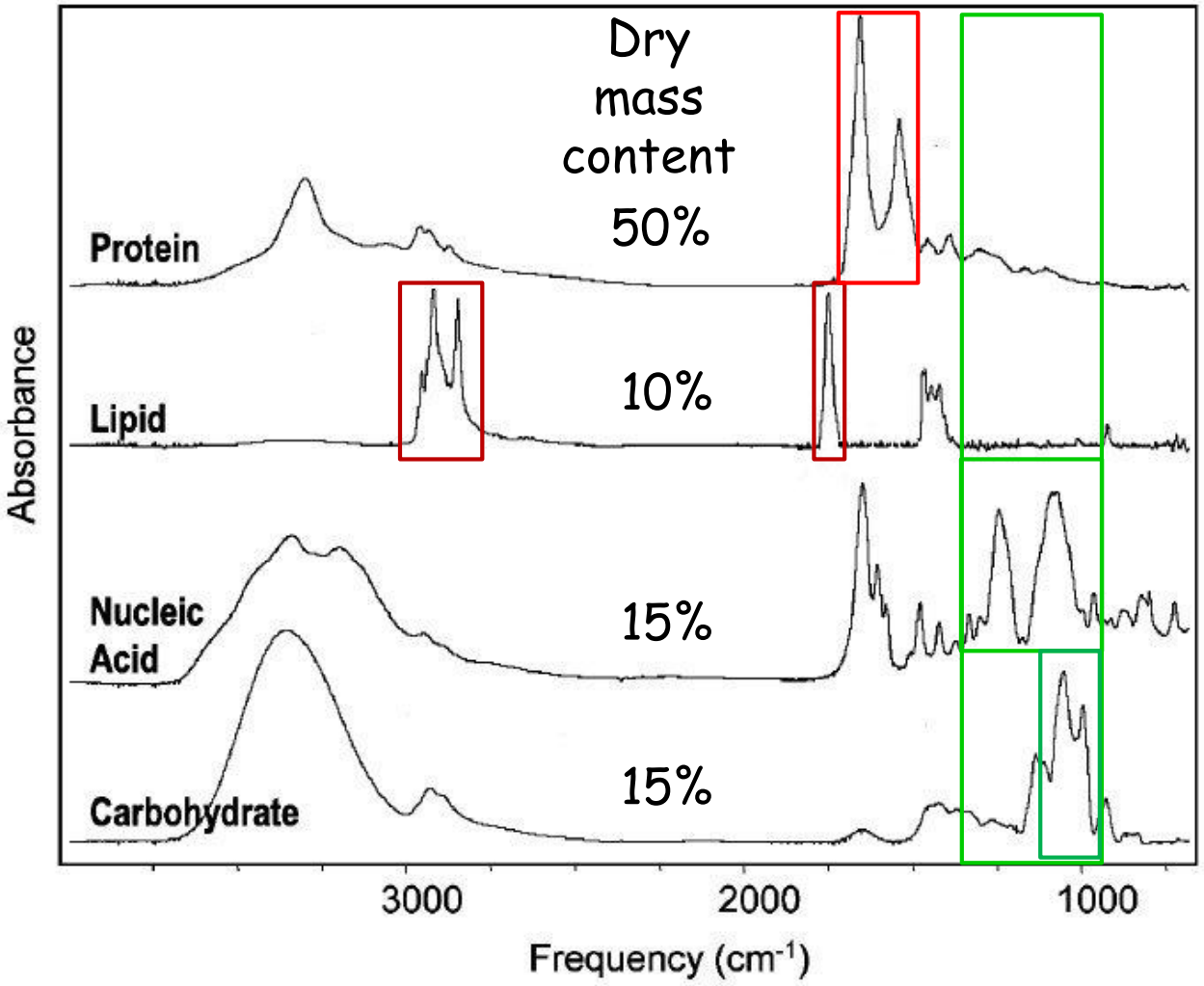

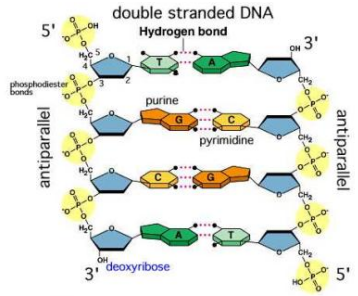

1250-1200

1244 : ν_{as} PO^{2-} RNA

1230 : ν_{as} PO^{2-} DNA

1100-1050

1089 : ν_{s} PO^{2-} DNA

1084 : ν_{s} PO^{2-} RNA

1100-1000

DNA and RNA ribose

ν C-O

Complex network of carbohydrate bands

The eukaryotic cell spectrum

Band intensity, position, width and shape (band components) are sensitive to subtle biochemical changes of bio-specimens.

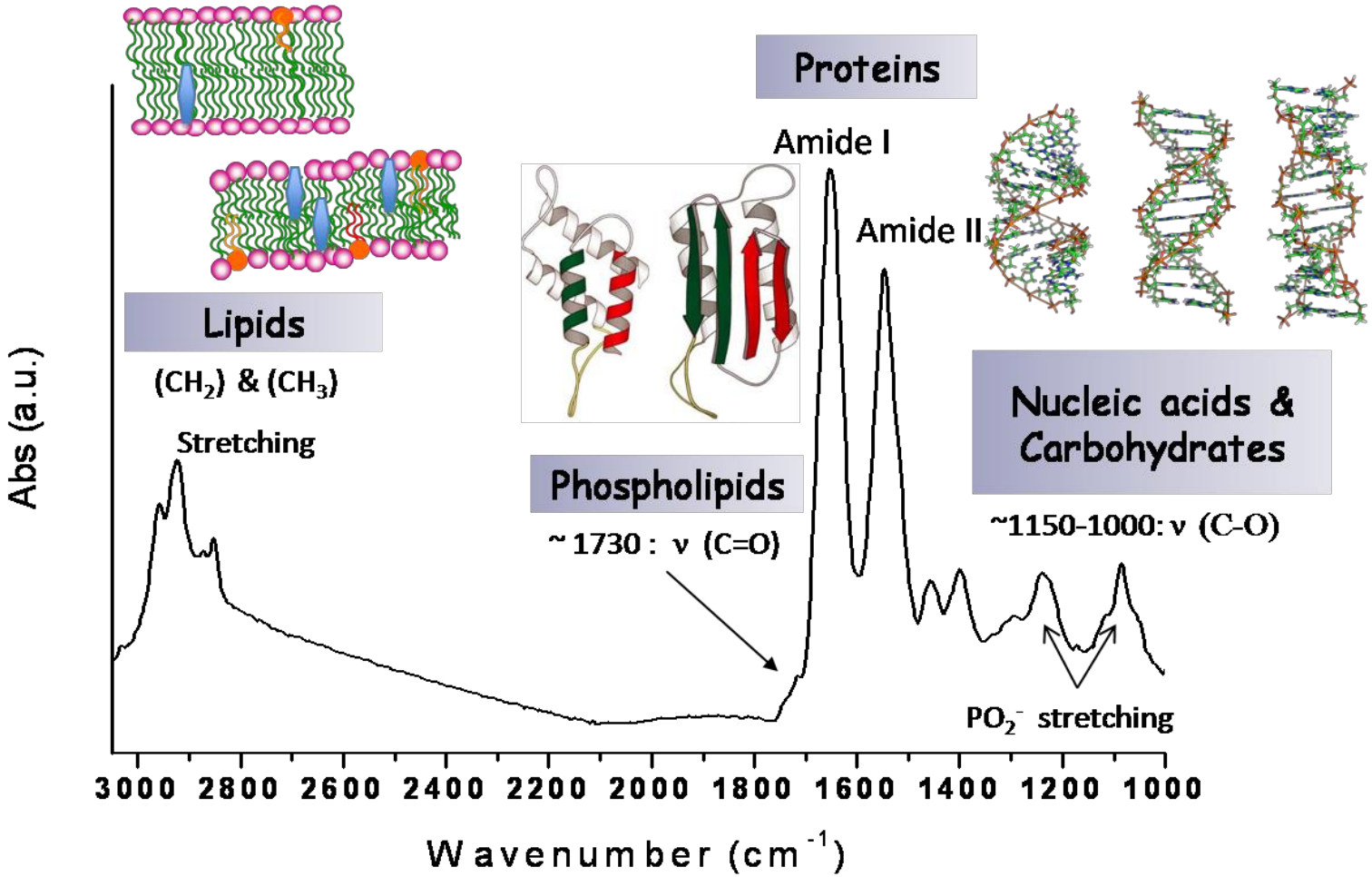

Compositional and structural information at tissue, cellular and sub-cellular level can be achieved by exploiting SR brightness advantage

The water absorption barrier

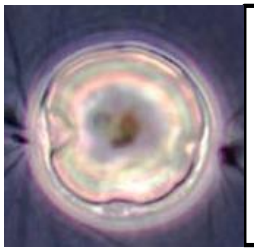

For the sampled volume:
~ 48% extra cellular water
~ 36% intra cellular water
~84% of water

Water: ~ 70% of the cell weight
Dry mass: ~ 50% of proteins
~ 15% of carbohydrates
~ 15% of nucleic acids
~ 10% of lipids
~ 15% other molecules

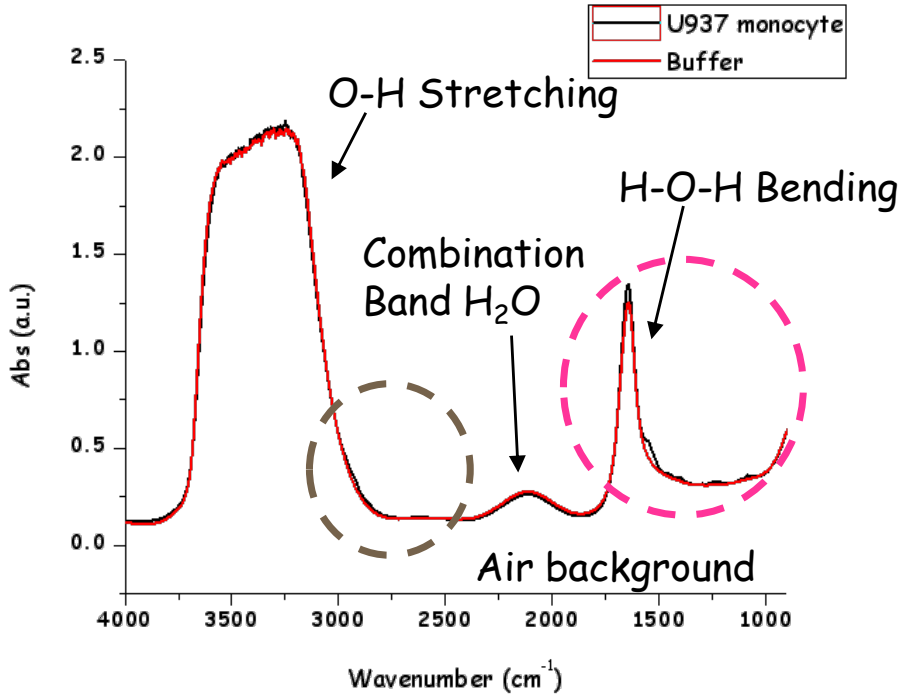

Living cell spectrum

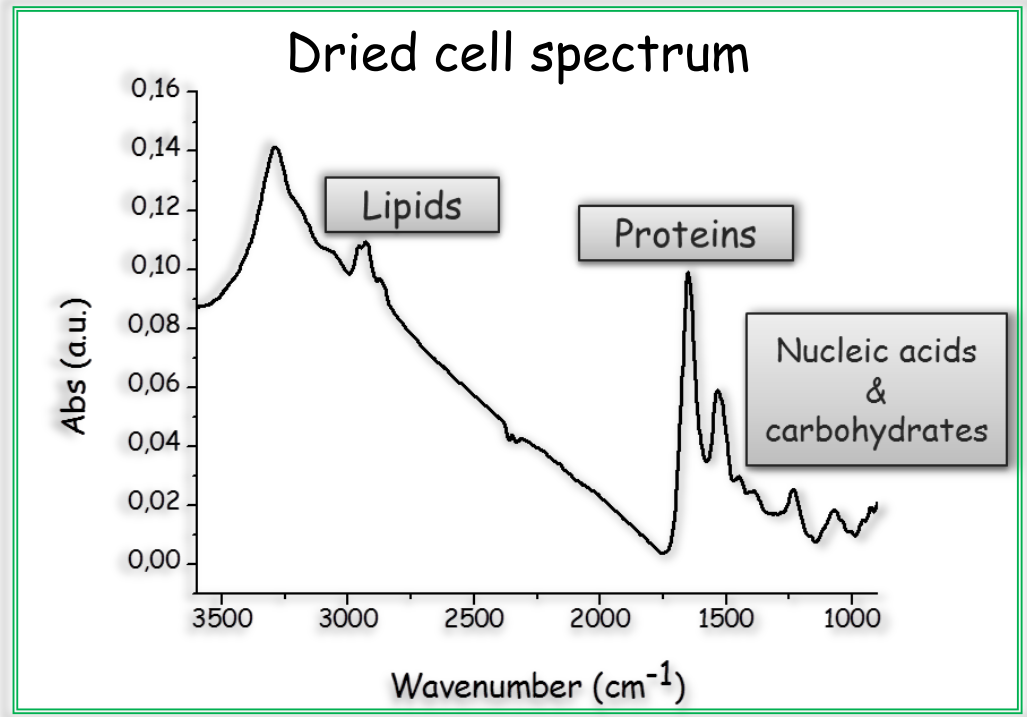

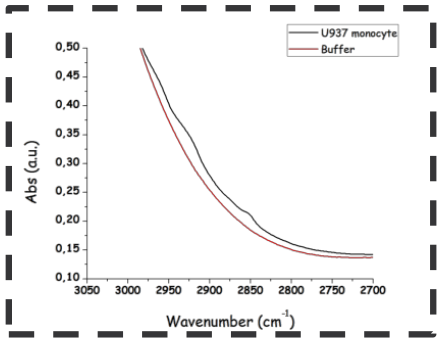

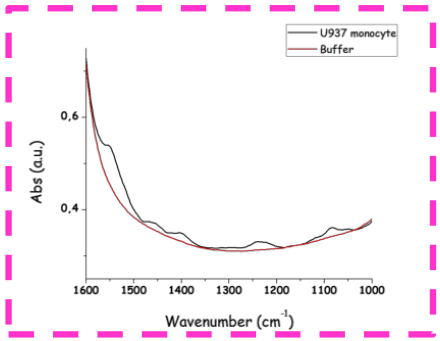

ε_{water} ~ 20 $L \cdot mol^{-1} \cdot cm^{-1}$

$\varepsilon_{Amide\ I} > \varepsilon_{water}$

$[C]_{water} >> [C]_{protein}$

Sample preparation

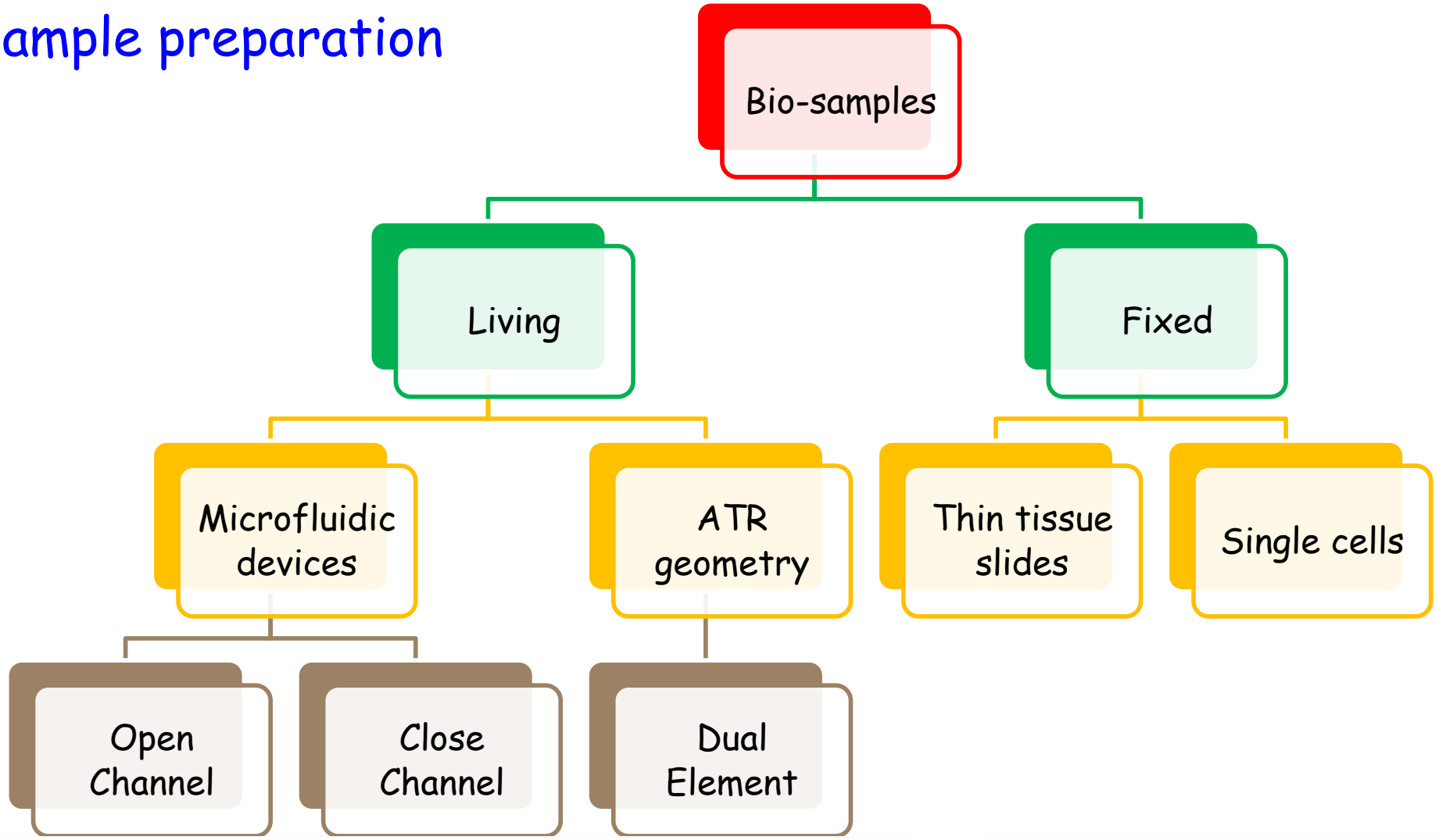

- IRMS of living versus fixed cells
- Real-time chemical imaging of bacterial activity in biofilms
- Dual element ATR

- Microspectroscopic Evidence of Cretaceous Bone Proteins
- Prion Disorders

Microscopic Evidence of Cretaceous Bone Proteins

Late Cretaceous mosasaur: ***Prognathodon***

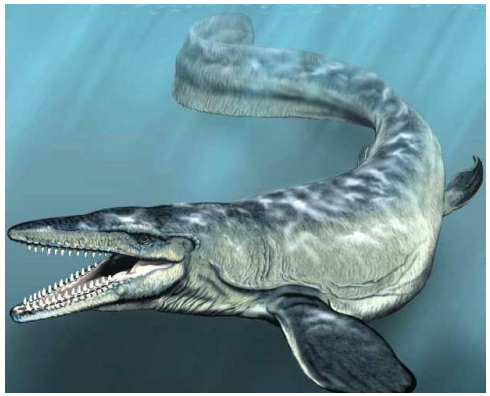

Demineralized bone sample
Transmission measurement

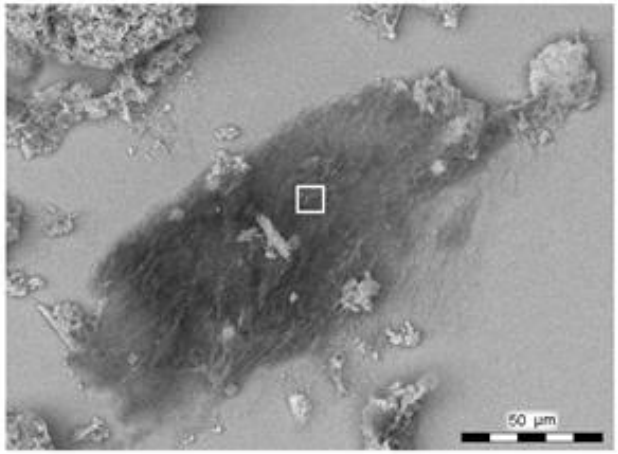

Existing monitor lizard:
Varanus exanthematicus

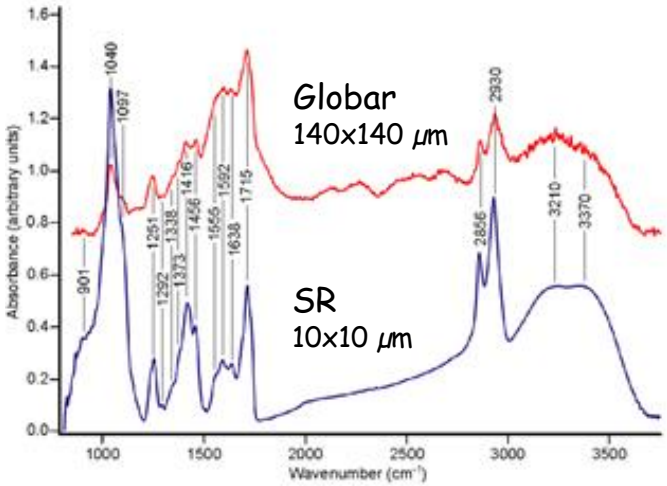

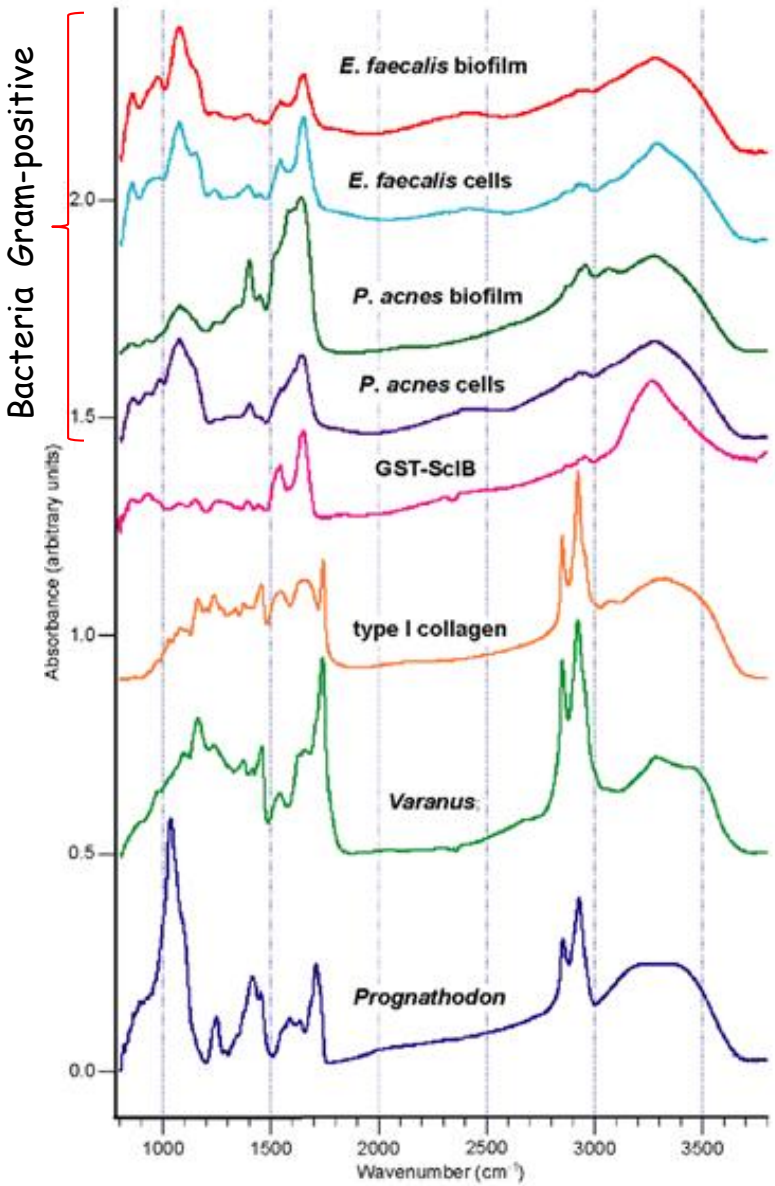

From Lindgren J, Uvdal P, Engdahl A, Lee AH, Alwmark C, et.al. (2011) PLoS ONE 6(4)

Prion disorders

Aberrant metabolism of the Prion Protein (PrP)

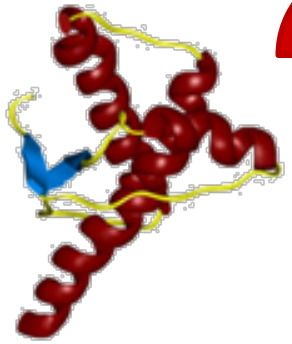

PrP^{C}

Alpha-helical

Protease sensitive

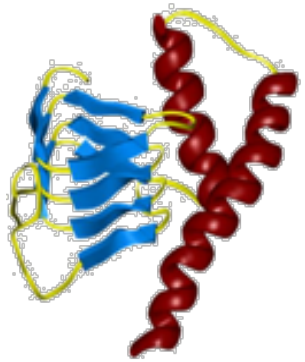

PrP^{SC} - PrP^{CJD}

beta- plated sheet

Protease resistant

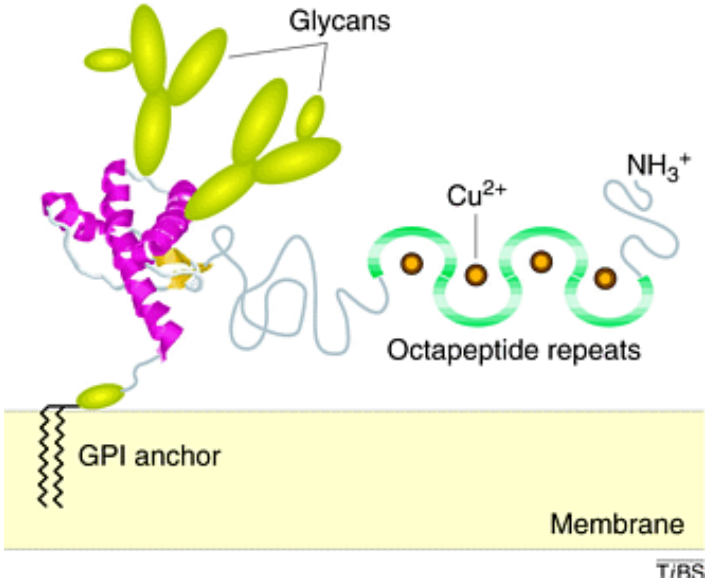

Prion rods

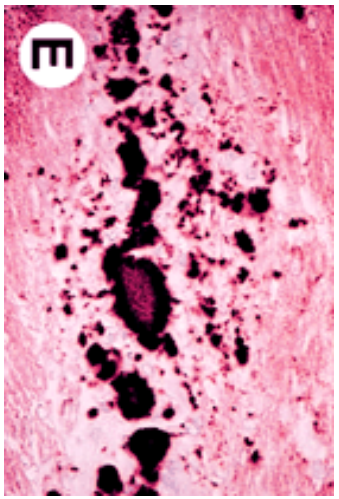

PrP amyloid plaques

PNAS 1999 vol. 96 no. 26 15137-15142

PNAS 1998 vol. 95 no. 23 13363-13383

SR-IRMS and prion research

- ✓ FTIR spectroscopy has been largely employed for studying the conformational changes associated to the conversion of PrP^{C} into PrP^{Sc}

PrP^{C} 42% α-helix; 3% β-sheet // PrP^{Sc} < α-helix; > β-sheet Phenotype dependent

- ✓ IRMS is able to distinguish between scrapie (S) and normal (N) brain tissues but the spectroscopic differences between different cerebellar substructures are much pronounced than disease alterations.

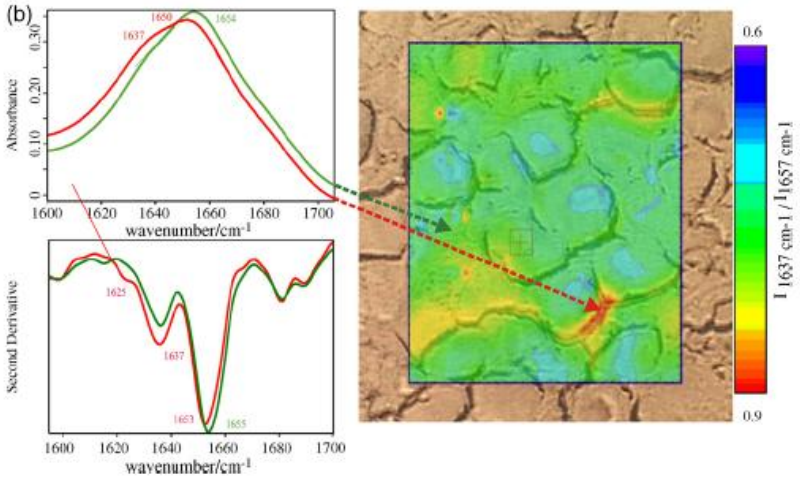

Differentiation is based on the superimposition of multiple contribution more than on the identification of structural protein alteration, evidenced only but not always in terminally ill animals (Dilution effect)

Tissue architecture complexity is limiting the understanding of cellular bases of disease

A. Kretlow wt al., FTIR-microspectroscopy of prion-infected nervous tissue, *Biochimica et Biophysica Acata (BBA) – Biomembranes* (2006), 7:948-959

M. Beekes et al., Analytical applications of Fourirer transform-infrared (FT-IR) spectroscopy in microbiology and Prion research, *Veterinary microbiology* (2007), 123:305-319

SR-IRMS and prion research: a cellular study

IRMS is a sensitive single-cell diagnostic tool for testing prion infection, faster than conventional Western blot PK digestion assay

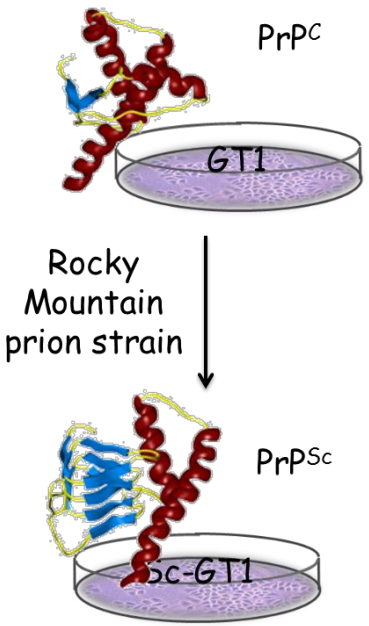

▪Multiple cell sensitivity
▪Execution time: many hours

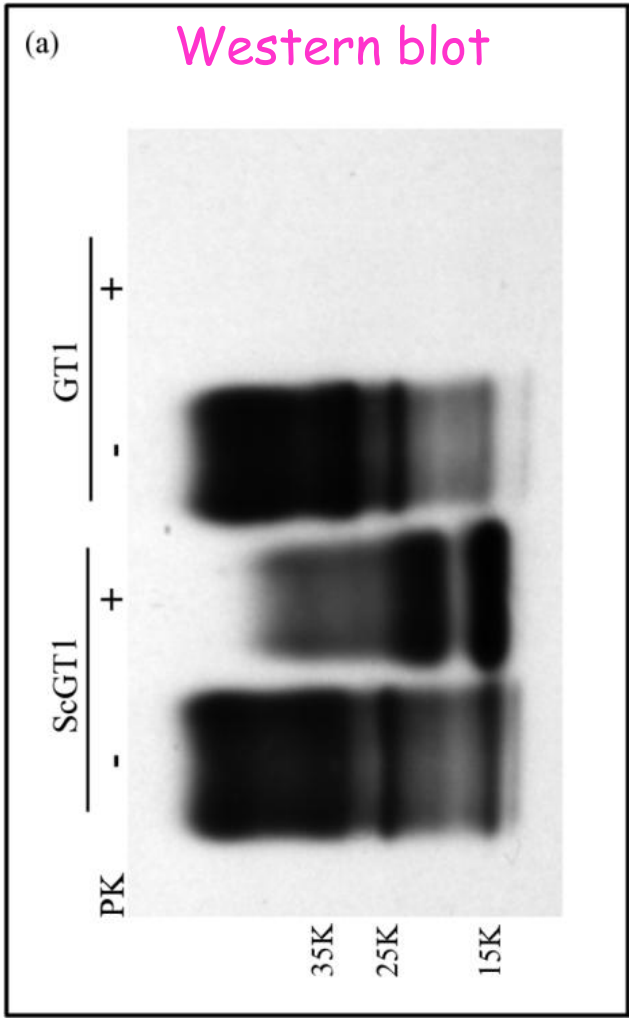

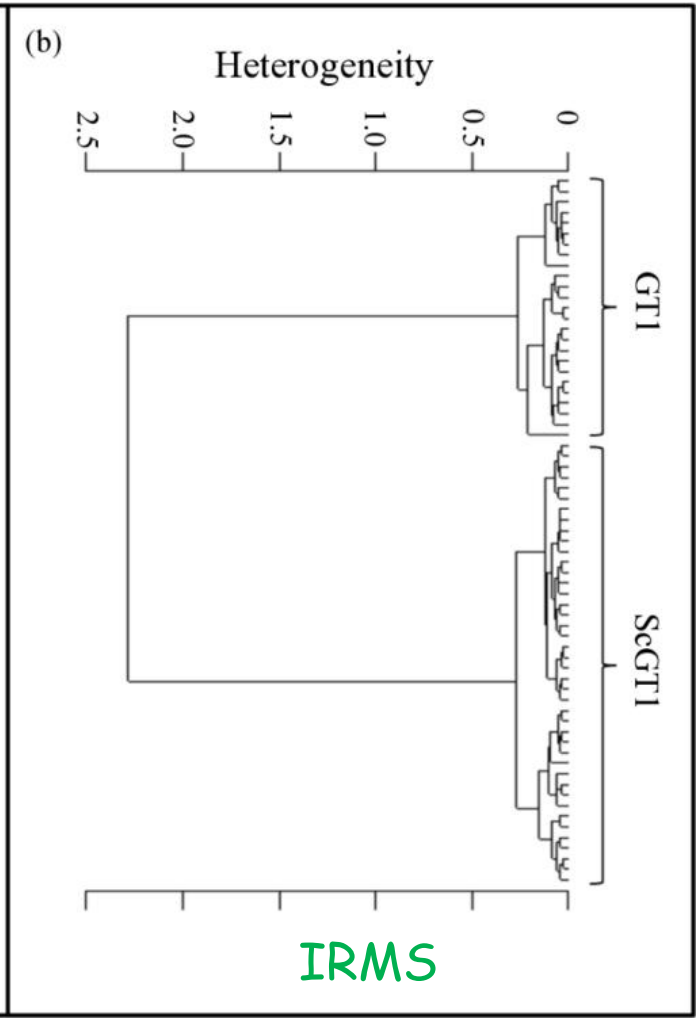

▪Single cell sensitivity
▪Execution time: few minutes

A. Didonna, L. Vaccari, et al., ACS Chemical Neuroscience 2011 2 (3), 160-174

IRMS revealed the biochemical reasons of classification

- Increase Glu and Asp protonated aminoacid

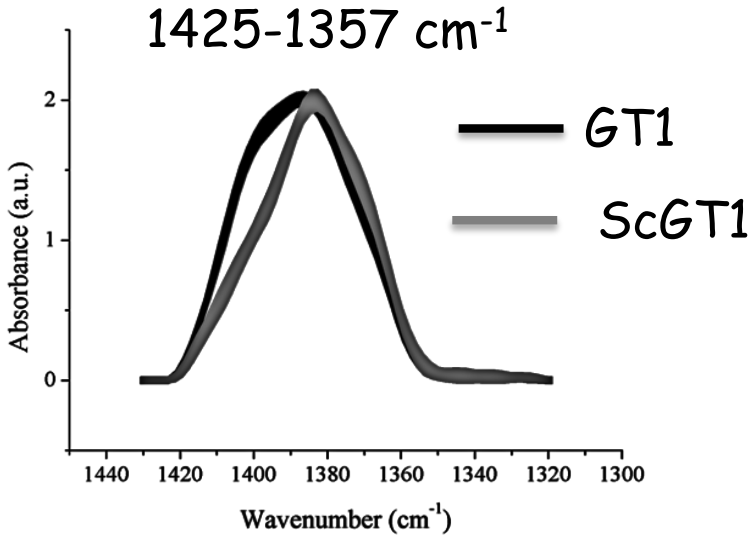

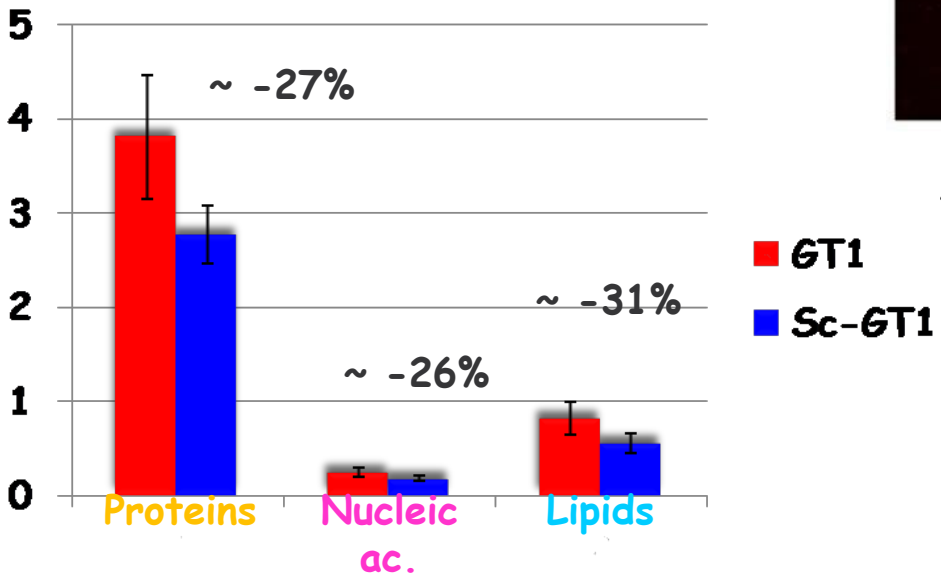

- Down-regulation in protein and lipid synthesis upon prion infection was elicited by semi-quantitative analysis

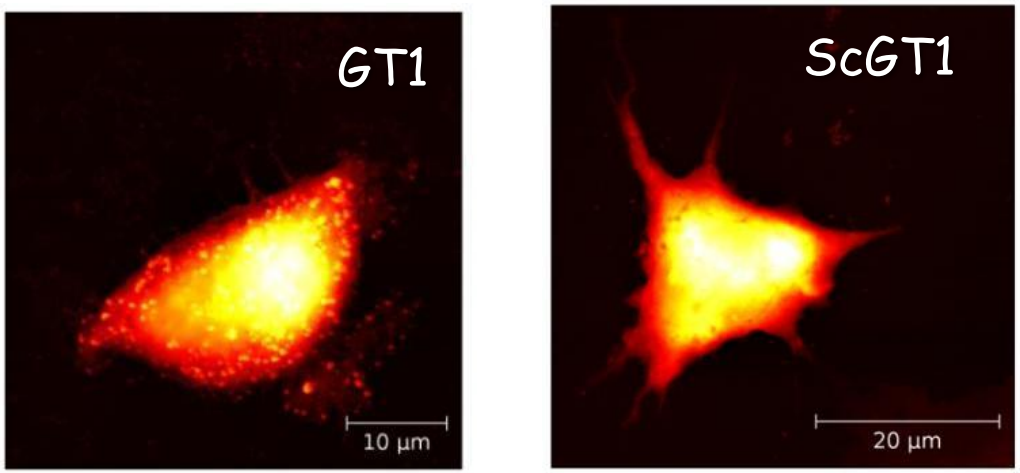

AFM: GT1 and Sc-GT1 have comparable pyramid like shape and effective cell height

IRMS revealed an increase in both number and dimension of lysosomal compartments upon prion infection

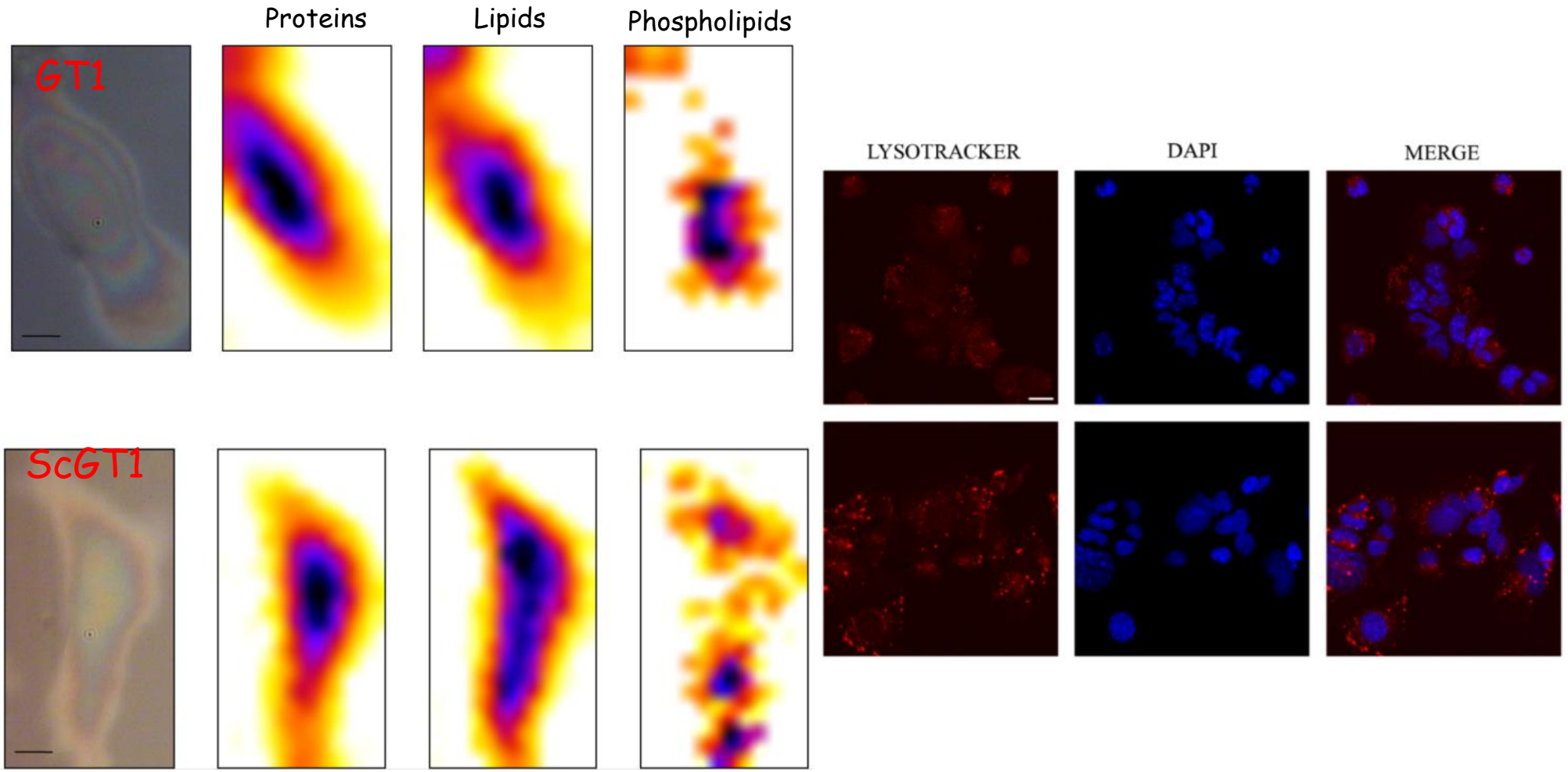

The synergic matching of IRMS with complementary investigation tools is a winning strategy for shining a light on cellular phenomena behind prion infection

SR-IRMS of living cells: toward label-free single-cell based assay

Label-free analytical methods that monitor living cells under physiological conditions for tracking the biochemical modification they undergo during their life cycle, both naturally occurring or once perturbed by external stimuli. Single-cell or better sub-cellular resolution is desirable.

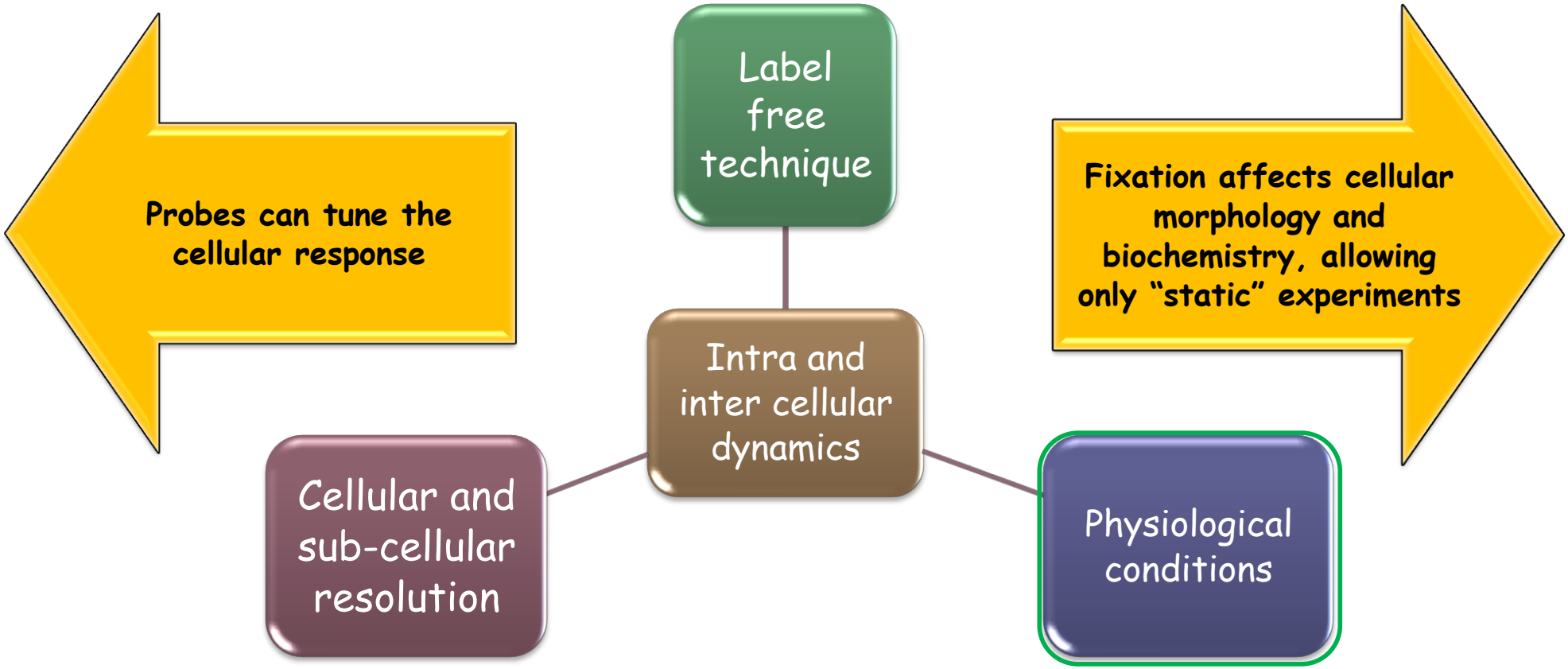

Strategies for living cell sampling

For disclosing cellular IR features, and in particular protein Amide I band, the spectral contribution of water has to be limited:

- By reducing the sampling depth within the cell: ATR sampling
  Suitable for prokaryotic cells , very thin adherent cells or special applications where the outermost cell layers are investigated
- By recording transmission or transflection spectra of living cells in liquid devices thinner than 9 microns for avoiding bending water band saturation and allowing water subtraction. A **microfabrication** approach is needed for controlling the water layer thickness and microchannel geometry.
  Materials conventionally employed for IR transmission measurements are not standard for microfabrication

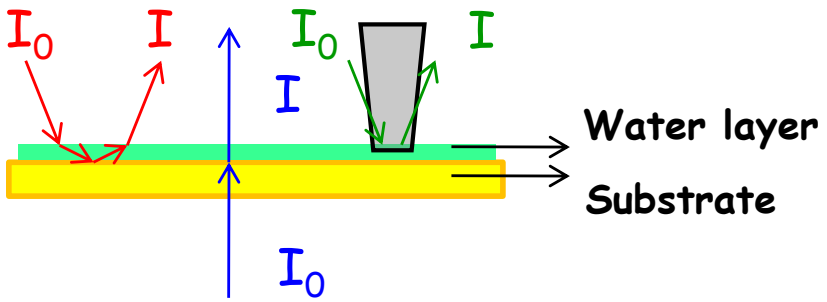

The IR spectral shape of both transmission and transflection single cell spectra are affected by **Resonant Mie scattering** effects.
Standing waves artifacts further complicate the interpretation of transflectance measurements.

Resonant Mie scattering

The anomalous modulation of the baseline of single cell spectra both in absorbance and transflection mode relates to the fact that the Mie scattering efficiency is dependent upon the refractive index of the sample (or better is ratio with the surrounding environment) and it changes on passing through an absorption resonance.

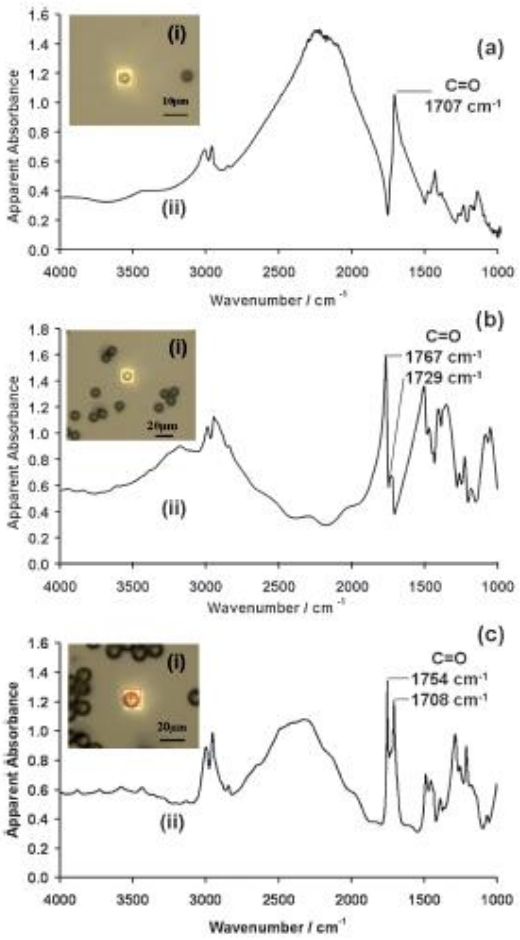

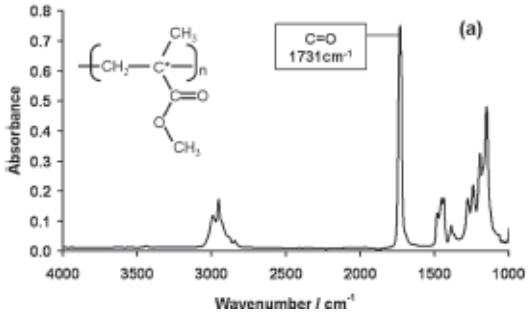

Thanks to the closer matching between the cell-water refractive indexes in the MIR, Mie scattering effects are minimal for living cell spectroscopy. RMieS algorithm has been developed for minimizing the Resonant Mie Scattering

Paul Bassan, Achim Kohler, et al., Analyst, 2010, 135, 268-277

Electrical field standing waves

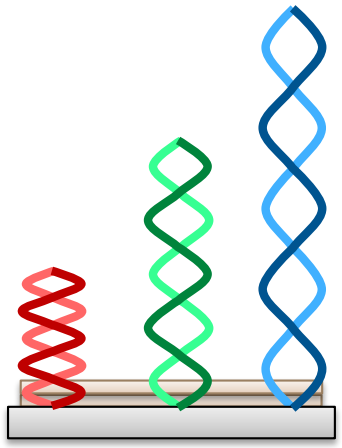

Transflectance spectra are further complicated by the electric field standing wave effect and in these cases the change in absorbance with thickness does not follow the Beer–Lambert relationship.

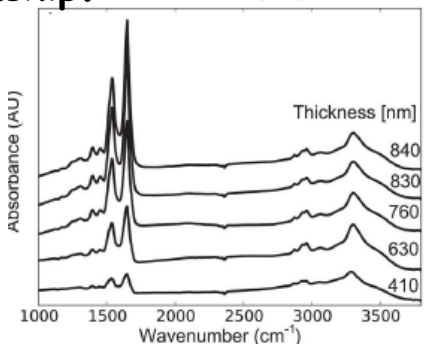

Jacob Filik , Mark D. Frogley , et al., Analyst, 2012, 137, 853-861

The microfluidic approach

Sampling technique	Material	Vis-Transparent	MIR-Transparent	MIR-Reflective	Biocompa-tibility	Other
Transflection	MirrIR-slides	No	No	Totally	Yes	Cheap
Both	Si, Ge	No	Partially	Partially	Yes	Cheap
Transmission	Diamond	Yes	Partially	No	Yes	Expensive +
	BaF_2	Yes	Totally	No	No	Expensive
	CaF_2	Yes	Partially	No	Possibly	Expensive
	ZnSe	Slightly	Partially	No	No	Expensive
	Si_3N_4	Slightly	Partially	No	Yes	Fragile
	TEM grids	Yes	Totally	No	Yes	Fragile

The optimal IR substrate

- Biocompatible, for performing cell culture on it
- IR transparent/reflective in the MIR
- Vis transparent/reflective, to easily match Vis and IR data
- Cheap and/or recyclable
- Exploitable also for other investigation techniques

Microfabrication

Bio-MEMS for single cell analysis with SR-IRMS

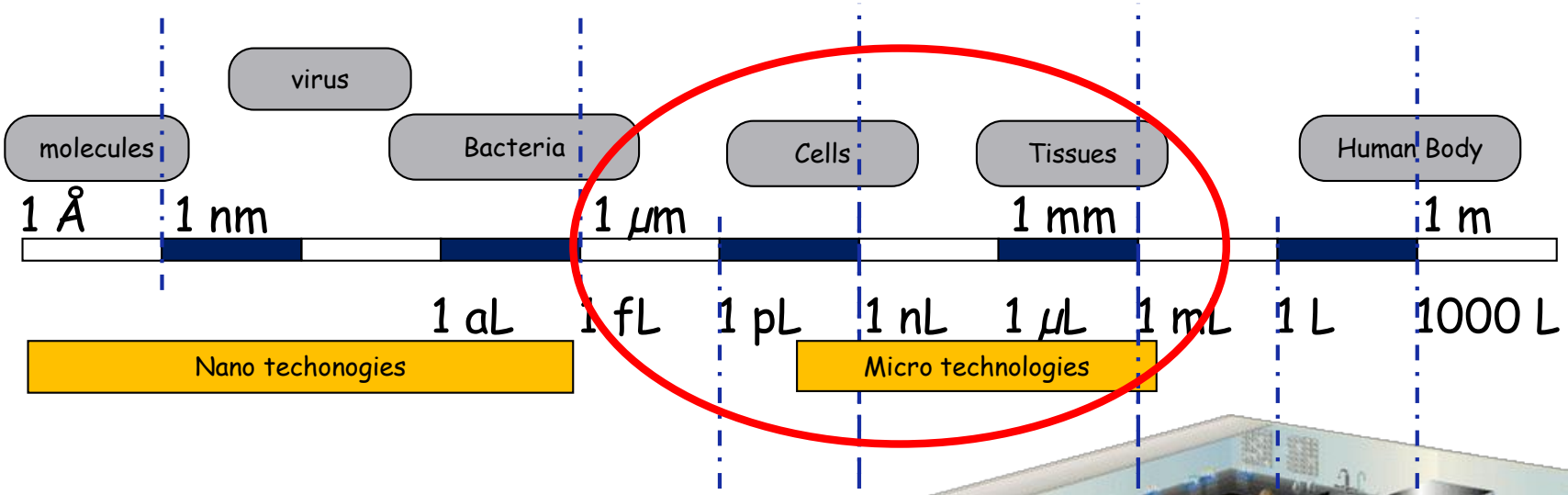

- The design flexibility is superior to any other manufacturing approach
- The lateral resolution fits with the SR-IRMS spatial resolution
- A nanometric control of the chip vertical dimension is guaranteed
- It offers the possibility to integrate many functionalities all together – sorting, filtering, mixing capabilities……

A complete laboratory under your Vis-IR microscope

Fully sealed microfluidic device for transmission measurements

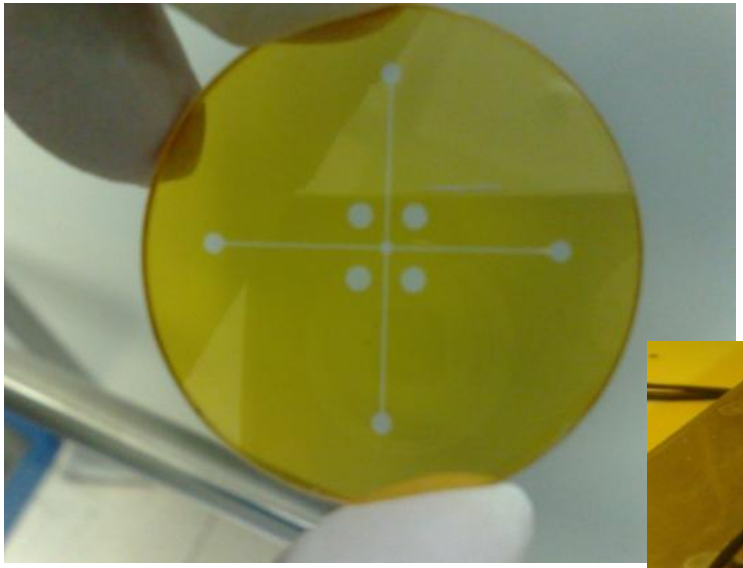

UV-lithography

Made on CaF_2 (raw or silicon coated) window
using a positive tone photoresist X-ARP
using a negative tone SU8 photoresist

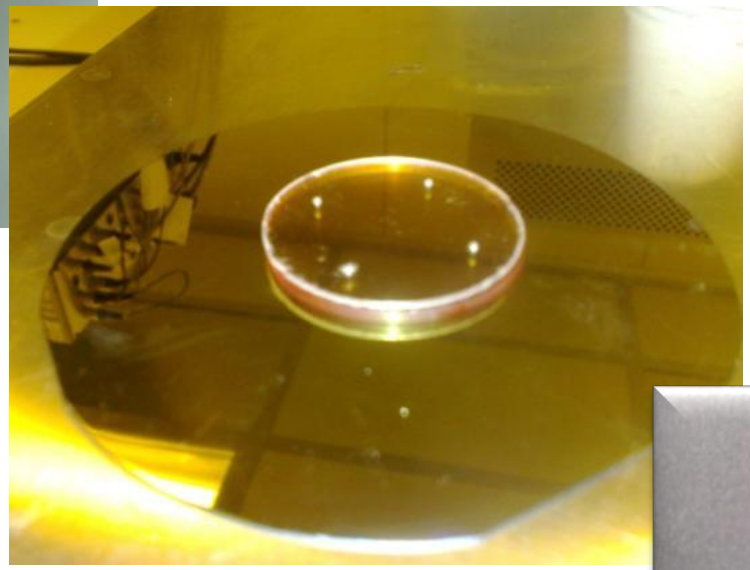

Sealing

Thermo-mechanical bonding
Chemical bonding

Raw CaF_2

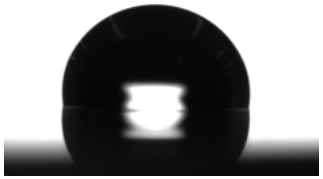

CaF_2 Silicon coated

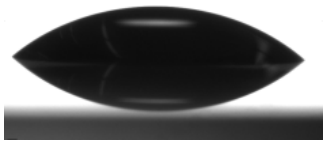

Connection with Outer world

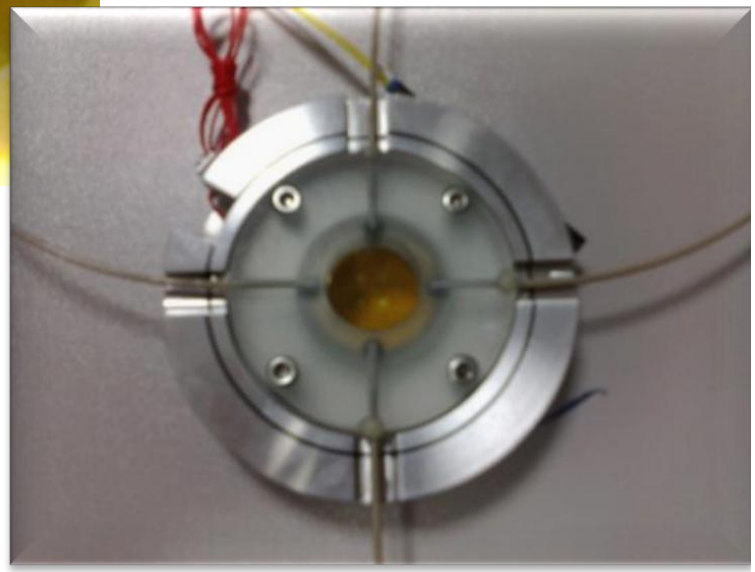

G. Birarda, et al., MNE (2010) Volume: 87,Pages: 806-809
G. Grenci, et al., MNE (2012) Accepted for publication

SR-IRMS of living versus fixed single-cells

The cellular model U937

- Circulating white blood cells
- Round shaped
- Average diameter 8-10 µm

Measured within fully sealed microfluidic CaF_2 devices, NaCl 0.9% buffer and complete medium

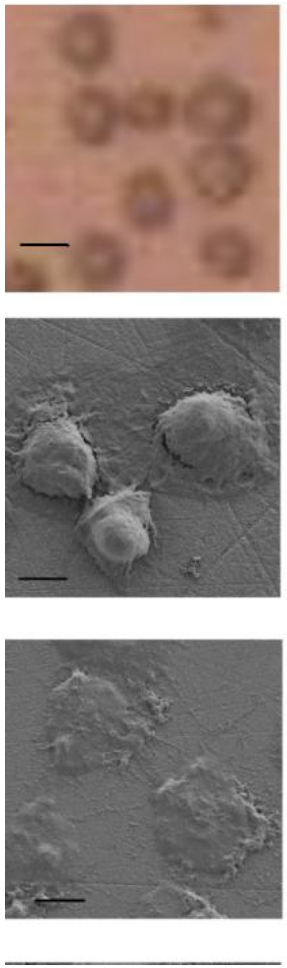

- **Living**

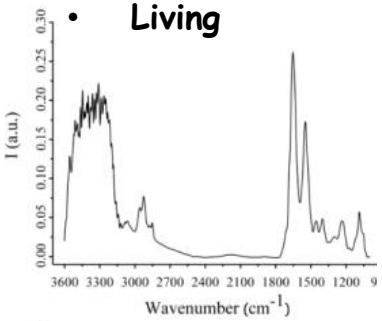

- **Formaline**

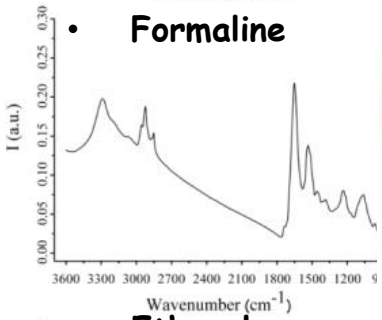

- **Ethanol**

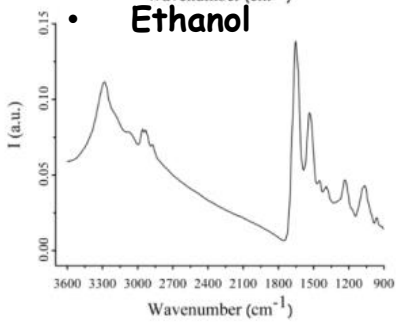

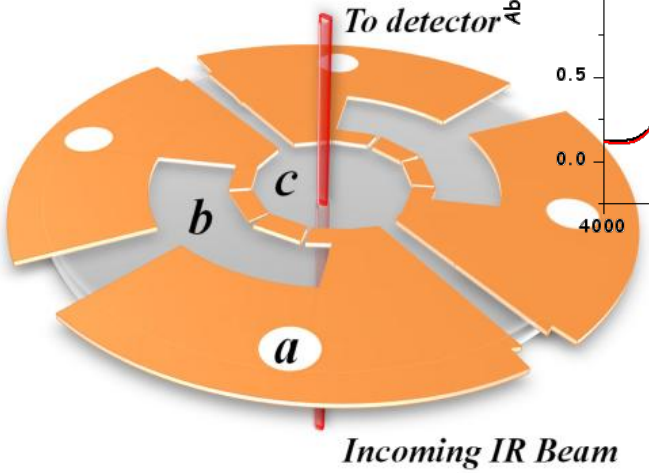

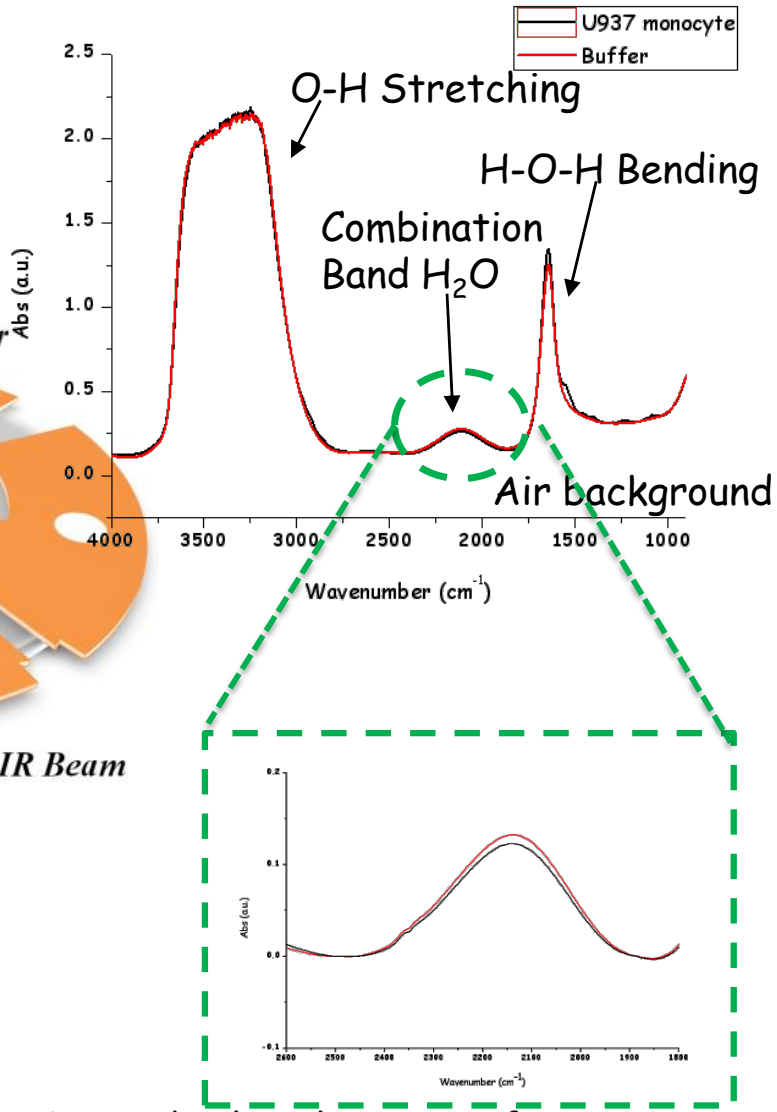

Lipid region

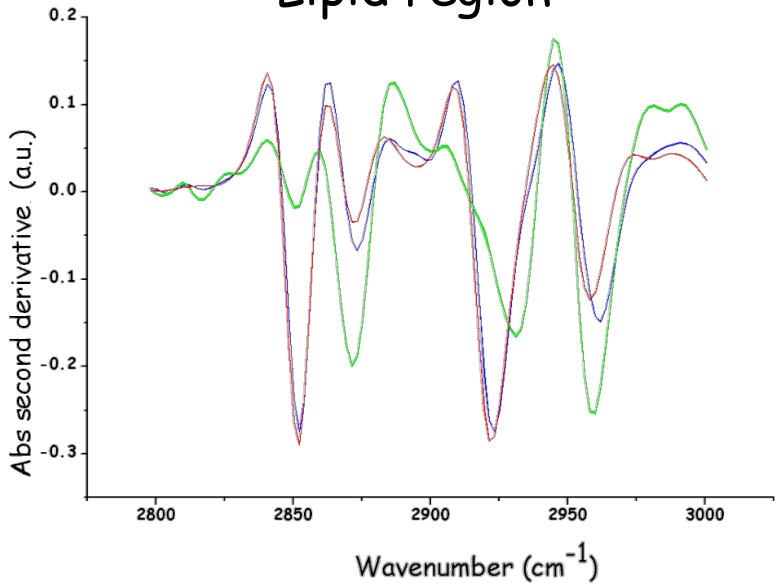

Nucleic acid region

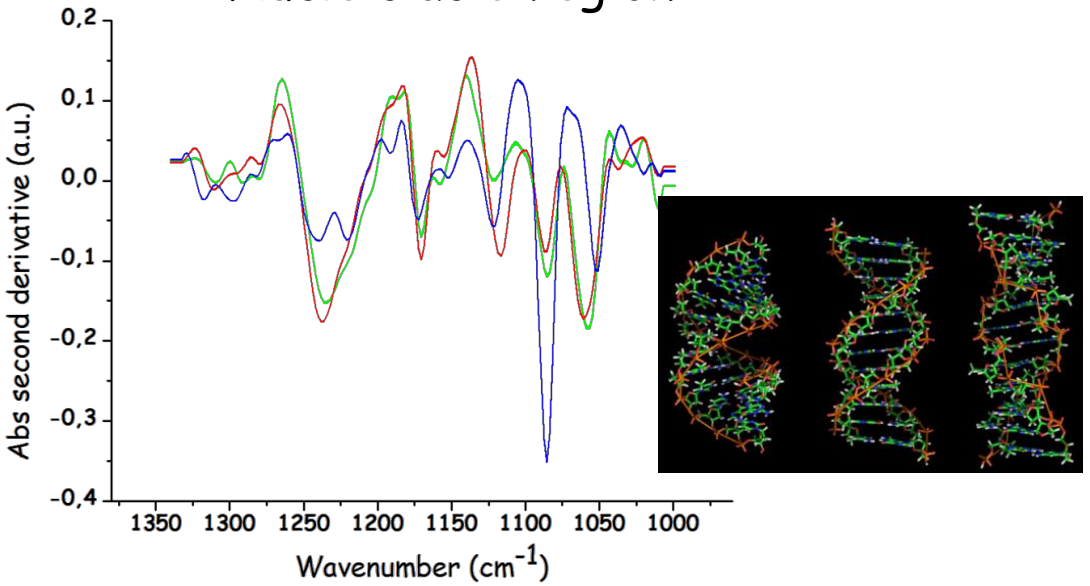

Protein region

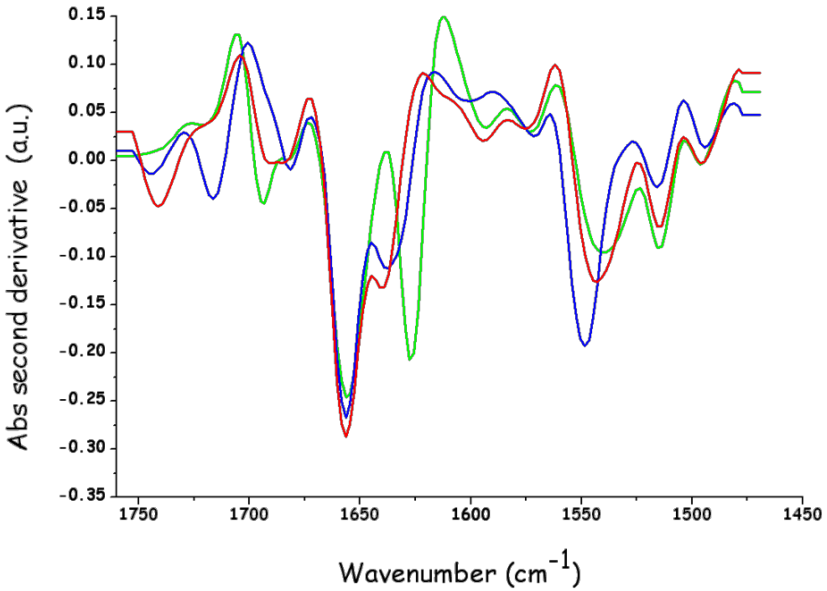

Formalin Ethanol Living

- **Ethanol is dramatically altering both membrane order (increased disorder) and composition. It induces also protein aggregation and precipitation.**
- **Formalin is well preserving both cellular membranes and protein secondary structure, similarly to unfixed air-dried cells. However, unfixed cells are not stable in time**
- **Nucleic acid structure, and DNA especially, is affected by both formalin and ethanol as well as by air-drying**

Real time monitoring of cellular adaptive response

U937 fMLP stimulation

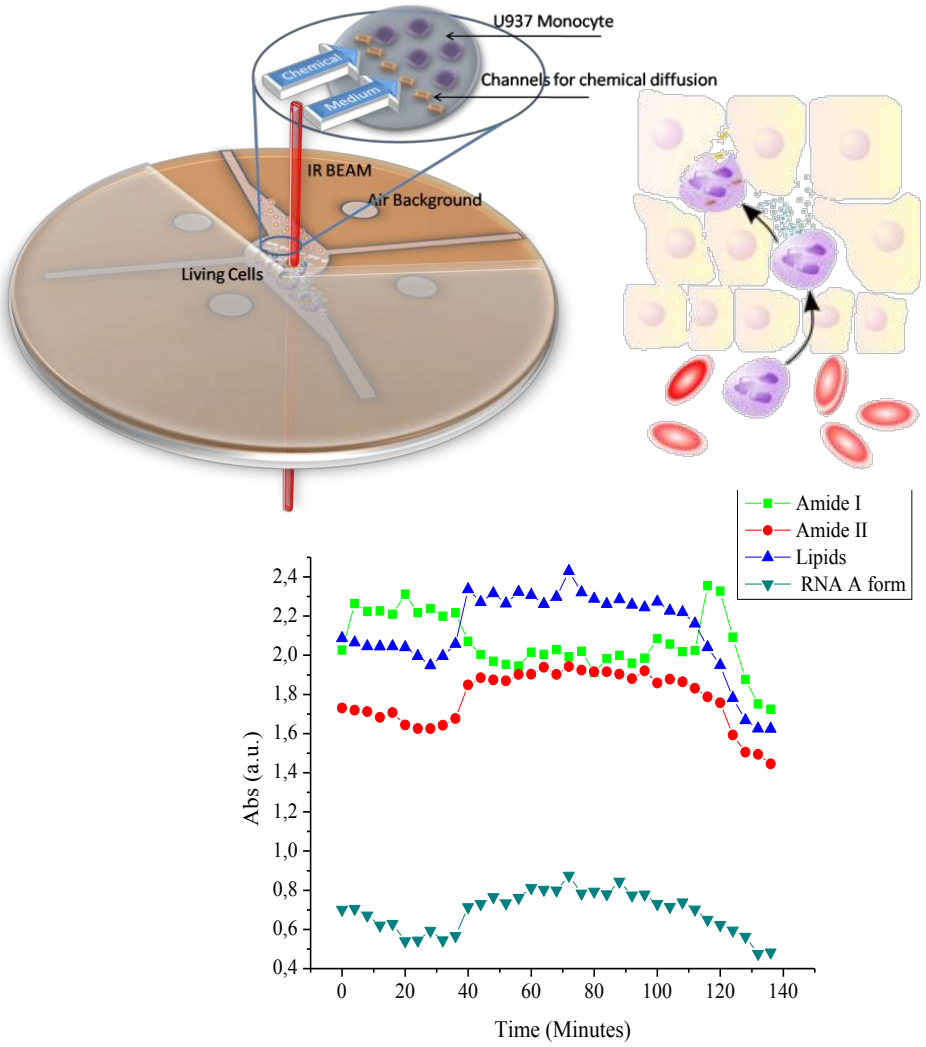

Protein expression and membrane extrusion have been monitored

Mechanical deformation of U937 monocytes

U937 monocytes (average diameter 8-10 microns)
D- Undeformed cells (★) [9 μm device]
D Deformed cells (✖) [5 μm device]
D+ Extremely deformed (▲) [3 μm device]

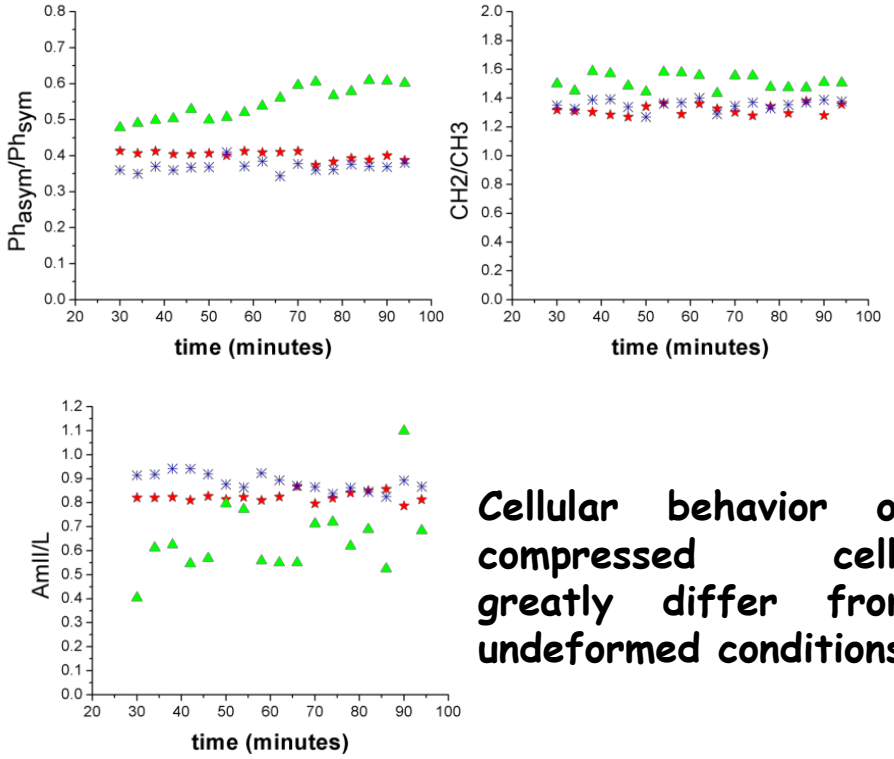

Cellular behavior of compressed cells greatly differ from undeformed conditions

G. Birarda, L. Vaccari et al., Vibrational Spectroscopy (2010) Volume: 53,Pages: 6-11

Real-time Chemical imaging of bacterial activity in biofilms

Uptake of mitomycin-C (MMC) by Escherichia coli within a biofilm

Open channel geometry for transflectance measurements

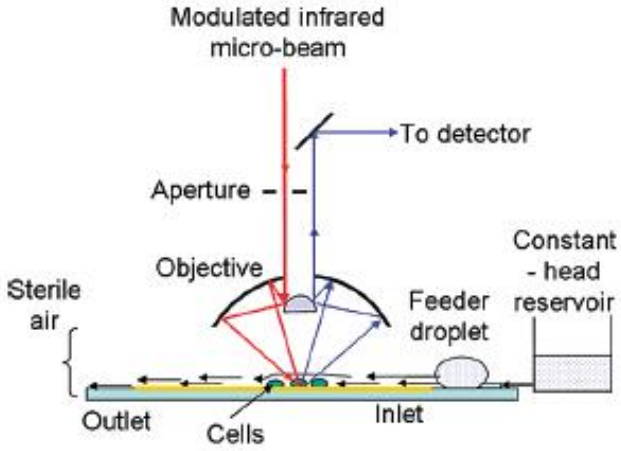

Diversification processes in response to MCC toxicity have been revealed

From H-Y H. Holman et al., Analytical Chemistry, 81:8564 (2009)

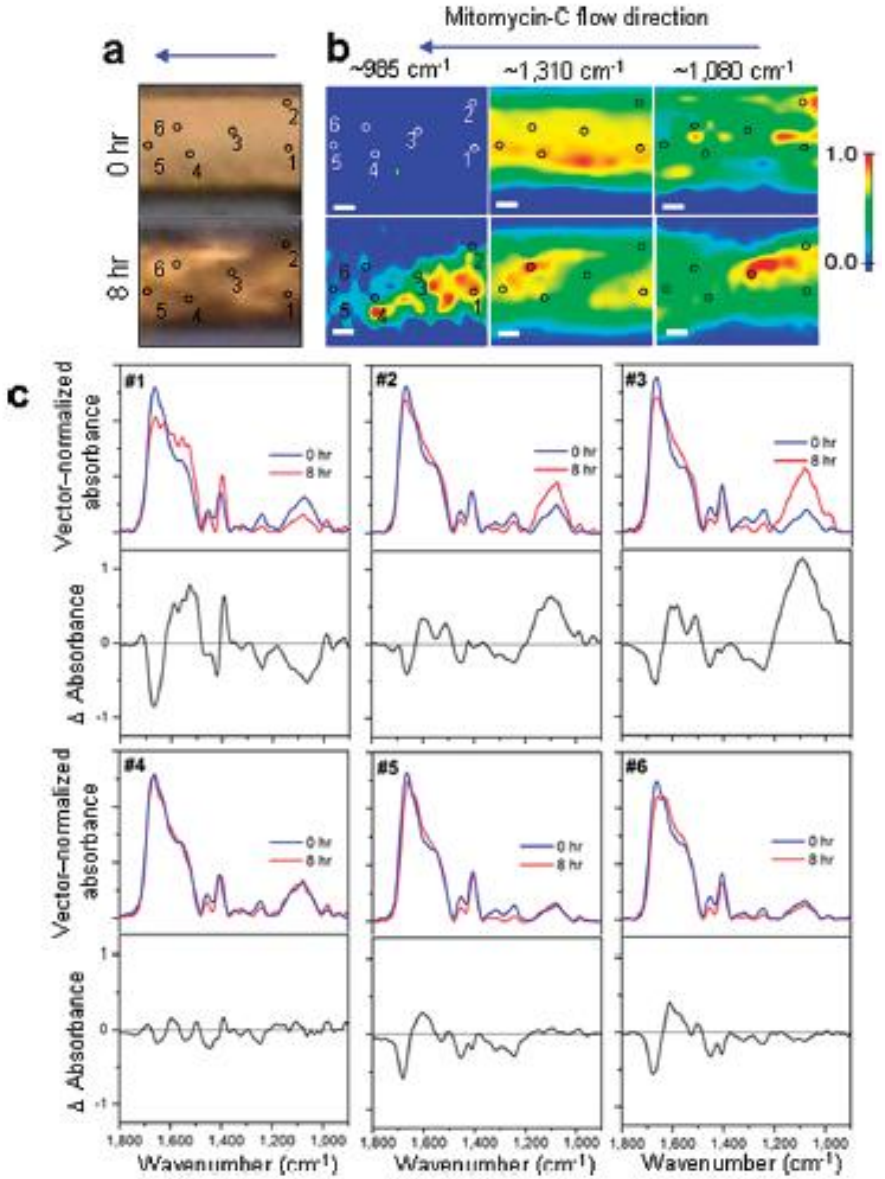

Dual element ATR microscopy

Sample windows and hemisphere are scanned

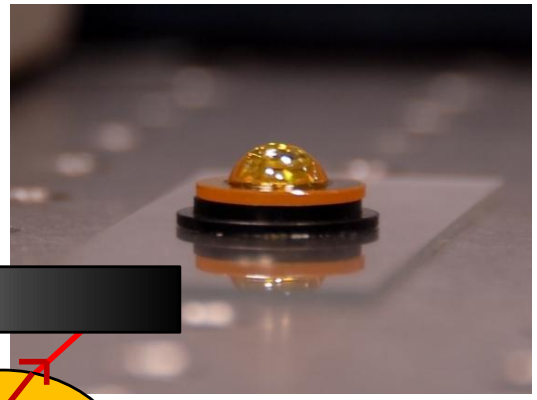

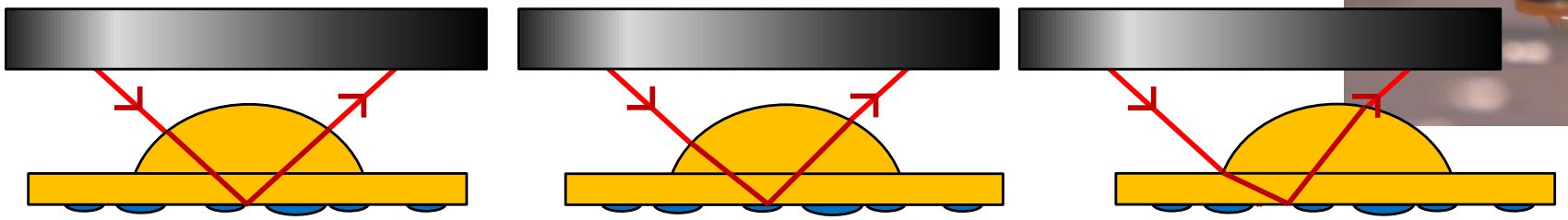

The lateral resolution is improved accordingly with the hemisphere-window refractive index, 2.4 for ZnSe

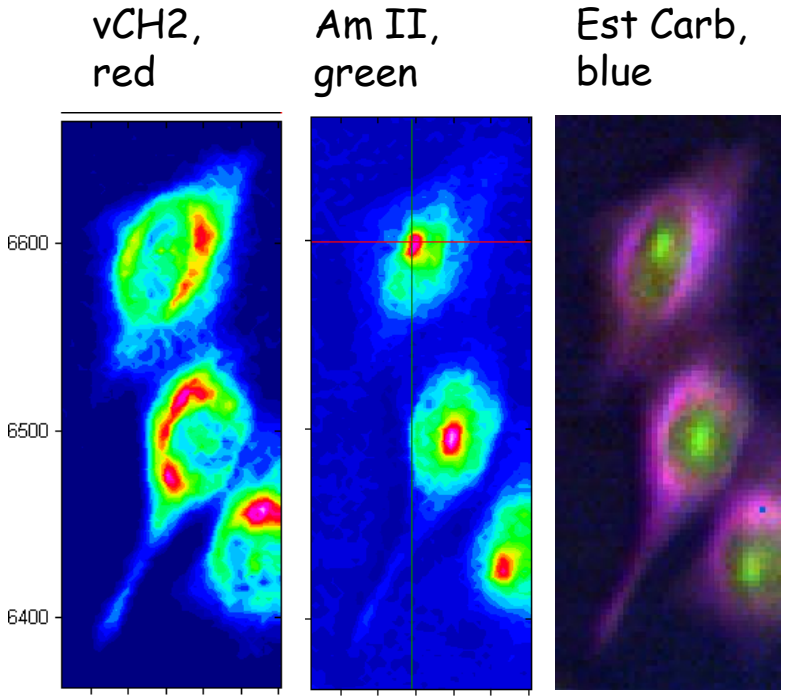

Geometry for living cell analysis

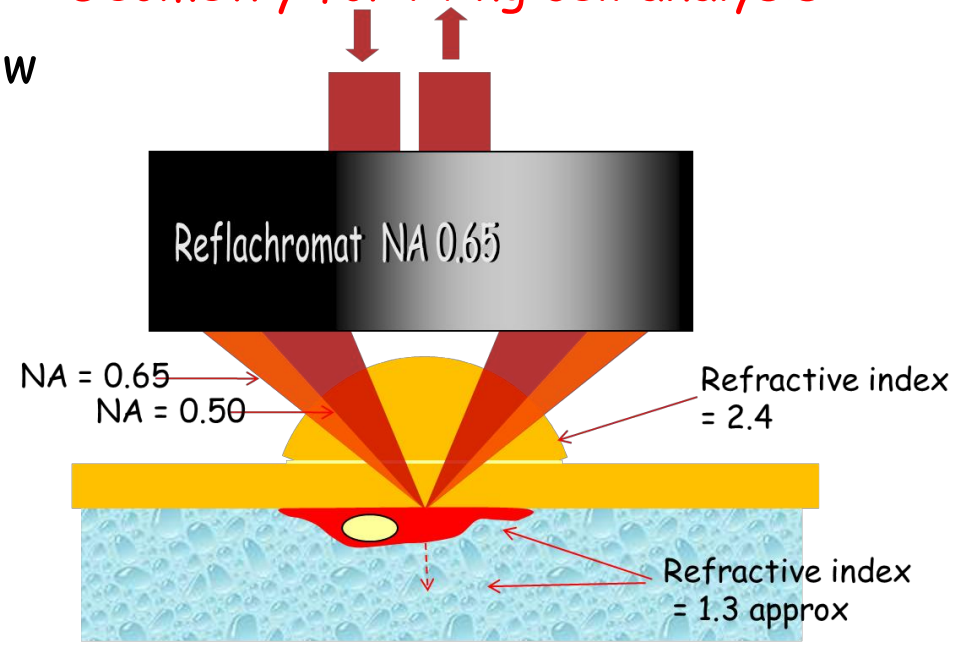

ZnSe toxicity toward cells
only highest angles will reflect internally at ZnSe interface.
Other rays at lower angles will be lost.

Summary and conclusions

- FTIR spectroscopy and microspectroscopy are quite versatile tools for probing chemo-physical properties of matter
- Chemo-physical features of a sample can be resolved at diffraction limited spatial resolution by exploiting the brightness advantage of SR sources
- The SR brilliance is fundamental for the full exploitation of microspectroscopic capabilities in the MIR, where vibrational features of a sample are investigated
- Samples with different size, morphology, composition, origin and nature can be investigated by using the appropriate sample preparation and sampling technique
- The complementation of SR-IRMS with other investigation tools allows to shed some light on many field of science, such as space science, earth science, cultural heritage, life sciences and many others